Synthesis and Characterization of CdSe and Au-CdSe hybrid nanoparticles

Leonor de la Cueva Castillo

Universidad Autónoma de Madrid (UAM)
Instituto Madrileño de Estudios Avanzados en Nanociencia (IMDEA-Nanociencia)
2017

Synthesis and Characterization of CdSe and Au-CdSe hybrid nanoparticles

Memoria presentada para optar al grado de Doctor en Ciencias por

Leonor de la Cueva Castillo

Directores

Concepción Alonso Fuente

Prof. Titular

Dpto. Química Física Aplicada (UAM)

Beatriz Hernández Juárez

Prof. Contratado Doctor

Dpto. Química Física Aplicada (UAM)

Universidad Autónoma de Madrid (UAM)

Instituto Madrileño de Estudios Avanzados en Nanociencia (IMDEA-Nanociencia)

AGRADECIMIENTOS

Por fin ha llegado el momento!!! Después de tanto tiempo trabajando en esta tesis llena de altibajos, ha llegado el momento de valorar y dar las gracias, y realmente me siento muy afortunada porque tengo muchas personas a las que agradecer. Si bien esta tesis ha requerido mucho esfuerzo y ha sido bastante difícil para mí, sé que no habría sido posible sin todas y cada una de las personas que han colaborado en su realización y que me han estado apoyando durante todo este tiempo.

En primer lugar quiero agradecer a mis directoras de tesis, Dr. Concepción Alonso y Dr. Beatriz H. Juárez, por todo lo que me han enseñado y ayudado durante estos años, por tener siempre la puerta abierta para resolver dudas, por vuestra dedicación y sobre todo por el trato que me habéis dado tanto en el terreno profesional como en el personal. Sinceramente, no sólo habéis sido mis directoras sino que sois amigas a las que siempre podré recurrir. Concha, muchas gracias por acordarte de mí y por querer contar conmigo para este trabajo, si no hubiera sido así seguramente ahora mismo no estaría en este punto. Bea, muchas gracias por la oportunidad que me diste cuando aún estaba terminando la carrera y por el esfuerzo que has hecho para que pudiera continuar esta tesis. Gracias a las dos por la confianza que habéis depositado en mí!

También quisiera mostrar mi agradecimiento al Dr. Roberto Otero, Dr. José María Gallego, Dr. Koen Lauwaet, Dr. Jonathan Rodríguez-Fernández y Dr. Fabiola Iacono, por la realización y la gran ayuda que me han prestado en los estudios de espectroscopía fotoelectrónica de rayos X.

I want to express my sincere gratitude to Prof. Christian Klinke and Dr. Michaela Meyns for their great collaboration in this thesis. Thank you for your support and motivation. I would also like to thank Prof. Christian Klinke for the images of the NPs.

Al Dr. Gorka Salas, muchísimas gracias por haberme dado todo el tiempo que he necesitado para trabajar en esta tesis, por la paciencia que has tenido conmigo, por tu apoyo, por ser un jefe genial y una bellísima persona. En fin, no sé cómo agradecer el buen trato que me has dado durante estos años, muchísimas gracias por todo!

Quisiera agradecer especialmente a los amigos que conocí al empezar esta tesis, Cristinita y Ramontxu, por todos los momentos geniales que me habéis hecho pasar y porque siempre puedo contar con vosotros. Vosotros sois uno de los muchos regalos que me llevo de esta tesis.

A mis compañeros y amigos del laboratorio un dos tres (y Sofi), María, Rebeca y Diego, gracias por aguantar mis cantos y lamentos, por levantarme en los peores momentos y por hacer que trabajar con vosotros sea tan divertido. También quiero agradecer al resto de compañeros de IMDEA Nanociencia, en especial a Álex, muchas gracias por tu incondicional ayuda y por los ánimos que me has dado.

A Miri, por todos los días geniales que hemos pasado juntas en el laboratorio de la uni.

A mis Terrors, Borja, Diego, Fer, Andrés, Juanje y Cosme, porque estos últimos años de tesis con vosotros han sido divertidísimos, por el terracismo de los viernes y por tratarme como a uno más... Ahora en serio, gracias por estar ahí cuando os he necesitado. También quería agradecer especialmente a Borja y Diego, porque esta última semana no sé qué habría hecho sin su ayuda.

Quiero agradecer a mis amigas de toda la vida, Eli, Lau, Aza, Patry, Pau y Mel, y a mis amigos de la universidad, María, Sergio, David, Andrea, Abraham, Jorge y Pablo, por aguantar mi quejas, por estar a mi lado en los peores momentos y conseguir animarme, y porque sois mi día a día.

A mis amigas del CGZ, Anuka y Olgui, gracias por vuestra sinceridad y sabios consejos, pero sobre todo gracias por estar ahí en todo momento.

A mi familia, en especial a mis hermanos y cuñados, Vanesa, Fernando, Sandra y Carlos, gracias por vuestra ayuda incondicional, por todos los consejos que me dais y porque con vuestro apoyo todo siempre es más fácil.

Pero mi mayor agradecimiento se lo debo a mis padres, por apoyarme en mis decisiones, por aguantar mis malos momentos y por enseñarme que todo se consigue con esfuerzo. A mi madre por cuidarme siempre y hacerme ver que con el tiempo todo se arregla. Y por último, quería agradecer especialmente a mi padre, por animarme a hacer esta tesis y por la confianza que depositó en mí cuando ni yo misma la tenía. Siempre creíste en mí y eso lo recordaré toda la vida. OS QUIERO.

Sinceramente,

MUCHAS GRACIAS!

A mi familia, en especial a mi padre.

SUMMARY

Semiconductor nanoparticles (NPs) are one of the most promising materials in nanoscience and nanotechnology due to their numerous applications in several fields, such as photocatalysis, photovoltaics, photodetectors and biomedicine. The nanostructuration of semiconductor materials in the nanometer scale and their combination with other materials yield interesting optical properties.

This thesis is focus on the synthesis and characterization of semiconductor CdSe NPs with different morphology and metal-semiconductor hybrid nanoparticles (HNPs) composed of pyramidal CdSe NPs and Au deposits. In addition, the reaction mechanisms and the surface chemistry including chemical composition and ligand shell have been studied.

Since the optical properties of semiconductor NPs are highly affected by the NP surface chemistry, the knowledge of the chemical composition and the redox reactions is essential for their performance in optoelectronic devices. To this aim, in the first part of this thesis, the changes on the chemical composition of CdSe NPs with different morphology synthesized by the so called *hot injection method*, and their transformation from rod-like to pyramidal shaped NPs due to the addition of 1,2-dichloroethane (DCE) as co-solvent in the reaction medium have been studied. It has been ascertained by several techniques that the inclusion of DCE in the NP synthesis produce the formation of ethane-1,2-dyilbys(trioctylphosphonium) dichloride as by-product, which is the source of chloride ions that causes the morphology changes from rod-like to pyramidal NPs and are incorporated in the ligand shell of pyramidal NPs. The incorporation of chloride ions in the NP ligand shell in a one-step synthesis is of great importance for their technological application, since it has been demonstrated that the exchange of the typical insulating long alkylchain ligands by halides improve the charge transfer between NPs.

The effect of the incorporation of chloride ions in the NP ligand shell and the redox processes that occur on the NPs surface during the application of different electrochemical treatments have been studied by correlated cyclic voltammetry and XPS experiments. According to XPS results, in the case of rod-like NPs the oxidation peaks corresponds to Se oxidation, whereas in the case of pyramidal NPs not only the Se oxidation takes place but also chloride ligands are oxidized, changing the chemical environment of Cd. These results demonstrate that the redox processes taking place at the NPs surface also depend on the ligand shell composition. These processes might alter the optical properties of the NPs and thus the performance of optoelectronic devices where they were integrated.

In this thesis it has also been demonstrated that electrochemical response of these NPs cannot be related with the injection of holes and electrons in the valence and conduction bands, respectively. Contrary to what has been published since 2001, the cyclic voltammetry studies of different size and shape CdSe NPs evidence that the electrochemical response of these NPs is exclusively related to redox processes on the NPs surface.

In the last part of this thesis, the synthesis of Au-CdSe HNPs has been carried out by the *multistage-seeded-growth method* and it has been demonstrated that the initial oxidation state of the Au precursor and the surface composition of the seed NPs drive the final morphology and composition of the Au deposits. Solution precursor studies by cyclic voltammetry and mass spectrometry in combination with the surface characterization of the HNPs by cyclic voltammetry and XPS, demonstrate that the use of a Au(I) precursor leads the formation of Au spherical dots on the corners of the pyramidal CdSe NPs, while the use of a Au(III) precursor produces the covering of the hole pyramidal NPs. The use of pyramidal CdSe NPs capped by chloride ligands as seeds trigger reaction mechanisms in which not only the chemical composition of the NPs but also the ligand composition are key factors in the deposition process, which has not been previously considered.

Finally, chapter 6 gathers a summary of the most relevant conclusions obtained during the course of this thesis.

RESUMEN

Actualmente, las nanopartículas (NPs) semiconductoras son uno de los materiales más prometedores en nanociencia y nanotecnología debido a las numerosas aplicaciones que tienen en diferentes campos, como en fotocatálisis, fotovoltaica, fotodetectores, biomedicina, etc. La nanoestructuración de materiales semiconductores a escala nanométrica y su combinación con materiales de otra naturaleza provoca la aparición de novedosas propiedades ópticas.

Esta tesis está centrada en la síntesis y caracterización de NPs semiconductoras de CdSe con distintas morfologías y en nanopartículas híbridas (HNPs) compuestas de NPs piramidales de CdSe y depósitos de Au con diferentes morfologías. También se han estudiado en profundidad los diferentes mecanismos de reacción y la composición química superficial de las NPs, incluyendo la esfera de ligandos.

Dado que las propiedades ópticas de las NPs semiconductoras se ven altamente afectadas por su composición química superficial, el conocimiento de ésta y de los procesos redox es esencial para su aplicación en dispositivos optoelectrónicos. Con este objetivo, en la primera parte de esta tesis, se han estudiado las diferencias en la composición química de NPs de CdSe sintetizadas mediante el *método de inyección en caliente* con distinta morfología, y su transformación morfológica desde NPs con forma cilíndrica a NPs con forma piramidal debido a la adición de 1,2-dicloroetano (DCE) como co-disolvente en el medio de reacción. Se ha comprobado mediante numerosas técnicas que la inclusión de DCE provoca la formación de dicloruro de etano-1,2-diilbis(trioctilfosfonio). Esta molécula es la fuente de iones cloruro que causan el cambio morfológico de las NPs y además forman parte de la cobertura de ligandos de las NPs con forma piramidal. La posibilidad de incorporar iones cloruro en la esfera de ligandos de las NPs mediante reacciones de una sola etapa es de gran importancia, ya que se ha demostrado que el reemplazo de los típicos ligandos aislantes con cadenas alquílicas largas por haluros mejora la transferencia de carga entre las NPs.

Se ha estudiado el efecto de la incorporación de cloruro en la esfera de ligandos y los procesos redox que ocurren en la superficie de las NPs durante la aplicación de diferentes tratamientos electroquímicos mediante las técnicas de voltametría cíclica y XPS. En el caso de las NPs con forma cilíndrica (sintetizadas en ausencia de cloro) los picos de oxidación corresponden a la oxidación de Se, mientras que en el caso de las NPs con forma piramidal no sólo tiene lugar la oxidación de Se sino que también se produce la oxidación de los ligandos cloruro, lo que afecta al entorno químico del Cd como ha sido comprobado por XPS. Estos

resultados demuestran que tienen lugar en la superficie de las NPs también dependen de la composición de la esfera de ligandos y posiblemente influyan en sus propiedades ópticas y en su funcionamiento en los dispositivos optoelectrónicos en los que suelen ser integradas.

Durante el curso de esta tesis se ha demostrado que la respuesta electroquímica de estas NPs no se puede relacionar con la inyección de huecos y electrones en las bandas de valencia y conducción, respectivamente. Contrariamente a lo que se ha publicado desde 2001, los estudios mediante voltametría cíclica de NPs de CdSe con diferentes formas y tamaños evidencian que la respuesta electroquímica se debe exclusivamente a procesos redox que tienen lugar en la superficie de las NPs.

En la parte final de esta tesis se han sintetizado HNPs de Au-CdSe mediante el *metódo de crecimiento por semillas* y se ha observado que la morfología y la composición de los depósitos de Au dependen del estado de oxidación del precursor de Au y la composición química de las NPs usadas como semillas. El estudio de las disoluciones precursoras de Au realizado por espectrometría de masas y voltametría cíclica en combinación con la caracterización superficial de las Au-CdSe HNPs realizada por voltametría cíclica y XPS, demuestran que el uso de precursores de Au(I) producen la formación de NPs de Au esféricas en los vértices de las pirámides, mientras que el uso de precursores de Au(III) generan un recubrimiento de Au alrededor de las NPs. El uso de NPs piramidales que contienen ligandos cloruro como semillas da lugar nuevos mecanismos de reacción en los que no sólo la composición química de las NPs sino que también la composición de ligandos son factores clave en los procesos de deposición, lo que no había sido previamente considerado.

Finalmente, en el capítulo 6 se resumen las conclusiones más relevantes obtenidas durante la realización de esta tesis.

INDEX

1. Introduction

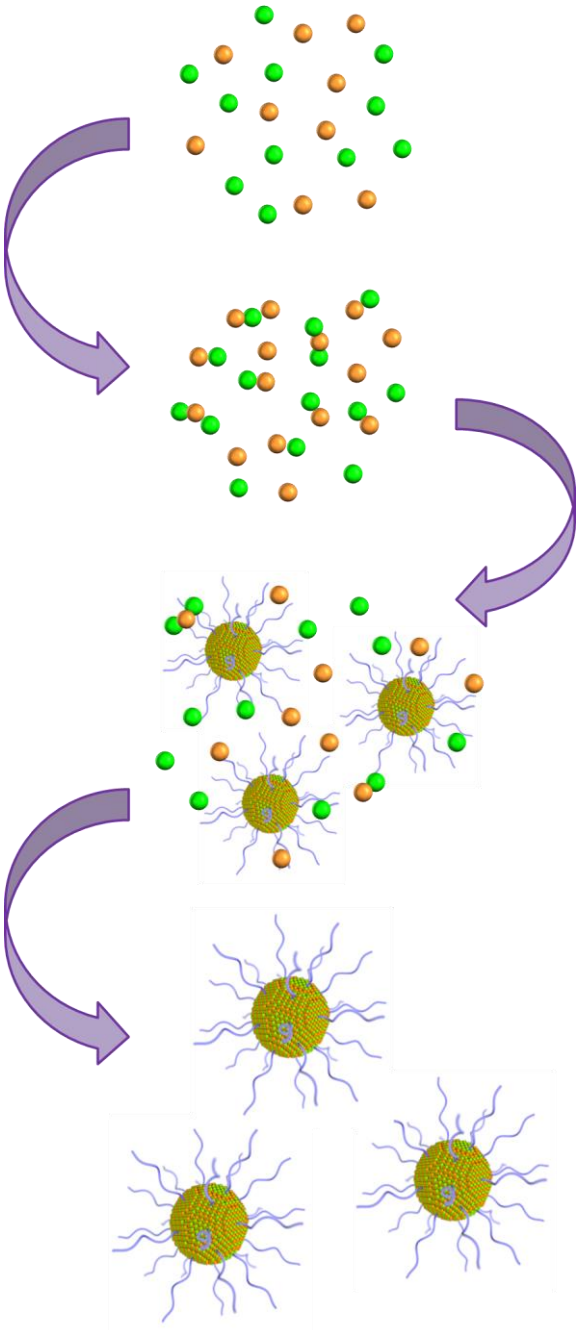

1. Introduction

1. 1. Semiconductor and hybrid nanoparticles (HNPs)

Nanoscience has become one of the most important research fields in the current science scene due to the intense investigation and the multiple advances that have been developed.[1, 2] Nanoscience focuses on phenomena arisen as consequence of the reduction of materials in size.[3] Among the different nanomaterials, nanoparticles became one of the most important and most studied materials due to their potential applications in areas such as photocatalysis, artificial water splitting, sensing, hyperthermia, etc.[4]

A nanoparticle (NP) could be defined as a material with a size smaller than 100 nm (at least in one dimension) and with defined properties which differ from those of the bulk materials.[5] Depending on the material, nanostructured metals, semiconductor or magnetic oxides exhibit different properties compared to their bulk counterparts. Semiconductor NPs show tunable optical properties due to the discretization of the energy levels.[6-11] Metallic NPs exhibit new absorption features as a result of the collective oscillation of the electrons on the metal surface (plasmon oscillations).[12-16] In the case of magnetic NPs, a change of the magnetic behavior from ferri- or ferromagnetic to superparamagnetic is observed upon size reduction.[17-20] Since these properties drastically change with mainly size and shape, an exhaustive effort has been made in the last 20 years to develop robust synthetic routes to produce monodisperse and high quality NPs. Among these routes, the colloidal synthesis, based on the controlled chemical precipitation from molecular precursors, has gained relevance due to its versatility, low-cost and reproducibility in the formation of many different types of materials.[21]

Besides, in the last decades, the interest in the production of combined or hybrid nanoparticles (HNPs) has been intensified due to the possibility to obtain complex nanostructures altering its properties.[22] HNPs are multicomponent NPs, consisting of two or more materials that are bound to each other exhibiting different chemical interfaces. By means of diverse colloidal synthetic methods HNPs with different morphology can be obtained depending on the materials nature, such as core-shell, oligomer-type or the direct fusion of both NPs with small connecting areas at concrete locations.[23] Basically, the final HNPs are platforms on which the contact across the different material sections produces the enhancement of the individual properties of the components and, in many cases, the emergence of synergetic effects that cannot be reproducible by the individual components alone. For example, the combination of semiconductor and metallic NPs results in changes in

the optical properties of the semiconductor part modifying the charge-carrier recombination and in the emergence of plasmon-to-exciton couplings due to the presence of the metal part.[24-26] On the other hand, the combination of semiconductor and magnetic phases leads to changes in the hysteresis parameters increasing the anisotropy of the magnetic part and even in the appearance of new magneto-optical or spintronic phenomena.[27-29]

This thesis is focused on the study of different size, shape, and surface compositions of colloidal semiconductor NPs and semiconductor-metal NPs (HNPs). This introductory chapter gathers the elemental information for the understanding of the formation of colloidal systems and the novel properties gained at the nanometer scale, as well as a brief overview of the different synthetic methodologies to produce NPs.

1. 2. From bulk semiconductors to nanoparticles: Quantum size effect

As it is known semiconductor materials exhibit several properties derived from the arrangement of atoms in an ordered crystal (ordered arrangement of the atomic potential), producing the formation of continuous electronic energy levels, called energy bands, as a result of the overlapping of the atomic orbitals of the constituent elements of the crystal.[30] These materials have two different energy bands, the valence and conduction bands, separated by the band gap or forbidden energy interval, E_g. At 0 K the valence band is filled with electrons while the conduction band is empty.

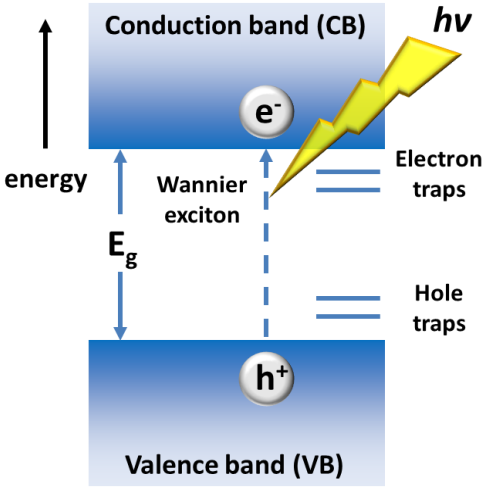

Scheme 1. *Electronic structure scheme of semiconductor materials.*

The semiconductor materials can be light excited by the absorption of a quantum of light, triggering the promotion of an electron from the valence to the conduction band and leaving a

hole (or a positive charge) in the valence band (Scheme 1). The electrical conductivity of these materials results from the free movement of these charges inside the crystals, but sometimes these charges can form a Wannier exciton (electron-hole pair) due to the Coulomb forces they experience. Usually, excitons of bulk semiconductors dissociate at room temperature.

When semiconductor materials are structured on the nanometric scale in the three dimensions the energy bands turn into quantized discrete energy levels.[5, 31] In this sense, the quantization and separation of the energy levels resembles the electronic structure of molecules. For this reason, in some cases, when the NP size is about 1-2 nm, is more appropriate to use the HOMO (highest occupied molecular orbital) and LUMO (lowest unoccupied molecular orbital) terms instead of referring to the valence and conduction bands, respectively. The discretization of the energy bands into energy levels is due to the quantum confinement of the electron-hole pair that occurs when the NP size is comparable to the Bohr exciton radius. The energy difference between these levels can be modulated as a function of the semiconductor material size. This fact is a consequence of the quantum size effect and it can be explained by the particle-in-a-box model. Using quantum mechanics to solve the Schrödinger equation, the following expression reported by L. Brus[32, 33] in 1983 was obtained:

$$E_g = E_{g-bulk} + \frac{\pi^2 \hbar^2}{2\mu_{ex} R^2} - \frac{1.786 e^2}{\epsilon R} \quad (1)$$

The first term, $E_{g\text{-}bulk,}$ is the band gap energy of the semiconductor bulk material. The second term corresponds to the quantum confinement correction, where $\hbar$ is the reduced Planck constant, μ_{ex} is the exciton effective mass that corresponds to the sum of the effective masses of the electron and hole and R is the NP radius. The third term corresponds to the Coulomb interaction between the electron and hole. In this term e is the electron charge, ε is the material dielectric constant that can be expressed as the product of the relative and the vacuum dielectric constants ($\varepsilon_r \cdot \varepsilon_0$) and 1.786 is a dimensionless constant obtained from the electron and hole ground-state enveloped functions for a spherical NP of radius R (using for the calculations the effective mass approximation (EMA)).[34] This expression describes the tunability of the semiconductor NPs E_g with respect to the bulk semiconductor.

To fully understand the effect of the material size on E_g it is important to remark that in the particle-in-a-box model the potential energy is 0 and only the kinetic energy has a contribution,[35] obtaining the following allowed energies:

$$\mathrm{E} = \frac{\pi^2 \hbar^2}{8 \mathrm{m} \mathrm{L}^2} \mathrm{n}^2 \quad (2)$$

Where *n* is the principal quantum number that indicates the electron state (*n = 1, 2, …*), *ħ* is the reduced Planck constant, *m* is the mass and *L* the box length. Therefore, the separation between adjacent energy levels with the quantum numbers *n* and *n+1* is:

$$E_{n+1} - E_n = \frac{\pi^2\hbar^2}{8mL^2}(n+1)^2 - \frac{\pi^2\hbar^2}{8mL^2}n^2 = (2n+1)\frac{\pi^2\hbar^2}{8mL^2} \quad (3)$$

From equation 3 it is inferred that the separation of the adjacent energy levels increases as the box length decreases. This means that E_g decreases as the NP size increases. This effect is represented in Figure 1, where several NPs dispersions under excitation with UV light, along with a scheme of the electronic structure as the NP size increases are shown. The dispersions correspond to CdSe NPs with sizes from approximately 2 (left vial) to 6 nm (right vial).

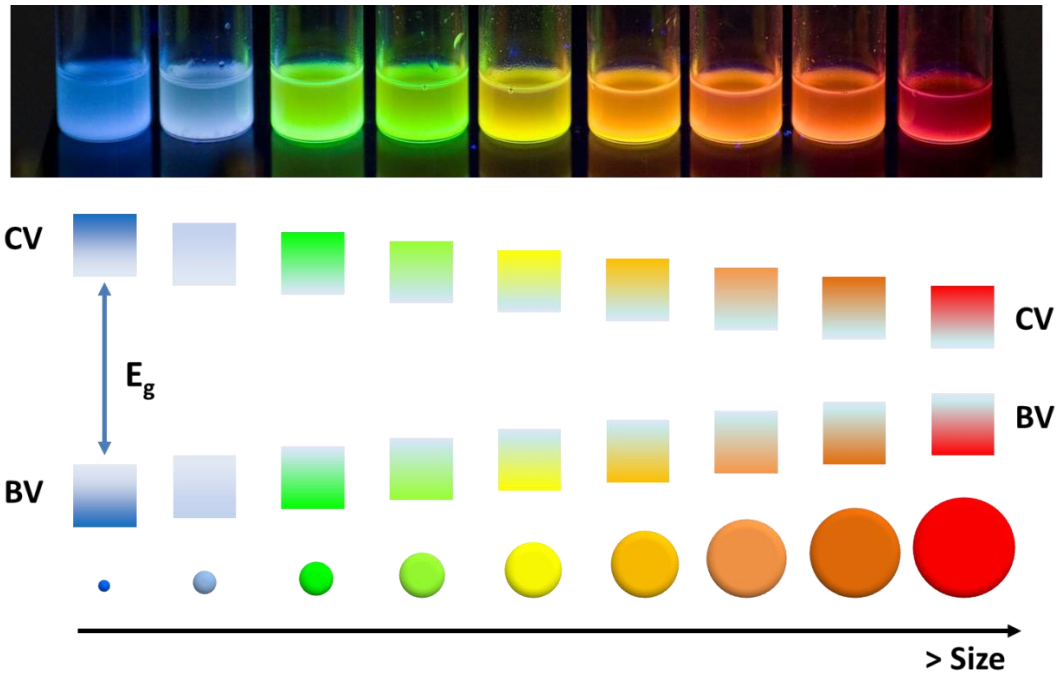

Figure 1. *Top: Emission of colloidal CdSe NP dispersions of different size under irradiation with UV light. Bottom: Scheme of the electronic structure of semiconductor NPs as the NP size varies. The energy difference between the valence and the conduction band increases as the NP size decrease due to the quantum confinement effect.*

1. 3. Optical properties of semiconductor NPs and semiconductor-metal HNPs

1. 3. 1. Semiconductor NPs

As has been explained above, semiconductor NPs present properties related to their size. Among them, the most important properties are their tunable optical properties,

particularly the UV-Vis absorption and the photoluminiscence emission. Semiconductor NPs can absorb a photon when its energy is similar or exceeds E_g. The lowest energy optical transition present in the NPs absorption spectrum is assigned to the promotion of an electron from the valence to the conduction band, and corresponds to the formation of the exciton.[4] Therefore, the position of this peak depends on E_g whereas the remaining absorption waves located at shorter wavelengths corresponds to the transition of electrons to higher excited states.[36] The absorption profile and the width of the peaks are strongly affected by the shape and the size distribution of the NPs. An increase in the NPs polydispersity causes a broadening of the peaks and even in extreme cases only an absorption shoulder can be discernible.

Another optical property of semiconductor NPs is the photoluminescence. The photoluminescence is based on the absorption of a photon producing the transition of an electron from the ground state to an excited state, the formation of the exciton and the subsequent emission of light by the recombination of the electron-hole pair. There are two types of photoluminescence depending of the excited state and the emission pathway, the fluorescence and the phosphorescence. In the fluorescence emission of semiconductor NPs, the absorption of light causes the promotion of the electrons from the ground state to a singlet excited state. Afterwards, the electrons undergo vibrational relaxation processes and drop to the lowest vibrational level of the singlet excited state via phonons in a non-radiative way. Finally, the recombination of the exciton produces the emission of light at higher wavelengths (lower energy) after a brief period of time, called fluorescence lifetime. The difference between the absorption energy and the energy of the emitted light is known as the Stokes-shift and has its origin in the energy loss suffered during the charge relaxation process.[4]

As has been mentioned above, the absorption and emission properties of the semiconductor NPs can be modulated as a function of their size due to the quantum confinement effect. In Figure 2 the absorption and emission peak shift to higher wavelengths as the semiconductor NP size increases.

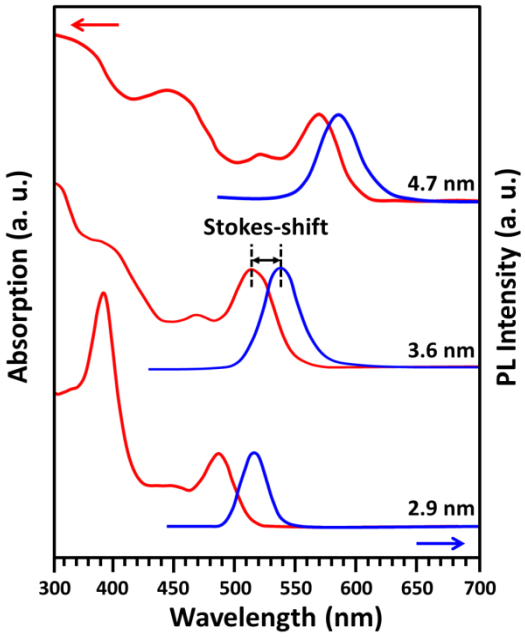

Figure 2. *Absorption (red line) and emission (blue line) spectra of different size semiconductor NPs. The Stokes-shift corresponds to the energy difference between the absorption energy and the energy of the emitted light (marked between two black dashed lines).*

The emission efficiency is expressed by the fluorescence quantum-yield (QY), which is the ratio between the number of absorbed photons and the number of emitted photons. To reach the maximum value of the QY (1) is difficult due to mainly the incomplete surface passivation with ligands, which implies the presence of surface trap states or defects that give rise to non-radiative processes decreasing the emission efficiency.

1. 3. 2. Semiconductor-metal HNPs

The unique properties of HNPs arise from the combination of those of each individual material and the synergistic properties that come from the contact between them. For this reason the HNPs can be classified in: (i) multifunctional NPs, in which the materials retain their initial properties, and (ii) hybrid NPs (HNPs), in which the properties of one of the material changes due to the presence of the other. Other factors that influence the final properties are the morphology of each material (the different growth domains) and if the domains are linked directly by chemical bonds or by molecular moieties. This section focuses on the optical properties of semiconductor-metal HNPs composed of CdSe and Au.[22, 37]

Due to the high proximity between the two types of materials several effects are expected in HNPs. Till the date, it has been demonstrated that the fluorescence can be

enhanced or quenched depending of the distance between both materials. Enhancement effects have been observed when the metal part is chemically linked (organic molecules with tunable length) to the surface of the semiconductor NPs and its origin was attributed to the interaction between the metal surface plasmon and the excitons of the semiconductor NPs.[38] Another reason is an increase in the absorption cross-section with reduced distance between both materials. In general terms, this effect is observed when both materials are separated by small distances and a large potential barrier is present between both domains.

On the other hand, fluorescent quenching is presented when the metal and the semiconductor domains are in close contact causing the charge separation at the materials interface.[39-41] The electron transfer from the semiconductor to the metal is facilitated because the energy of the metal Fermi level is between the energy of the valence and the conduction bands of the semiconductor NP. Once the exciton is created the electron relaxes into the metal Fermi level in a non-radiative way leaving a hole in the semiconductor part. This fact makes the HNPs suitable nanostructures for their implementation in photocatalysis and solar cells.

1. 4. Synthetic methods

There are two different methods to synthesized NPs, namely the top-down and the bottom-up approach (Figure 3).[5]

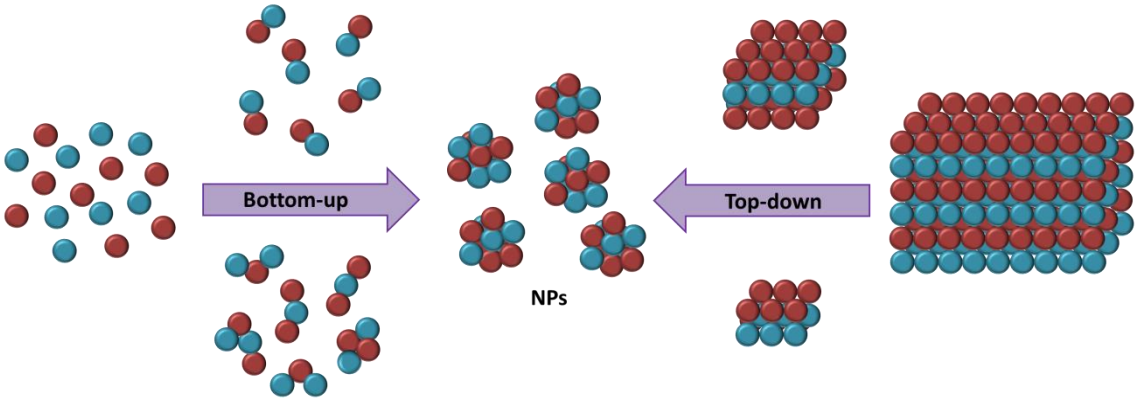

Figure 3. *Scheme of the bottom-up and top-down processes.*

The first one consists of physical methods which imply the mechanical treatment of bulk materials to reduce their size, like lithography, or the use of electron or ion beams or X-rays. The second one consists of chemical syntheses, which involve the nucleation and growth of nanocrystals from precursor atoms or molecules to produce nanomaterials. Both methodologies have advantages and disadvantages. In the case of the top-down processes it is possible to produce large quantities of NPs but control over their size and uniformity is more

challenging and entail high costs, whereas by means of the bottom-up approach there is a high control over the size, shape, and monodispersity of the NPs, although only small quantities can be produced.

In this thesis a colloidal liquid-phase bottom-up approach has been performed to produce the NPs, thus, in the following a brief description of the different bottom-up synthetic methods is presented.[42]

1. 4. 1. Vapor phase deposition methods

These methods are frequently used in the fabrication of semiconductor thin-films, but they can be also used to produce different nanomaterials, as carbon nanotubes or nanoparticles. Within this group, the methods can be classified in physical vapor deposition (PVD) and chemical vapor deposition (CVD) ones. The latter consist on the introduction of volatile precursors in the reaction chamber, their reaction or thermal decomposition at high temperatures (500-1000 °C) and its deposition on a substrate. One of the most used CVD techniques is the molecular beam epitaxy (MBE), which allows the growth of single atomic layers and the thickness of the final deposits can be finely controlled.

1. 4. 2. Vapor-liquid-solid method

The vapor-liquid-solid (VLS) method is commonly used to create 1D nanostructures like rods, wires or whiskers. It has been used since 1970s to synthesize micrometric and millimetric whiskers of different materials. The mechanism governing deposition can be divided in three different steps: (i) a metal catalyst is introduced and the temperature is increased to form catalyst liquid droplets where the nanostructure grows, (ii) the volatile precursor materials are included and adsorb and diffuse into the droplets, and (iii) the continuous inclusion of the precursor materials produces the supersaturation of the alloy-droplets leading the nucleation of the solid material at the liquid/solid interface and the 1D growth.

1. 4. 3. Liquid-phase methods

The liquid-phase methods consist of chemical precipitation reactions and can be divided into two different groups: sol-gel and colloidal methods.[42]

1. 4. 3. 1. Sol-gel methods

The sol-gel methods are based on the formation of small particles or colloids (sols) by hydrolysis and condensation reactions in a liquid phase. The increase of the dispersed phase concentration and changes of the external conditions (pH, solvents, etc.) produce the contact and aggregation of the colloidal particles forming a gel. The subsequent drying processes of the gel leads the production of different materials, such as xerogels, aerogels, ambigels or cryogels. With this type of synthesis it is possible to produce differently shaped materials, powders, fibers, etc. The most synthesized materials by these methods are silicon and titanium oxides.

1. 4. 3. 2. Colloidal methods

Colloidal synthetic methods can be used to produce several nanomaterials. With these methods not only the shape and chemical composition of single materials can be varied but also the production of alloyed, doped, and combined materials is feasible. This section will focus on the synthesis of single semiconductor NPs and metal-semiconductor HNPs.[43]

Colloidal syntheses are based on the formation of NPs by chemical precipitation reactions from their molecular precursors in different solution media. To achieve homogeneous dispersions of NPs in solution different stabilizers or surfactants, which bind to the NPs surface, have to be included in the syntheses. Finally, the obtained NPs are composed by an inorganic core that confers the optoelectronic properties, and an organic shell of molecules or species that attributes to the NPs the colloidal stability in solution and controls the different physico-chemical properties.

The colloidal NP syntheses can be carried out in several liquid media. Initially, the NP syntheses were carried out in aqueous media using different molecules or polymers as stabilizers.[44] At the same time, a bi-phase method, named microemulsion, was developed to synthesize the NPs inside confined volumes, such as micelles (organic solvent droplets stabilized in a continuous aqueous phase) or inverse micelles (water droplets stabilized in an organic continuous phase).[42] These droplets served as nanoreactors for the NP growth and prevent the aggregation between NPs. Both methods are carried out at room temperature and the produced NPs have relatively broad size distributions. This forces to perform several post-synthetic treatments to separate the different sized NPs, like size/selective precipitation from solvent-non-solvent mixtures. In 1993 Murray and co-workers introduced a new synthetic procedure called "*hot-injection method*" where the colloids were performed in organic

solvents at relatively high reaction temperatures (around 300 °C).[6] This method is based on the "burst nucleation" concept proposed by LaMer and Dinegar in 1950,[45] in which many nuclei are generated simultaneously at high temperature, allowing their growth at lower temperature without additional nucleation. The “burst nucleation” refers to the separation of the nucleation and growth processes, which are illustrated in the LaMer plot (Figure 4). This method permits obtaining NP dispersions with size distributions below 5%. During the reaction at high temperatures the monomer (minimum subunit of the nanoparticle) concentration increases constantly by the *in-situ* generation or by the exterior supply of precursors, producing the supersaturation of the solution (S>1). In this phase (stage I), no nuclei are formed due to the high energetic barrier for the spontaneous homogeneous nucleation. Later, in stage II, the nucleation starts when the supersaturation is highly enough to exceed the critical saturation value ($S>S_C$), causing the formation of stable nuclei in the solution. As the monomers are consumed during the formation of the nuclei, the supersaturation decreases below S_C, and thus the nucleation rate is zero and the nuclei grow (stage III).

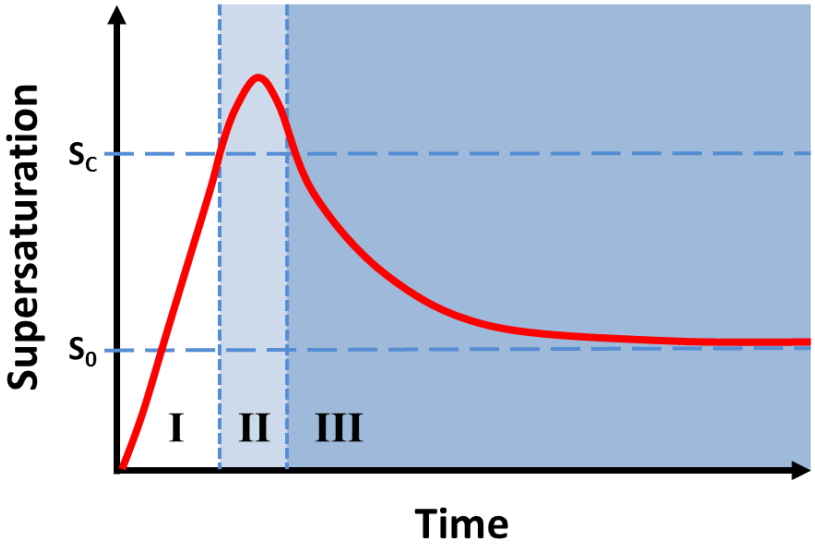

Figure 4. *LaMer plot: illustration of the supersaturation degree with time during the nanoparticle formation. Stage I: supersaturation of the solution without any nucleation process. Stage II: beginning of the nucleation process above the critical saturation degree. Stage III: stop of the nucleation process and initiation of the growth process due to the supersaturation decrease.*

Experimentally, by the *hot-injection method* the separation of the nucleation and growth processes is achieved by the rapid injection of cool precursors into a hot solvent, reaching a sufficiently high concentration to overpass the energetic barrier for homogeneous nucleation. After the precursor injection, the temperature is quickly decreased to stop the

nucleation process and separate it from growth. Another synthetic method that offers the possibility to separate these processes is the *heating-up method*. This method is based on the mixture of the different precursors in an organic solvent at room temperature and heated it up to a certain temperature at which the nucleation starts. In this process, there is a moment in which the number of nuclei stops increasing and a maximum particle concentration is reached. After this moment, the growth process starts without coinciding with the formation of new nuclei. This method allows the production of large-scale NPs and, in some cases, their sizes and uniformity could be comparable with the NPs obtained by the *hot injection method*.

In the case of HNPs, the colloidal syntheses are based on the growth of a different material over a pre-existing NP or seed.[5, 43] Among the colloidal methods there are two essential strategies: (i) the "one-pot" or single-stage approach that lies on the synthesis of the initial seeds and the subsequent precursor addition of the new material in the same reaction pot, and (ii) the multistage-seeded-growth approach. The "one-pot" synthesis is experimentally easy and fast, but it is almost impossible to avoid the alloying of the different materials (especially at the interface) and cannot provide high control over the final composition. Instead, the multistage-seeded-growth approach allows the separation of the nucleation of the seeds and the growth of the other materials, the change of the reaction conditions of each structure, the possibility to perform different post-treatments to the initial seeds and the suppression of the interfacial alloying due to the possibility to perform low temperature reactions.

Among the multistage-seeded-growth methods there are different ways to perform the addition of new precursors. The most used strategy is the precursor addition to the seeds under vigorous stirring, which is most suitable when a slow growth is required. The growth rate should be maintained constant during the reaction to avoid the homogeneous nucleation of the added precursor. For this purpose the precursors can be included in different ways: (i) dropwise addition of the mixed precursors, (ii) dropwise alternating the precursors, and (iii) by the alternating injection of the different precursors, known as SILAR method (Successive Ion Layer Adsorption and Reaction). The choice between the different additions depends on the precursor's nature and its reactivity in the reaction media. Another strategy for the multistage-seeded-growth is the seeded injection, which consist in the injection of the seeds mixed with one of the precursors into a hot solution that contains the second precursor under vigorous stirring. This methodology leads to the heteroepitaxial growth of the new material on the NP seeds and prevents the homogeneous nucleation, which will be explained below.

There are other methods to produce HNPs. In the last two decades, a method commonly used in bulk materials and called ion exchange, has been applied for the HNPs synthesis.[46] This post-synthetic method is based on the displacement of the original NP ions with new ions under certain conditions that favor their diffusion. The diffusion coefficient of ions in bulk materials is much lower than in NPs. Further, the surface area to volume ratio is large in nanostructures, producing a fast ion exchange. These reactions are often carried out in solution, both in organic and aqueous solvents, but it has also been successfully applied in solid materials. Most of the reported works in the literature focus on the cation exchange. In this case, the anion lattice is practically unaltered while the cations are exchanged in a topotactical way. The conditions to reach a topotactic cation exchange depend on the nature of the initial and new material cations and their stabilities both in solution and in the NPs. By this post-synthetic method it is possible to obtain different HNPs, such as core-shell, alloyed, gradient composition, and even periodic compositional HNPs.

A parallel method to ion exchange is the galvanic replacement.[46, 47] The galvanic replacement is an electrochemical method carried out in solution, in which one of the metals is oxidized acting as a sacrificial template by ions of a second metal having a higher reduction potential. In this method two redox reactions occur: (i) the oxidation or corrosion of the lower reduction potential metal in the anode, and (ii) the ions reduction of the highest reduction potential metal and its deposition on the cathode. By means of this method the native metal of the seed is dissolved (oxidized) and diffuse into the solution leaving a hole in the NP structure. At the same time, the ions of the new metal are reduced and deposited on the NP surface creating novel HNPs with a different material shell or alloyed HNPs.

1. 5. Formation mechanisms of NPs: nucleation and growth processes

As already mentioned, the formation of NPs takes place in two well-differentiate steps: the nucleation and further growth. The understanding of these processes is essential to improve the synthetic procedures and to obtain high quality NPs.

1. 5. 1. Nucleation process

The formation of the NPs evidently starts with the nucleation process. There are two types of nucleation processes: (i) the homogeneous nucleation that occurs when several atoms assemble forming a small crystal through density fluctuations of the media, as in the case of semiconductor NPs, and (ii) the heterogeneous nucleation that occurs on surfaces of formed nuclei or pre-existing NPs which is typical in the synthesis of HNCs.[5, 31]

1. 5. 1. 1. Homogeneous nucleation

As has been mentioned in the previous section, the monomer concentration should be high enough to reach the critical supersaturation value (S_C) and overcome the energy barrier to form stable nuclei. The nucleation in a solution at constant pressure and temperature is driven by the difference in free energy between the crystalline phase (atoms bound forming part of the NPs) and the solution phase (atoms free in solution). Thus, the total change in free energy (ΔG_{TOT}) for the nucleation process is given by equation (4):

$$\Delta G_{TOT} = \Delta G_V + \Delta G_S = \frac{4}{3}\pi r^3 \rho \Delta\mu + 4\pi r^2 \gamma \quad (4)$$

Where the first term ΔG_V is the volume excess free energy, which is negative because it is the energy freed by the formation of bonds. The second term ΔG_S is the surface excess free energy, which is positive because it takes into account the correction for the incomplete saturation of the surface bonds. The symbol ρ corresponds to the density of the crystalline phase, γ is the interfacial tension between the nuclei and the solution, r is the radius of the nuclei and $\Delta\mu$ is chemical potential difference between the nucleus and the monomers in the solution, which can be described as $-kT \cdot ln(S)$. The supersaturation degree can be also expressed as the factor between the monomer activity in the growth solution at a certain temperature (T) and the monomer activity in equilibrium with the macroscopic particle at the same temperature. Taking into account equation 4 and the fact that ΔG_V and ΔG_S have opposite sign, it can be deduce that ΔG_{TOT} will reach a maximum for nuclei that have a critical radius (r_C) and decreases as the nuclei radio increase creating an energy barrier for the nucleation process (Figure 5).

This fact implies that the nuclei with a radius under the r_C will be re-dissolved into monomers in the solution (will not be stable), whereas the nuclei with radius above r_C will form an stable nuclei that will grow to form a NP. The critical radius, r_C, can be expressed as:

$$r_C = -\frac{2\gamma}{\rho k T \ln S} \quad (5)$$

This equation shows that high T and/or supersaturation values lead to smaller critical values favoring the nucleation processes, as it was experimentally demonstrated by the *hot-injection synthesis.*

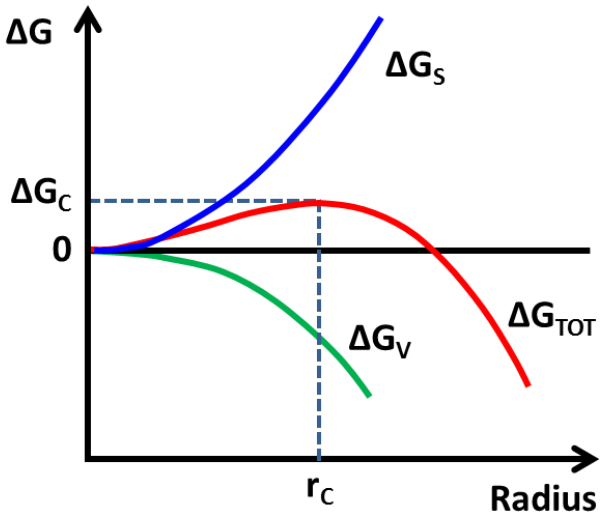

Figure 5. *Change in the free energy during the nucleation process. In this graphic ΔG_S is the surface excess free energy, ΔG_V is the volume excess free energy, and ΔG_{TOT} is the free energy change. The activation energy for the nucleation process is indicated by ΔG_C.*

1. 5. 1. 2. Heterogeneous nucleation

The presence of a seed in the nucleation process lowers the activation energy (ΔG_C) for the nucleation since it provides the system with a low-energy interface between the NP and the solution (Figure 6).

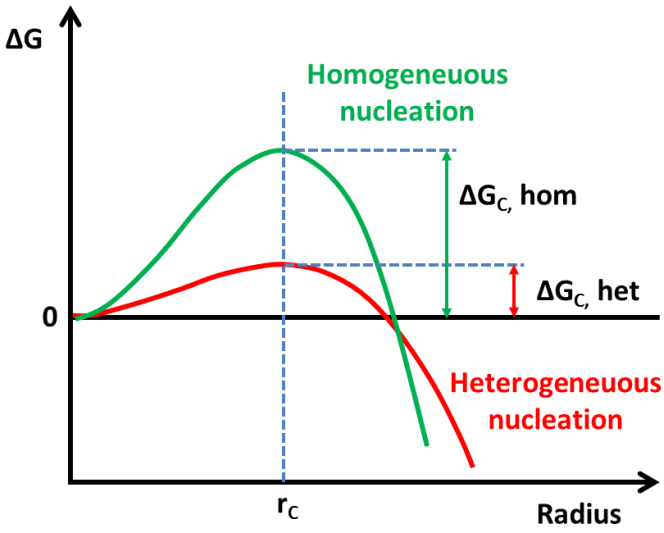

Figure 6. *Change in free energy for the heterogeneous and homogeneous nucleation. The critical radius, which is the same for homogeneous and heterogeneous nucleation under identical conditions, is indicated by r_C. The activation energy for the nucleation process is indicated by ΔG_C.*

For this reason, the nucleation process occurs at low monomer concentrations and temperatures, which also aids the suppression of the homogeneous nucleation as previously mentioned for the multistage-seeded-growth.

The critical free energy for the heterogeneous nucleation can be expressed by:

$$\Delta G_C(\text{het}) = \Delta G_C(\text{hom}) \times f(\theta) \quad (6)$$

Where f(θ) is a parameter that depends on the contact angle (θ) between the new nucleation NP and the pre-existing surface of the seed ($f(\theta) = 0.25[(2+\cos\theta)\cdot(1-\cos\theta)^2]$).

The most important difference between the homogeneous and the heterogeneous nucleation is the number of interfaces of the system. In the homogeneous nucleation there is only one interface between the nuclei and the solution (with an interfacial energy, Υ_{LG}), whereas in the heterogeneous nucleation there are three different interfaces with their own interfacial energies: the solution-nuclei (Υ_{LG}), the nuclei-substrate (Υ_{SL}) and the substrate-solution (Υ_{SG}). The final contact angle (θ) will depend on the interplay between these energies since the nucleation of the new material should happen where the interfacial energy is minimum (equation 12):

$$\gamma_{SL} + \gamma_{LG}\cos\theta = \gamma_{SG} \quad (7)$$

It is also important to mention that the interfacial tension in the solid-solid interface play an important role and is related with the lattice mismatch of the different materials. In the heterogeneous nucleation small lattice mismatch between the new material nucleation and the seeds is required. Finally, the orientation of the new nucleation process depends on the materials' nature and will take place in high energy sites, such us defects or corners, to minimize the interfacial tension, as it will be shown in Chapter 4.

1. 5. 2. Growth process

There are several factors that affect the growth process, such as the temperature, the chemical composition of the reaction media (including surfactants that bind to the NPs surface and slow down the growth rate), the initial concentration, the concentration upon monomer depletion during the NPs growth, etc. Apart from these factors, it is important to mention that the growth process also depends on the previous nucleation. The nucleation may vary the initial conditions for the growth due to non-homogeneities, density fluctuations of the reaction

media or even slight variations in the reaction temperature during the NPs nucleation. Thus, the growth of the NPs is affected by the size, shape and structure of the initial nuclei.[5, 31]

The growth of NPs may take place either by the monomer addition over pre-existing nuclei or by coalescence of smaller NPs. The growth by coalescence is inhibited by the presence of surfactants that anchor to the NPs surface and prevent the aggregation between NPs. In the case of the here reported CdSe NPs the NPs growth is produced by monomer addition. Thus in this section only this type of mechanism will be presented.

The growth by monomer addition occurs in two different steps: (i) the monomers diffusion to the NPs surface, and (ii) the monomers incorporation into the NPs (reaction). It is important to remark that, simultaneously to the growth, monomers are removed from the NP and diffuse into the solution. However, these two competing process are only relevant at low monomer concentrations. Initially the growth rate of NPs can be expressed by:

$$\frac{dr}{dt} = \frac{DV_m(a_b - a_r)}{r - (D/K_S)} \quad (8)$$

Where D is the diffusion coefficient of the monomer, V_m is the molar volume of the solid, a_b is the monomer activity in the bulk of the solution, a_r is the monomer activity on the surface of the NPs with a radius r, and K_s corresponds to the reaction constant between the monomers and the NP surface.

The monomer diffusion step depends on the concentration gradient between the NPs surface and the bulk of the solution. When this is the limiting step ($D \ll K_s r$), the reaction is in the diffusion controlled regime and can be approximated to:

$$\frac{dr}{dt} = \frac{DV_m(a_b - a_r)}{r} \quad (9)$$

On the other hand, the monomer incorporation on the NP surface involves the reaction between the monomers and the surfactant capped NPs surface and its rate depends on the release of the surfactant molecules and the available NP surface sites. When the monomer incorporation is the limiting step ($D \gg K_s r$), the growth is under reaction control and can be expressed by:

$$\frac{dr}{dt} = DV_m(a_b - a_r) \quad (10)$$

As it is shown in equation 10, that under reaction control the growth rate is size-independent and the size distribution remains constant during the growth. Under reaction controlled

conditions the growth rate depends on the free surface sites for the monomer reaction and the NP size becomes irrelevant at this stage of the growth.

The growth mechanism is initially dominated by the reaction controlled regime, where the monomers' activities (concentrations) are high and the monomer diffusion can be neglected. At later stages, when the monomer concentration is depleted the growth mechanism is expected to be in the diffusion controlled regime. During this phase, the dissolution rates of the NPs increase. According to the Gibbs-Thomson relation, the particles that have experienced dissolution processes have an extra chemical potential, causing an increase of its solubility in a size dependent way:

$$a_r = a_0 \, exp(2\gamma V_m / r k_B T) \tag{11}$$

Where a_0 is the monomer activity in equilibrium with the bulk material and K_B is the Boltzmann constant. This relation can be also used to define the critical size that is in equilibrium with the monomer activity in the bulk of the solution (r_C=r when a_r=a_b), which is equivalent to the previously mentioned critical radius, r_C, for the nucleation process (equation 5). Finally, the growth rate can be expressed in terms of the critical size as stated in the following equation:

$$\frac{dr}{dt} = \frac{2\gamma D a_0 V_m^2}{k_B T r} \left(\frac{1}{r^*} - \frac{1}{r}\right) \tag{12}$$

This equation shows that NPs with sizes similar to the critical one, in equilibrium with the solution do not grow. In contrast, smaller NPs will re-dissolved and larger NPs will grow. By this equation it can be also inferred that the monomer activity during the growth process controls the size distribution of the final NPs ensemble. At high monomer activities the r_C is small and the majority of the NPs grow. The small NPs grow faster than the larger ones reducing the initial broad size distribution and increasing the average size. Under these conditions the system is said to be in the size focussing regime (Figure 7). On the contrary, at lower monomer activities the r_C is large and the dissolution rate of the smaller NPs increases producing the broadening of the size distribution. Under these conditions the larger NPs grow at expense of the dissolution of the smaller ones. This process is known as the defocussing regime or Ostwald ripening (Figure 7).[48]

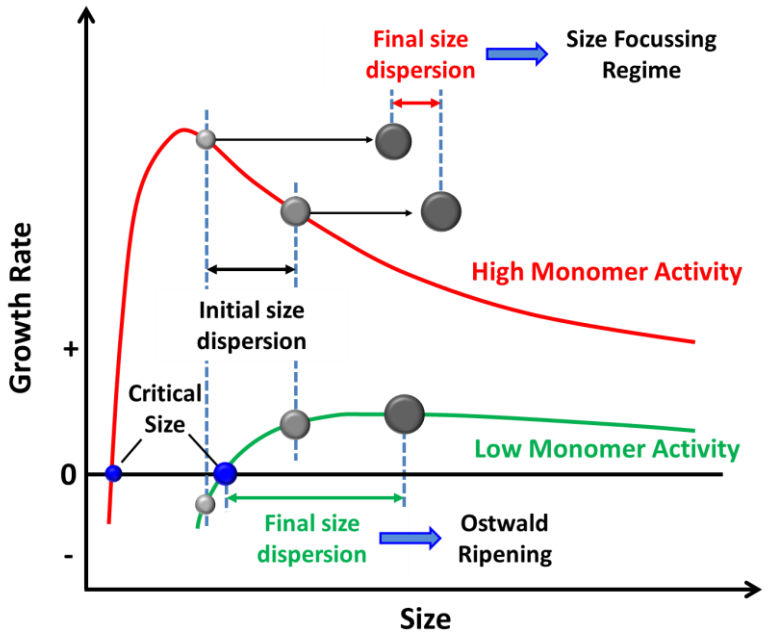

Figure 7. *Size dependence of the NP growth rates in two monomer activity regimes: high (red upper curve) and low (green lower curve). At high monomer activities the size focussing regime is favour, whereas at low monomers activities the Ostwald ripening occurs.*

In the last decades several efforts have been done to avoid the NPs ripening. It has been proved that some types of surfactants prevent re-dissolution of the NPs while others accelerate it. Another possibility to prevent the ripening is to perform repeated injections of the precursor solution. In this case it is necessary to keep the monomer activity under the homogeneous nucleation threshold to avoid secondary nucleation. Another alternative is to carry out the reactions under a large excess of one of the precursor. In this way the depletion of one of the monomers will control the growth but the supersaturation of the other will still be enough to prevent defocussing avoiding the NPs dissolution. This is the path in which CdSe nanorods grow, as it will be presented in Chapter 3.

1. 5. 2. 1. Heteroepitaxial growth

The principles explained above for the NP growth process are the same for the heteroepitaxial growth, but in the latter the morphology control is more difficult due to the need of the lattice matching. Analogously to the nucleation process, the essential difference between the growth processes is that the heteroepitaxial growth depends on the surface and the heterointerfacial free energies. Therefore, the morphology of the final HNPs depends on the shape, size, composition and surface defects of the seed, the nature of the growing material and the misfit strain at the heterojunctions. Even so, HNPs with very complex

morphologies can be obtain, such as core-shell, heterodimers, nanodumbbells, heteronanorods or multipods.

As the HNPs growth is determined by the interfacial free energies and thus, by the lattice mismatching, a classification of the different growth modes depending on the lattice matching is presented: (i) the layer-by-layer growth for lattice matched systems (or also called the Frank Van der Merwer mode, FM), (ii) the layer growth followed by self-organization in islands for systems with small lattice mismatch (or the Stransky-Kastranow mode, SK), and (iii) the island growth for systems with large lattice mismatch (or the so-called Volmer-Weber mode, WB). In the FM mode the strain is suppressed and the thickness of the growth layer can be unlimited. Oppositely, in the SK mode first a monolayer grow but is strained due to the lattice mismatch, then as the concentration and the thickness increase the strain is accumulated producing the self-organization of the layers into islands. At the other end, in the VW mode the material minimized the interfacial area growing directly in islands.

For colloidal HNPs the morphology control is even more difficult than for NPs synthesized by vapor-deposition methods, since colloidal NPs have larger degrees of interfacial strain producing the growth with larger lattice mismatching. Moreover, the different facets of the colloidal NPs present distinct free energies, reactivities and also offer different lattice mismatches. Besides, the surfactant bond strength is different for each facet changing its growth rates and resulting in the anisotropic growth of the new material. All these factors must be taken into account for the production of the desired HNPs and prevent the formation of amorphous phases.

1. 6. Applications of semiconductor and hybrid nanoparticles HNPs

1. 6. 1. Semiconductor NPs

The unique size dependent optical properties of semiconductor NPs have boosted their application in several fields. Colloidal NPs possess optical properties, such as bright, narrow PL emission and tunability of the wavelength that make them perfect sources of saturated emission colors for their application in light emitting devices (LEDs).[49] Moreover, colloidal NPs are easily deposited on different substrates by low-cost techniques, such as spin-coating, inkjet printing, or microcontact printing. Therefore, these NPs are also good candidates for their integration in flexible displays, offering an alternative for Organic LED´s (OLEDs). Another possibility is the use of these NPs in photovoltaic applications: The high absorption cross-section at tunable wavelengths gives the possibility to produce high efficiency

solar cells.[50-52] These NPs can be also applied in photocatalysis. In this sense, some of the most exciting objectives are the hydrogen generation from water or the synthesis of methanol from water and CO_2, using the photogenerated charge carriers to produce the necessary redox reactions.[53]

Finally, in the biomedical field, colloidal semiconductor NPs are promising materials for their application in imaging.[54] Their exceptional optical properties, such as the broad and strong absorption, the narrow emission, the high quantum yields and chemical resistance to photobleaching and degradation, make them materials competitive with the typical fluorescent dyes.

1. 6. 2. Semiconductor-metal HNPs

As has been commented above, the combination of different materials in the same nanostructure may lead to the enhancement of their properties and even in the generation of new ones not present in their individual counter parts. The profuse research in this field has demonstrated the possibility of applying these HNPs in several fields. For example, the hybrid metal-semiconductor materials can be integrated in electrical devices in which the metal part of the HNP can act as electrical contact points. By the use of these HNPs is not necessary to deposit the metals by different methods, as electron-beam lithography or others, and the irreproducibilities and the high contact resistances can be avoided.[55] For these systems, it has been demonstrated that the electrical conductivity of the semiconductor part to the circuit is highly improved. Moreover, the metals of these HNPs can be used as anchor points for self-assembly to create more complex nanostructures. The metal part can be used a selective site for the attachment of certain molecules, as the bond enthalpy between metals and thiol groups (among others) is very high, which allows these sites suitable for molecule bonding.[56, 57]

One of the most recent applications of the HNPs is their use in photocatalysis and solar energy fields. These applications require prevention of electron-hole recombination, which is achieved by the arrangement of semiconductor and metal NPs. In these systems the semiconductor part absorbs photons generating electron-hole pairs, followed by charge separation through the fast transfer of electrons to the metal part. This process produces quenching of the photoluminescence and provides both materials with separated charge carriers that will be used in the redox reactions.[25, 58, 59] One of the most challenging aims is the photochemical water splitting to generate hydrogen as a green source of energy.[60, 61]

Nowadays, it is necessary to improve the efficient absorption of the visible light by the semiconductor part to obtain successful results.

On the other hand HNPs have been used as multifunctional biological markers. These materials can be used for the diagnosis of diseases by combining magnetic and semiconductor functions in only one NP. The semiconductor part can be used as fluorescent tag and the magnetic part can be employed as contrast agent in MRI. For bio-applications it is important to encapsulate the HNPs with biocompatible materials, like silica.[29] Alternative HNPs used as contrast agents are those combining noble metals and magnetic NPs taking advantage of the plasmonic features and the strong response to magnetic fields.[62]

1. 7. References

1. S. Logothetidis, ed., *Nanomedicine and Nanobiotechnology*, Springer Berlin Heidelberg, 2012.
2. S. Logothetidis, ed., *Nanostructured Materials and Their Applications*, Springer Berlin Heidelberg, 2012.
3. E. Roduner, *Chemical Society Reviews*, 2006, **35**, 583-592.
4. M. V. Kovalenko, L. Manna, A. Cabot, Z. Hens, D. V. Talapin, C. R. Kagan, V. I. Klimov, A. L. Rogach, P. Reiss, D. J. Milliron, P. Guyot-Sionnnest, G. Konstantatos, W. J. Parak, T. Hyeon, B. A. Korgel, C. B. Murray and W. Heiss, *ACS Nano*, 2015, **9**, 1012-1057.
5. C. D. M. Donega, ed., *Nanoparticles. Workhorses of Nanoscience*, Springer Berlin Heidelberg, 2014.
6. C. B. Murray, D. J. Norris and M. G. Bawendi, *Journal of the American Chemical Society*, 1993, **115**, 8706-8715.
7. C. B. Murray, C. R. Kagan and M. G. Bawendi, *Annual Review of Materials Science*, 2000, **30**, 545-610.
8. M. Gao, S. Kirstein, H. Möhwald, A. L. Rogach, A. Kornowski, A. Eychmüller and H. Weller, *The Journal of Physical Chemistry B*, 1998, **102**, 8360-8363.
9. X. Peng, L. Manna, W. Yang, J. Wickham, E. Scher, A. Kadavanich and A. P. Alivisatos, *Nature*, 2000, **404**, 59-61.
10. A. P. Alivisatos, *The Journal of Physical Chemistry*, 1996, **100**, 13226-13239.
11. L. Manna, D. J. Milliron, A. Meisel, E. C. Scher and A. P. Alivisatos, *Nature Materials*, 2003, **2**, 382-385.
12. L. M. Liz-Marzán, *Langmuir*, 2006, **22**, 32-41.
13. P. Mulvaney, J. Pérez-Juste, M. Giersig, L. M. Liz-Marzán and C. Pecharromán, *Plasmonics*, 2006, **1**, 61-66.
14. R. Jin, Y. Charles Cao, E. Hao, G. S. Metraux, G. C. Schatz and C. A. Mirkin, *Nature*, 2003, **425**, 487-490.
15. I. Ojea-Jiménez, F. M. Romero, N. G. Bastús and V. Puntes, *The Journal of Physical Chemistry C*, 2010, **114**, 1800-1804.
16. M. Grzelczak, J. Perez-Juste, P. Mulvaney and L. M. Liz-Marzan, *Chemical Society Reviews*, 2008, **37**, 1783-1791.
17. T. Hyeon, *Chemical Communications*, 2003, 927-934.
18. J. Park, E. Lee, N.-M. Hwang, M. Kang, S. C. Kim, Y. Hwang, J.-G. Park, H.-J. Noh, J.-Y. Kim, J.-H. Park and T. Hyeon, *Angewandte Chemie International Edition*, 2005, **44**, 2872-2877.

19. A. Akbarzadeh, M. Samiei and S. Davaran, *Nanoscale Research Letters*, 2012, **7**, 144-144.

20. S. Sun, H. Zeng, D. B. Robinson, S. Raoux, P. M. Rice, S. X. Wang and G. Li, *Journal of the American Chemical Society*, 2004, **126**, 273-279.

21. J. Park, J. Joo, S. G. Kwon, Y. Jang and T. Hyeon, *Angewandte Chemie International Edition*, 2007, **46**, 4630-4660.

22. R. Costi, A. E. Saunders and U. Banin, *Angewandte Chemie International Edition*, 2010, **49**, 4878-4897.

23. P. D. Cozzoli, T. Pellegrino and L. Manna, *Chemical Society Reviews*, 2006, **35**, 1195-1208.

24. A. Vaneski, A. S. Susha, J. Rodríguez-Fernández, M. Berr, F. Jäckel, J. Feldmann and A. L. Rogach, *Advanced Functional Materials*, 2011, **21**, 1547-1556.

25. R. Costi, A. E. Saunders, E. Elmalem, A. Salant and U. Banin, *Nano Letters*, 2008, **8**, 637-641.

26. H. Y. Lin, Y. F. Chen, J. G. Wu, D. I. Wang and C. C. Chen, *Applied Physics Letters*, 2006, **88**, 161911.

27. H. Gu, R. Zheng, X. Zhang and B. Xu, *Journal of the American Chemical Society*, 2004, **126**, 5664-5665.

28. K.-W. Kwon and M. Shim, *Journal of the American Chemical Society*, 2005, **127**, 10269-10275.

29. S. T. Selvan, P. K. Patra, C. Y. Ang and J. Y. Ying, *Angewandte Chemie International Edition*, 2007, **46**, 2448-2452.

30. H. Weller, *Angewandte Chemie International Edition in English*, 1993, **32**, 41-53.

31. A. L. Rogach, ed., *Semiconductor Nanocrystals Quantum Dots. Synthesis, Assembly, Spectroscopy and Applications.*, SpringerWienNewYork, 2008.

32. R. Rossetti, S. Nakahara and L. E. Brus, *The Journal of Chemical Physics*, 1983, **79**, 1086.

33. L. E. Brus, *The Journal of Chemical Physics*, 1984, **80**, 4403.

34. A. Franceschetti and A. Zunger, *Physical Review Letters*, 1997, **78**, 915-918.

35. P. Atkins and J. De Paula, *Physical Chemistry*, Oxford University Press.

36. D. J. Norris, A. Sacra, C. B. Murray and M. G. Bawendi, *Physical Review Letters*, 1994, **72**, 2612-2615.

37. U. Banin, Y. Ben-Shahar and K. Vinokurov, *Chemistry of Materials*, 2014, **26**, 97-110.

38. J. Lee, A. O. Govorov, J. Dulka and N. A. Kotov, *Nano Letters*, 2004, **4**, 2323-2330.

39. T. Mokari, E. Rothenberg, I. Popov, R. Costi and U. Banin, *Science*, 2004, **304**, 1787.

40. E. Elmalem, A. E. Saunders, R. Costi, A. Salant and U. Banin, *Advanced Materials*, 2008, **20**, 4312-4317.

41. D. Mongin, E. Shaviv, P. Maioli, A. Crut, U. Banin, N. Del Fatti and F. Vallée, *ACS Nano*, 2012, **6**, 7034-7043.

42. C. Burda, X. Chen, R. Narayanan and M. A. El-Sayed, *Chemical Reviews*, 2005, **105**, 1025-1102.

43. C. d. M. Donega, *Chemical Society Reviews*, 2011, **40**, 1512-1546.

44. A. L. Rogach, T. Franzl, T. A. Klar, J. Feldmann, N. Gaponik, V. Lesnyak, A. Shavel, A. Eychmüller, Y. P. Rakovich and J. F. Donegan, *The Journal of Physical Chemistry C*, 2007, **111**, 14628-14637.

45. V. K. LaMer and R. H. Dinegar, *Journal of the American Chemical Society*, 1950, **72**, 4847-4854.

46. S. Gupta, S. V. Kershaw and A. L. Rogach, *Advanced Materials*, 2013, **25**, 6923-6944.

47. M. Ibáñez and A. Cabot, *Science*, 2013, **340**, 935.

48. W. Ostwald, ed., *Lehrbuch der Allgemeinen Chemie*, Leipzig, 1887.

49. Y. Shirasaki, G. J. Supran, M. G. Bawendi and V. Bulovic, *Nature Photonics*, 2013, **7**, 13-23.

50. G. Konstantatos and E. H. Sargent, *Nature Nanotechnology*, 2010, **5**, 391-400.

51. I. J. Kramer and E. H. Sargent, *ACS Nano*, 2011, **5**, 8506-8514.

52. P. V. Kamat, *The Journal of Physical Chemistry C*, 2008, **112**, 18737-18753.

53. W. Fan, Q. Zhang and Y. Wang, *Physical Chemistry Chemical Physics*, 2013, **15**, 2632-2649.

54. T. L. Doane and C. Burda, *Chemical Society Reviews*, 2012, **41**, 2885-2911.

55. Y. Cui, U. Banin, M. T. Björk and A. P. Alivisatos, *Nano Letters*, 2005, **5**, 1519-1523.

56. A. Salant, E. Amitay-Sadovsky and U. Banin, *Journal of the American Chemical Society*, 2006, **128**, 10006-10007.

57. N. Zhao, K. Liu, J. Greener, Z. Nie and E. Kumacheva, *Nano Letters*, 2009, **9**, 3077-3081.

58. A. Mills, R. H. Davies and D. Worsley, *Chemical Society Reviews*, 1993, **22**, 417-425.

59. M. Gratzel, *Nature*, 2001, **414**, 338-344.

60. N. S. Lewis, *Science*, 2007, **315**, 798.

61. N. Bao, L. Shen, T. Takata and K. Domen, *Chemistry of Materials*, 2008, **20**, 110-117.

62. N. Pazos-Pérez, Y. Gao, M. Hilgendorff, S. Irsen, J. Pérez-Juste, M. Spasova, M. Farle, L. M. Liz-Marzán and M. Giersig, *Chemistry of Materials*, 2007, **19**, 4415-4422.

2. Objectives

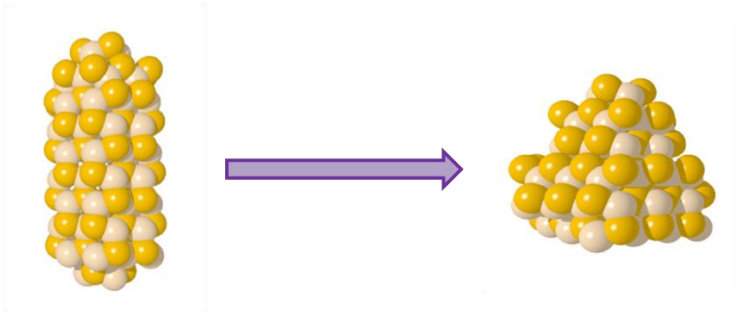

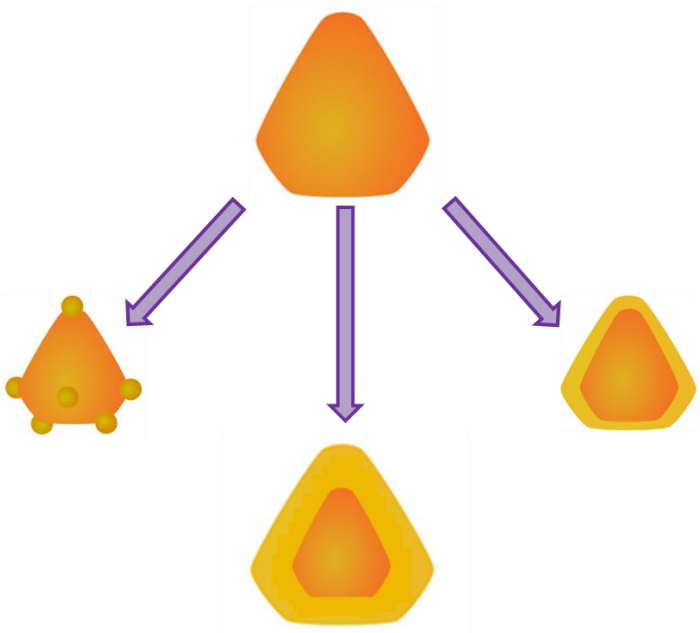

2. Objectives

The main objective of the first part of this thesis is the study of the electrochemical response of different CdSe nanoparticles in order to evaluate surface changes in the chemical environments after different electrochemical treatments. To this aim, CdSe NPs with different morphology, rod-like and pyramidal shaped, have been synthesized and characterized by means of several techniques, including cyclic voltammetry (CV) and X-ray photoelectron spectroscopy (XPS).

In the second part of this thesis, the main objective is the elucidation of the heterodeposition mechanisms of Au deposits with different morphology on pyramidal CdSe NPs to produce hybrid Au-CdSe HNPs.

3. Synthesis and Characterization of Rod-like and Pyramidal Nanoparticles (NPs)

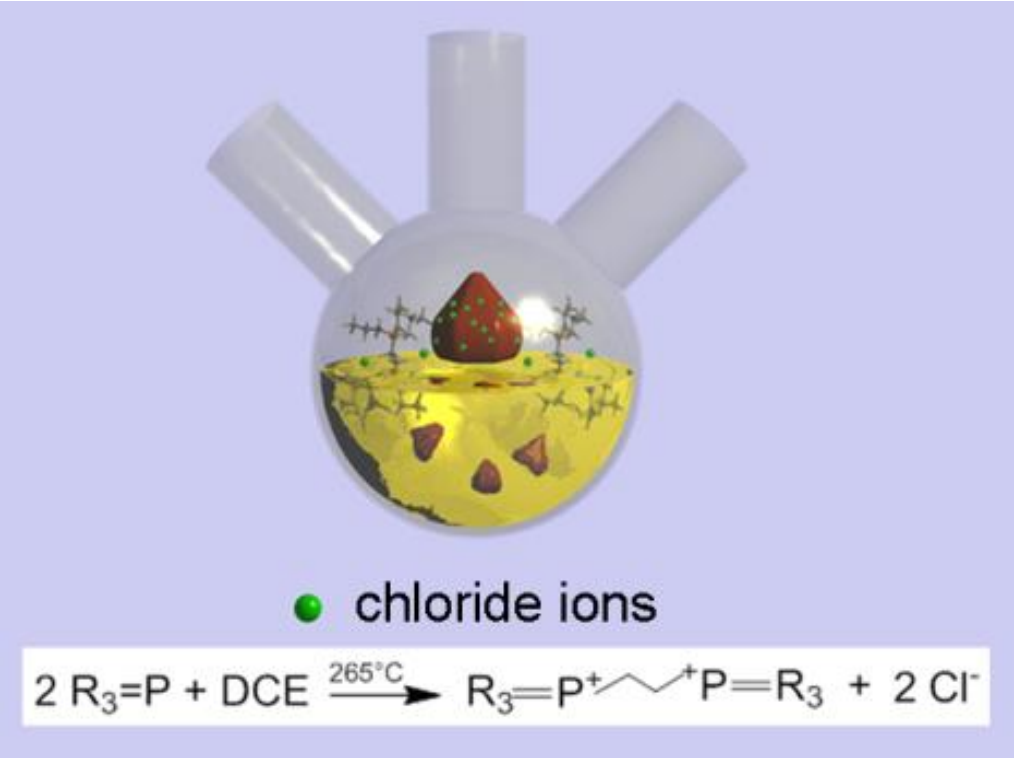

3. Synthesis and Characterization of Rod-like and Pyramidal Nanoparticles (NPs)

3. 1. Abstract

In this chapter the morphological change from rod-like to pyramidal shaped CdSe nanoparticles (NPs) synthesized by the so-called hot injection method, in the absence or presence of a chlorinated co-solvent, has been studied. Rod-like CdSe NPs were synthesized in a mixture of octadecylphosphonic acid (ODPA), trioctylphosphine (TOP), and trioctylphosphine oxide (TOPO). The initial morphology changes from rod-like to pyramidal by the addition of a chlorinated co-solvent (dichloroethane, DCE) in the reaction mixture. The effects that the inclusion of DCE produces on the reaction mechanism, on the final morphology and on the surface chemistry have been studied by Mass Spectrometry, Nuclear Magnetic Resonance (NMR) Spectroscopy and X-ray Photoelectron Spectroscopy. It has been ascertained that chloride ions are in-situ formed during the synthesis, as a sub-product of the reaction between DCE and TOP, and that these chloride ions are incorporated on the shell of the NPs upon partial and selective displacement of the original ODPA ligands, producing the re-shape from rods to pyramids.

3. Synthesis and Characterization of Rod-like and Pyramidal Nanoparticles (NPs)

3. 2. Introduction

In the last decade, it has been demonstrated that the addition of a halogenated source during the synthesis of semiconductor NPs produced by the hot injection method is a versatile way to control NP´s morphology and properties. By means of this approach it is possible to tune the NPs morphology of some II-IV semiconductor NPs,[1-5] to create 2D materials by oriented attachment of the individual NPs,[6] and even to obtain hybrid materials where semiconductor NPs decorate the Csp^2 surfaces such as those of carbon nanotubes or graphene.[1, 3, 7] The interest to include halogenated species in the NPs synthesis not only lies on the formation of new morphologies or hybrid materials, but also on the incorporation of such halogenated species as X-type (ionic) ligands, replacing the initially insulating organic shell. It is known that halides can displace the L (coordinative) and/or others X-type (ionic) ligands.[8, 9] This ligand exchange of the insulating long alkyl chain molecules by short halide ions improves the charge transfer among NPs and may improve their optical properties due to a better surface passivation, for this reason a detailed knowledge of the distribution of ligands on the NPs surface is extremely important for their application in NPs-based devices.[10, 11, 12, 13] For these reasons several groups have also developed different routes to incorporate these halide X-type ligands in post-synthetic treatments.[14]

Concerning the morphological control, the *in-situ* changes in the NPs morphology during the reaction could be achieved by the addition of different halogenated sources in the reaction medium. Some authors include $CdCl_2$ along with CdO as cadmium precursor to control de formation of octapod-shaped CdSe/CdS NPs,[4] while others add chlorine containing organic molecules as surfactants to obtain CdS pencil-shaped NPs.[5] In the particular case of CdSe NPs, it has been demonstrated that the addition of chloroalkanes as co-solvents (1,2-dichloroethane, 1,1,2-trichloroethane, etc.)[15] in the reaction medium changes the rod-like NPs morphology (obtained in mixtures of octadecylphosphonic acid (ODPA), trioctylphosphine (TOP) and trioctylphosphine oxide (TOPO)[16-18] into pyramidal-like ones.[2, 19] Furthermore, it has been shown that the use of haloalkanes, exhibiting different nucleophilic character (bromide or iodine compounds), also yields NPs with slightly different morphology. Interestingly, the nucleophilic character of the additive modifies the kinetics of the reaction, in good agreement with the mechanism of substitution reactions. [15]

Chloride ligands can be also incorporated on the NPs surface in post-synthetic treatments. Some research groups exchange the original alkylphosphonates capping ligands by

chloride employing different ammonium chloride salts,[9] while others describe similar procedures using silylating agents.[8, 20] In many cases minimum shape variations are observed (probably due to shorter reaction times). However, other authors report on anisotropic etching of the original NPs,[21] what suggests that halogenated compounds present in the reaction media may produce similar etching effects during the reaction course.

In this chapter the morphological change from rod-like to pyramidal shaped CdSe NPs synthesized in the absence or presence of DCE is presented. The effect of the chlorinated source on the reaction mechanism has been studied by means of mass spectrometry (ESI-TOF) and nuclear magnetic resonance (^{1}H NMR). Furthermore, a detailed characterization of the ligand composition of the organic shell has been performed by means of X-ray photoelectron spectroscopy (XPS) and solid ^{31}P CP/MASS NMR (cross-polarization/magic angle spinning nuclear magnetic resonance) techniques.

3. 3. Synthesis of different shape CdSe NPs

3. 3. 1. Synthesis of rod-like CdSe NPs

The CdSe NPs synthesis was performed following a variation of a method previously reported.[1, 3, 18] The NPs were prepared by stirring and heating (under nitrogen) 0.025 g (0.2 mmol) of CdO (cadmium precursor) and 0.20 g (0.6 mmol) of ODPA, using 2.9 g (8 mmol) of TOPO as reaction medium. The solution turned clear at around 250 °C, evidencing the $Cd(ODPA)_2$ complex formation. Afterwards, the temperature was increased to 265 °C and 0.43 mL of Se dissolved in TOP (TOPSe, selenium precursor) (1 M) (0.4 mmol) were injected for nucleation. For the growth regime, the temperature was kept at 255 °C. After 21 h of growth, the reaction was quenched by decreasing the temperature to 70 °C and adding 3 mL of toluene. Then, the NPs were purified by centrifugation (5 minutes at 14000 rpm) and re-dispersion processes, using toluene as solvent and methanol as non-solvent. Finally, the purified NPs were redispersed in toluene and stored in the dark at 4 °C.

3. 3. 2. Synthesis of pyramidal CdSe NPs

This synthesis was performed in a similar way than the rod-like NPs reaction with slight variations.[1, 3] Once the optically clear $Cd(ODPA)_2$ complex solution was obtained, the temperature was decreased to 80 °C and 3-4 µL (0.05 mmol) of DCE were injected with a Hamilton glass micro-syringe. After the addition of the chlorinated source, the temperature

was increased to 265 °C and the reaction continued as in the case of rod-like NPs. NPs under different molar Cd/Se molar ratios have been synthesized, as describe in Table 1 (ANNEX II). In all cases, the Cd/ODPA molar ratio has been kept constant to 3 to ensure the complete complexation of Cd.

As previously mentioned, pyramidal CdSe NPs are able to decorate graphitic surfaces.[1, 3, 22] To this aim, NPs are allowed to nucleate and grow in the presence of the Csp^2 system, previously added to the reaction mixture. Thus, the CdSe synthetic reactions were carried out in the presence of HOPG (highly oriented pyrolytic graphite) substrates (1 cm^2) included in the pot. The HOPG substrates were purified by washing the substrates in toluene baths. NPs not attached to the HOPG substrates were purified and stored as in the case of rod-like NPs.

These substrates have been used for XPS measurements because the deposition methodology guarantees the coverage of one single monolayer of NPs avoiding the possible charge effects during measurements.

3. 4. Results and discussion

3. 4. 1. Reaction conditions to obtain different morphology CdSe NPs

3. 4. 1. 1. Rod-like CdSe NPs

For this particular synthesis it is known that the conversion of Cd and Se precursor molecules to metal chalcogenide rod-like NPs is possible due to the use of phosphonic acids as reagents. The first step of the CdSe NPs synthesis consists on the complexation reaction between the cadmium precursor (CdO) and the ODPA to form the $Cd(ODPA)_n$ complex. When the molar ratio between the surfactant and the cadmium precursor is 2, the Cd atoms are coordinated with two surfactant molecules obtaining a $Cd(ODPA)_2$ complex,[17] according to the following reaction (1):

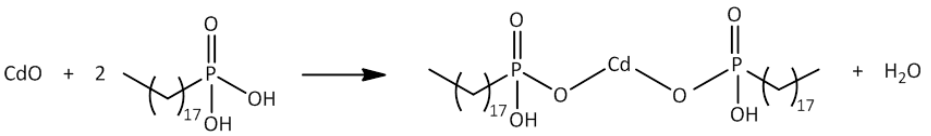

(1)

Once the $Cd(ODPA)_2$ complex is formed, the Se precursor (Se dissolved in TOP; TOPSe) is injected. The Lewis acidity of the Cd^{2+} ion center permits the binding of the electron rich Se

atoms of the TOPSe precursor, releasing the oxide and the anhydrides of the initial ODPA,[23] according to reaction (2):

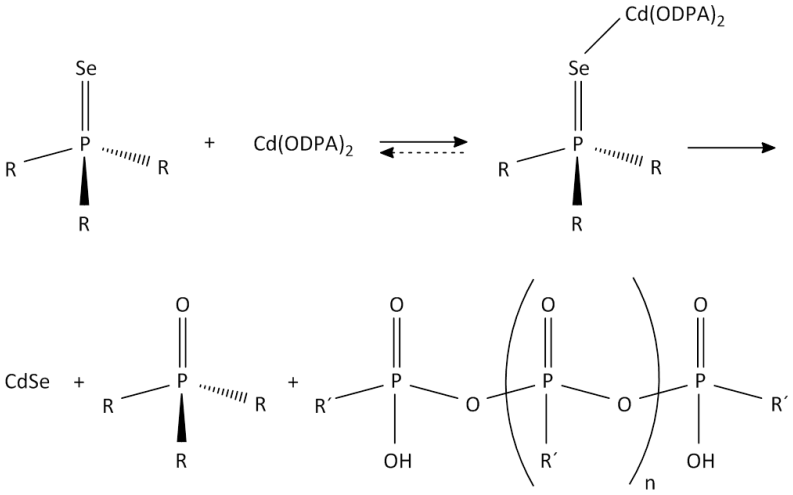

(2)

$R = C_8H_{17}$ $R' = C_{18}H_{37}$

The formation of the phosphonic oxides after the reaction between precursors agrees with a two-step substitution reaction where first, an electrophile binds to the chalcogenide atom of the TOPSe and second, nucleophile oxygens bind to the P atom producing the cleavage of the P=Se double bound. It has been also observed that changing the concentration of ODPA modifies the TOPSe cleavage kinetics, evidencing that not only ODPA but also its anhydrides are capable to break the P=Se double bound.[23]

In general, there are several factors influencing the morphology of the NPs obtained by hot-injection, including precursor monomer concentrations, surfactant molecules, temperature and reaction time. Surfactants and in this particular case, ODPA molecules, accomplish several functions: first they act as complexing agents as explained above. Second, they act as ligands, binding to certain facets of the NPs and driving the growing directions. Finally, they act as stabilizers of the NPs in organic solvents. Since the correct choice of the surfactant controls the final NP morphology,[17] in order to understand the formation of a rod, the affinity of ODPA to the different crystallographic facets should be taken into account. It is reported that the binding energy of phosphonic acid-based ligands is relatively small for the basal (0001) and (000-1) polar facets of CdSe (see Figure 3.1), which are terminated either on Cd or Se atoms, respectively, compared to the much greater binding energy calculated for the lateral (10-10) and (11-20) non-polar facets containing both types of atoms (Cd and Se).[24]

Furthermore, since ligands are electron-donating species, passivation of non-metal terminated facets is also less favoured. Thus, the high ODPA affinity for the lateral facets along with a generally accepted dipole moment along the c-axis,[25] favours the formation of elongated one dimensional nanostructures. Additionally, Cd atoms growing on the (0001) facet shows one dangling bond, while three dangling bonds are feasible for Cd growing on the (000-1) facet, which provides a higher chemical potential to this facet. This circumstance also favours anisotropic growth along the c-axis in the presence of ODPA.

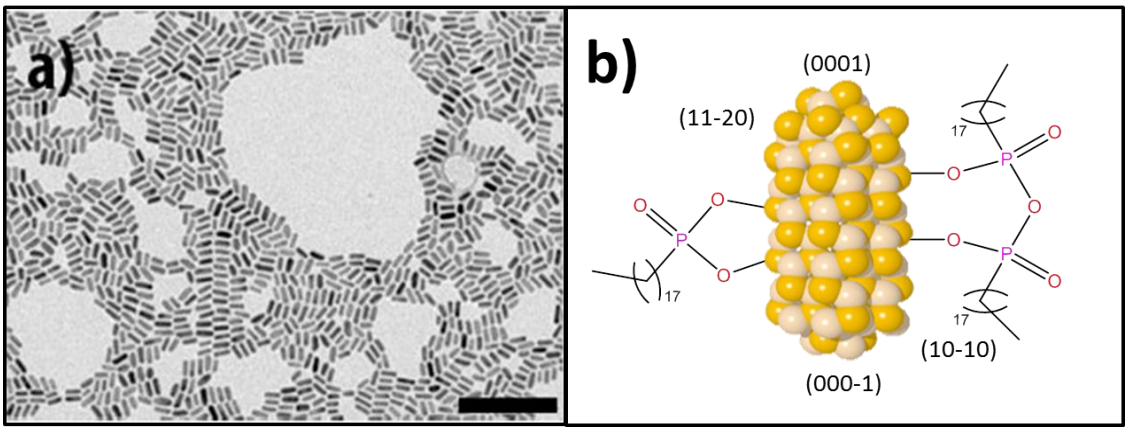

Figure 3.1. *a) TEM image of rod-like NPs of 21 hours of reaction. Scale bar 100 nm. b) Scheme of the rod-like NPs morphology with the polar (0001) and (000-1) and the non-polar (11-20) and (10-10) facets and the surface ligand composition.*

Once the NP is formed, the composition of the ligand shell has been regularly studied by several characterization techniques, including FTIR (ATR) and mainly NMR. For CdSe rod-like NPs an organic shell composed of ODPA phosphonates ($ODPA^{2-}$) and ODPA anhydrides has been previously proposed,[9, 13, 18, 23, 26] as depicted in Figure 3.1, where a TEM image of rod-like NPs (a), along with a scheme of the NPs and its ligand shell composition (b), are depicted.

3. 4. 1. 2. Pyramidal CdSe NPs

When the synthesis is performed under the same conditions used for rods but DCE is added as chlorinated co-solvent, the NPs growth process drastically changes, obtaining pyramidal NPs. In Figure 3.2 TEM images of three aliquots taken at different reaction times in the presence of DCE, along with a scheme of the NPs evolution are depicted. As it is shown, in the first stages of the growth process rod-like NPs are obtained (left image: 5 min). After 2 hours of growth (middle image), the NPs morphology changes to bullet shaped, while at longer reaction times (right image: 21 h), the morphology of the NPs is pyramidal.

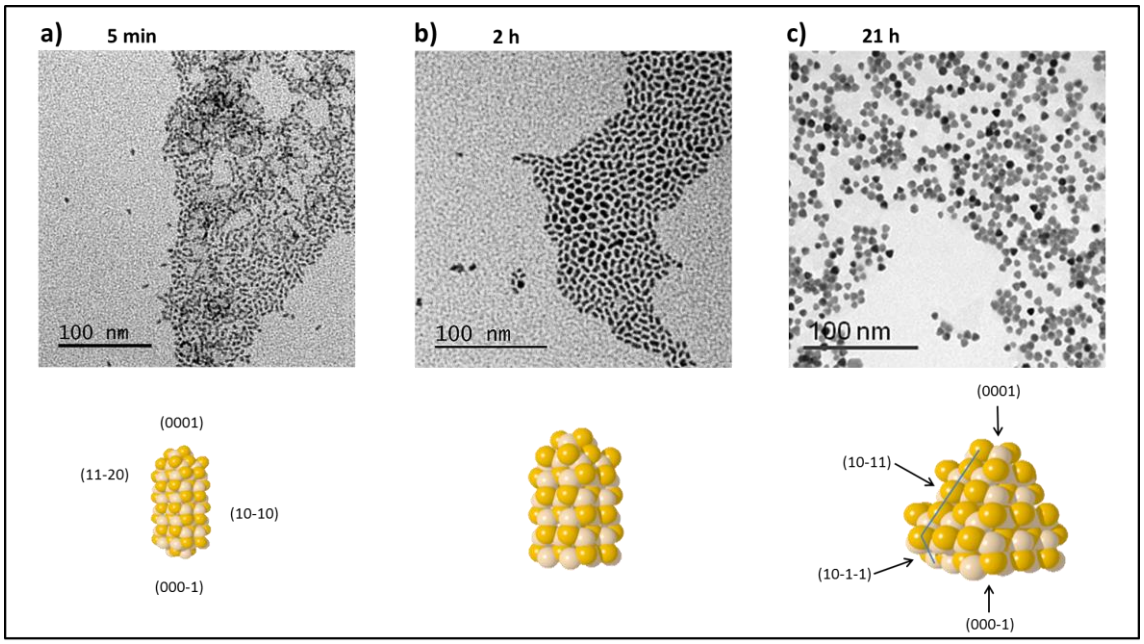

Figure 3.2. *TEM images of three aliquots taken at different reaction times (from left to right: 5 min, 2 h and 21 h) in the synthesis of CdSe NPs (a). These images show the shape evolution from rod-like at 5 min (left) through bullets at 2h (middle) to pyramids at 21 h (right).*

3. 4. 1. 3. Different Cd/Se ratios

To study in detail the effect of DCE on the reaction several syntheses with different Cd/Se molar ratios from 4 to 0.25 and a fixed DCE concentration were carried out. Representative TEM images of CdSe samples obtained for Cd/Se precursor molar ratios of 2, 1 and 0.5 are depicted in Figure 3.3 along with size histograms both for the diameter and the length of the NPs. When the NPs synthesis is carried out in the absence of DCE, the shape of the NPs is rod-like regardless the Cd/Se precursor molar ratio. As it can be observed in the TEM images in Figure 3.3, for stoichiometric Cd/Se conditions or under Se excess precursor conditions (Cd/Se = 0.5) the addition of DCE during CdSe synthesis leads to a re-shaping from rods into pyramids. However, under excess Cd precursor conditions (Cd/Se = 2 or higher, not shown) the addition of DCE does not trigger the re-shaping. Thus, the NPs morphology changes might be driven by a chlorine-containing species (different from the precursor, DCE) which must be generated in situ by reaction between DCE and the Se precursor. In order to quantify the effect of DCE in the shape evolution, the size of rod-like and pyramidal NPs has been measured for the samples shown in Figure 3.3.

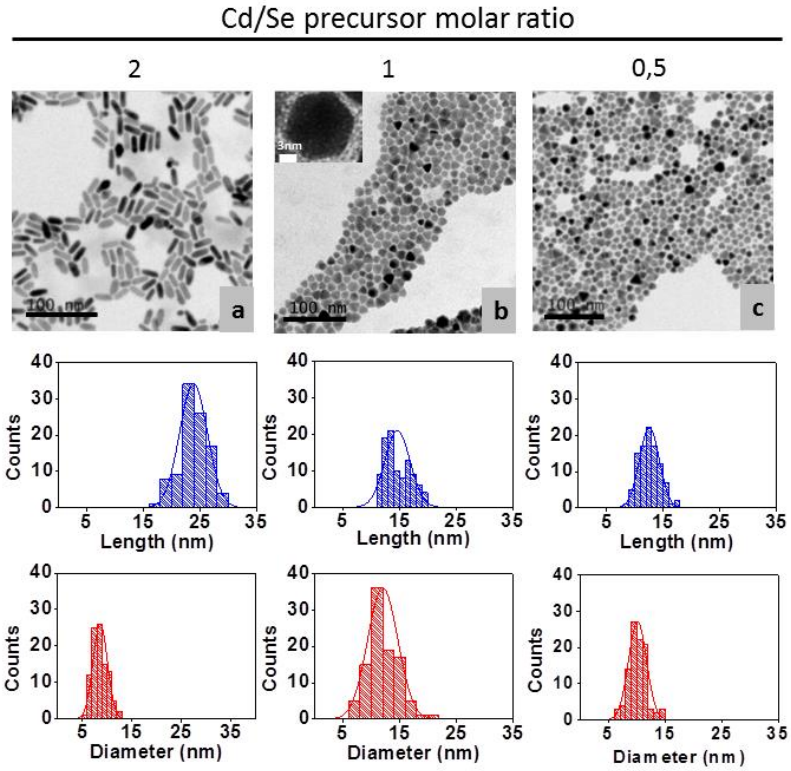

Figure 3.3. *TEM images of CdSe NCs obtained after 21 hours of reaction from Cd/Se precursor molar ratios of 2, 1 and 0.5 in the presence of DCE. The inset in (b) shows a pyramidal NC in the [001] direction. The histograms correspond to the length (blue) and diameters (red) of the NCs.*

As clearly seen in the histograms, the morphological anisotropy observed for samples obtained under excess of Cd precursor (Figure 3.3 a) turns into a more isotropic shape for samples with stoichiometric Cd/Se ratios or excess of Se precursor (Figures 3.3 b,c). Aspect ratios around 3 are observed for rods and close to 1 for pyramids. The width of the size distribution of the NPs does not exceed 10% of the mean radius for Cd/Se precursor molar ratios ranging from 2 to 0.5. The synthesis with molar ratios out of this range yields either bigger NPs and/or highly polydispersed ones (i.e. NPs obtained from Cd/Se precursor molar ratios of 4 and 0.25, images not shown). We attribute such polydispersity to the large difference between Cd and Se precursor concentrations, which might enable a high monomer saturation regime only for one of the precursors during nucleation and first growth stages, promoting further severe Ostwald ripening.[18]

Clearly, the generation of chlorinated species during the reaction must modify the morphology of the NPs probably due to its incorporation on the NPs surface. In order to obtain information about the composition of the NPs synthesized under different precursor's molar

ratios and to elucidate differences in the ligand shell composition, XPS analyses have been carried out. Out of these analyses, the presence of P and Cl has been evidenced.[22, 27] Since the P *2p* and Cl *2p* XPS peaks are related exclusively to the NPs ligand shell,[22] we calculated the normalized areas Cl/Cd and P/Cd, between elements comprising the ligand shell (Cl or P) and a component of the NP core (Cd).

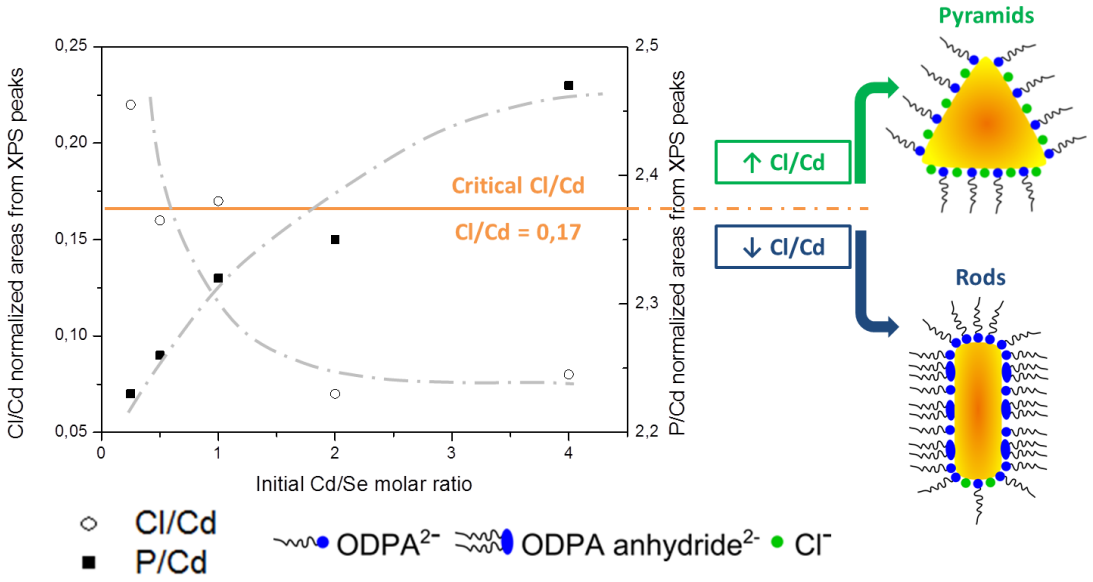

Figure 3.4. *Cl/Cd (circles) and P/Cd (dark squares) normalized areas calculated from XPS data and plotted versus the Cd/Se precursor molar ratios. The horizontal continuous line indicates the minimum Cl value to promote the re-shaping of rod-like to pyramidal-like NCs. The discontinuous curved lines are only a guide for the eyes. The experimental error associated with the relative peak areas is around 10%.*

Figure 3.4 shows the XPS Cl/Cd and P/Cd normalized areas plotted as a function of the Cd/Se precursor molar ratio in the synthesis. It is worth noting that these ratios do not correspond to quantitative concentration values of elements present in the samples, but to qualitative amounts of different elements composing the shell relative to a given amount of Cd. The presence of Cl indicates that chlorinated species are incorporated in the ligand shell. The small Cl/Cd ratio detected for rod-like NPs suggest a minor contribution of chlorinated species in contrast to pyramids where the ratio significantly increases. It can be observed that high Cl/Cd and low P/Cd ratio values are obtained under Se precursor excess (Cd/Se < 1) whereas under Cd excess (Cd/Se > 1) the trend is the opposite. These results suggest that the chlorine incorporation in the NPs is favoured for high Se precursor contents and it can be stablished that the critical amount of chlorine (Cl/Cd) to produce the NPs re-shaping is around 0.17.

As it has been mentioned above, under Cd precursor excess (Cd/Se = 2) the initial rod-like NP morphology does not change even when large amounts of DCE are added, pointing to different reaction mechanisms depending on the precursor concentrations and the presence or absence of DCE. Under Cd precursor excess DCE might react with the $Cd(ODPA)_2$ complex producing different chlorinated compounds[4, 5, 21, 28, 29] which does not lead the NPs morphology change. If this would be the case, it could be assumed that DCE is able to displace the ODPA molecules of the Cd complex, avoiding its reaction with the Se precursor (TOPSe). The reactivity between the $Cd(ODPA)_2$ complex and Cl is further proved by a series of experiments in which DCE/CdO molar ratios exceeding 1.3 make the Cd precursor unable to react with TOPSe. This result evidences the ability of DCE to displace ODPA ligands from the Cd complex, which may also lead to partial substitution of ODPA in the complex (i.e. Cl–Cd–ODPA). Therefore, under excess Cd precursor conditions, the Cd complex might mainly have evolved to $CdCl_2$ (not triggering the re-shaping), although a small amount may form Cl–Cd–ODPA complexes.

On the contrary, under Se excess conditions the chlorine incorporation on the NPs surface is favoured and thus, the re-shaping should be related with the reaction between TOP (or TOPSe) with the DCE. Further blank experiments (not shown) confirmed that the reaction between DCE and TOP causes the morphology change of the rods into pyramids.

All these results demonstrate that the morphology change is produced by the release of a reactive chlorine specie during the reaction but now two different questions arise: i) which chemical species are generated after the reaction between TOP and DCE promoting the NPs re-shaping? and ii) Do the generated species produce changes in the chemical composition of the initial ligands? To clear these points up different characterization techniques as NMR (^1H and ^{31}P), mass spectrometry, and X-ray photoelectron spectroscopy were used.

3. 4. 2. Elucidation of the reaction mechanism

With the aim finding the conditions under which the NP re-shaping is achieved a series of blank experiments were done, finding that the reaction between DCE and TOP promotes the NPs re-shaping. To ascertain which chlorinated species are formed during this reaction, equimolar mixtures of TOP and DCE at different conditions were analysed by ^1H NMR and Mass Spectrometry.

3. 4. 2. 1. ^{1}H NMR studies

First, it is important to mention that the reactions between DCE and TOP were carried out in a Schlenk line under a nitrogen atmosphere to prevent the oxidation of TOP into TOPO. Secondly, the samples were dissolved in deuterated chloroform ($CDCl_3$) for the analysis. In Figure 3.5 the ^{1}H NMR spectra of the simple mixture of TOP and DCE at room temperature (top spectrum, a) is compared to the mixture after 21 hours of reaction at 265 °C (bottom spectrum, b). As it can be seen in the top spectrum, the simple mixture of the reagents without increasing the temperature shows the characteristic peaks of the individual unreacted species. The multiplets observed at low chemical shifts correspond to the protons of the alkyl chains of TOP. The peak at around 0.9 ppm is in agreement with the chemical shift of methyl groups, while the peak at around 1.3 ppm is related to the protons in methylene groups corresponding to C_4, C_5, C_6 and C_7 of TOP molecules. The small shoulder at around 1.4 ppm has been assigned to the protons situated in C_1 and C_2 in TOP, since they might be more deshielded by P. The smaller peaks between 1.5 and 1.7 ppm are in agreement with protons C_1 and C_2 in the alkyl chains in TOPO. Thus, a slight oxidation of TOP into TOPO during the reaction due to impurities in DCE or even during the analysis procedure cannot be discarded. The pronounce singlet observed at around 3.7 ppm corresponds to the protons presented in the methylene groups of DCE. This result discards any reaction at room temperature, while in the spectra of the mixture after 21 hours of reaction at 265 °C some changes can be found (b in Figure 3.5). The most significant change is the lack of the singlet around 3.7 ppm previously assigned to DCE. The series of peaks observed between 0.9 and 1.7 do not allow us to establish a clear identification of the reaction product beyond that it might have a structure similar to trioctylphosphines. The chemical shift observed at 1.1 ppm could be attributed to protons situated close to chlorine and oxygen atoms.

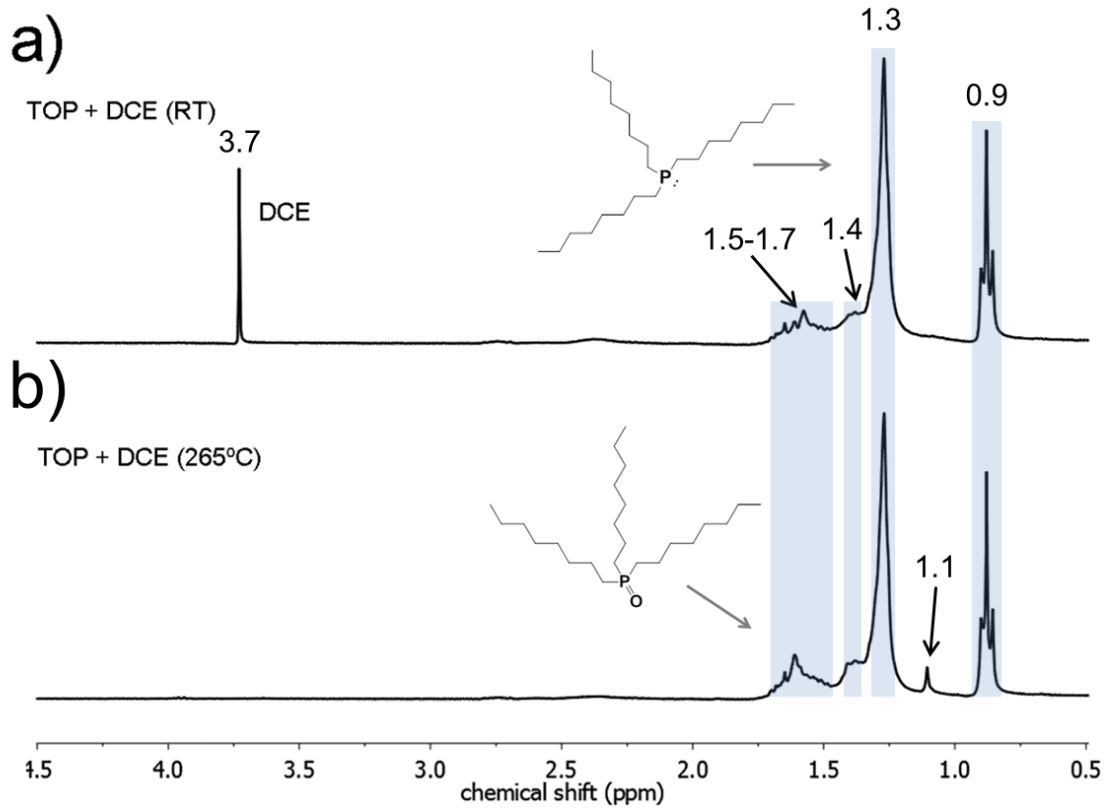

Figure 3.5. *^{1}H NMR spectra of the direct mixing (under nitrogen) of DCE and TOP (a) and the product obtained after reaction at 265 °C (b).*

3. 4. 2. 2. Mass Spectrometry analysis

Due to the impossibility of the clear identification of the chorine-containing species by ^{1}H NMR, ESI-TOF mass spectrometry was performed. Figures 3.6 (a,b) show the mass spectra of TOP and the product obtained after the reaction of DCE and TOP at 265 °C, respectively. As can be seen in Figure 3.6 a, the TOP spectra does not present impurities and only a main peak at m/z of 371.38 corresponding to the $(M+1)^{+}$ signal of TOP is observed (also its corresponding isotopes could be observed in the inset of the image). In the spectra of the product new mass peaks are discernible (Figure 3.6 b). First, the signals at m/z of 371.38 and 387.37 correspond to unreacted TOP and TOPO, respectively. These signals are characteristic of the singly charged species with the peaks of M+1 and M+2 separated by a difference of 1. The small amount of TOPO present in this spectrum is also supported by the ^{1}H NMR results and could be attributed to the oxidation of TOP during the reaction or even during the measurements.

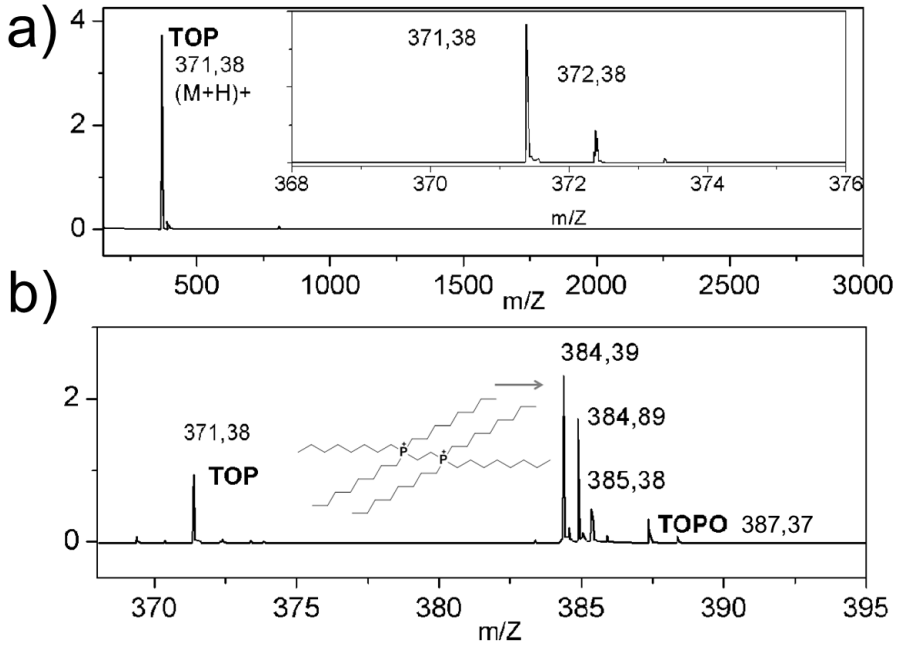

Figure 3.6. *a) ESI-TOF mass spectrum of TOP, demonstrating no relevant impurities. The inset shows a smaller spectral range where the $(M + 1)^+$ and its corresponding isotopes are observed. b) ESI-TOF mass spectrum of the product obtained from the reaction between DCE and TOP at 265 °C (ethane-1,2 diylbis(trioctylphosphonium)dichloride).*

The most important change consists on the appearance of a main peak in the spectrum at m/z 384.39, which can be unequivocally assigned to ethane-1,2-dyilbys(trioctylphosphonium) dichloride. This signal has the characteristic peaks of a doubly charged product at M+1 and M+2 separated by a difference of 0.5. The vanishing of the DCE signal in the ^{1}H NMR spectra and the appearance of the new signal in the mass spectrum after the reaction between DCE and TOP evidences the formation of ethane-1,2-dyilbys(trioctylphosphonium)dichloride at high temperatures (265 °C) and long reaction times. This reaction may occur through a substitutional mechanism, as depicted in Scheme 3.1.

Thus, it can be concluded that the formation of ethane-1,2-dyilbys(trioctylphosphonium)dichloride during the NPs synthesis generate chloride ions as subproduct, which are believed to be the active specie that promote the shape transformation of rod-like NPs into pyramidal ones.

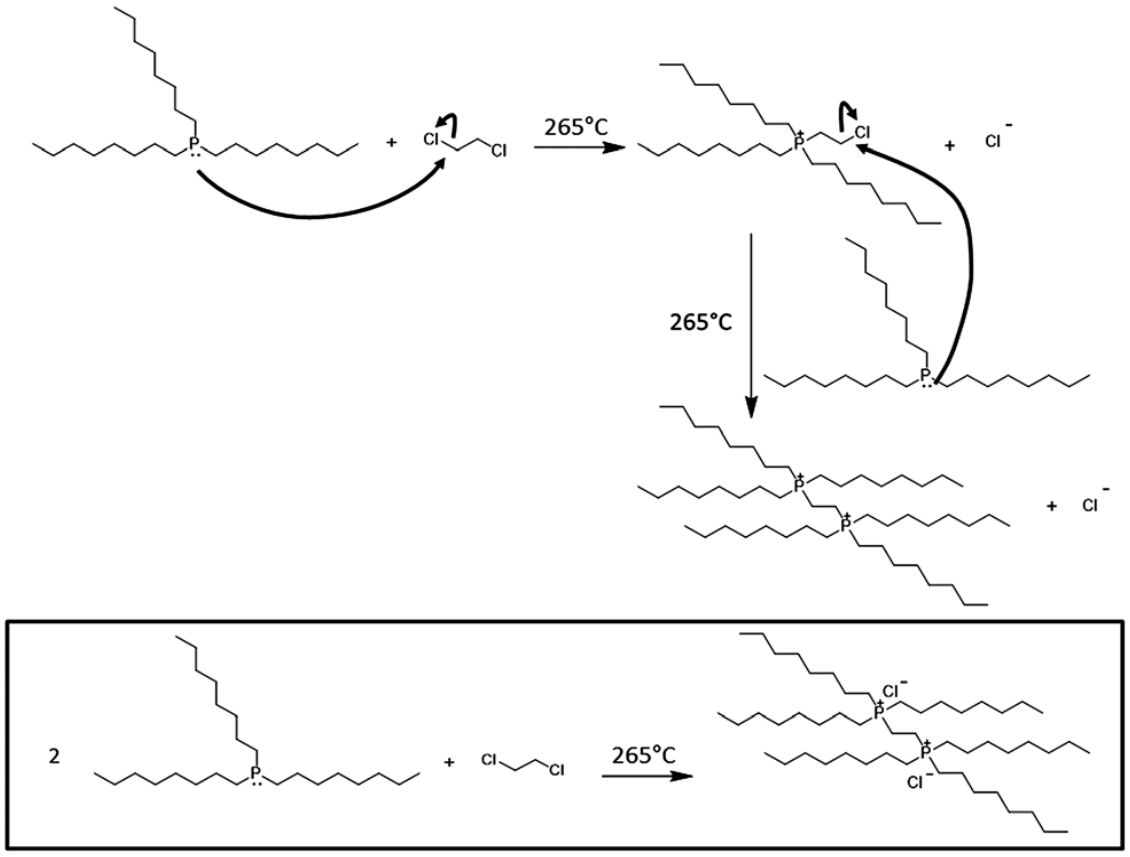

Scheme 3.1. *Proposed mechanism for the chloride anions generation as products of the reaction between DCE and TOP at 265 °C.*

3. 4. 3. Study of the composition of the ligand sphere by XPS, solid NMR and DFT

In order to identify the different ligands anchored to the NPs surface and evidence differences in the ligand composition produced by the inclusion and/or exchange of chloride ions in the ligand sphere, XPS and solid ^{31}P CP/MAS NMR analysis of the NPs were performed.

3. 4. 3. 1. XPS studies

The XPS experiments were carried out on NPs assembled on highly oriented pyrolytic graphite (HOPG) substrates. As expected, in the Cl *2p* region a peak centered at 199 eV appears only for pyramidal NPs suggesting that chloride anions are part of the ligand sphere (not shown).[27] This binding energy value has been previously reported for $CdCl_2$.[30] The ionic nature of ethane-1,2-dyilbys(trioctylphosphonium)dichloride suggests that probably the chloride ions present in the reaction media may bind to the Cd^{2+} surface sites as X-type ligands.[9]

To elucidate any effect on the phosphonic acid related ligands produced by the incorporation of chloride, the P *2p* regions of both, rods and pyramids, were also analysed. The natural line shape for *2p* levels is that of an asymmetric spin-split doublet composed of two contributions separated 0.87 eV (P $2p_{3/2}$ and P $2p_{1/2}$). In Figure 3.7 the P *2p* spectrum of rod-like NPs is shown (upper gray line).

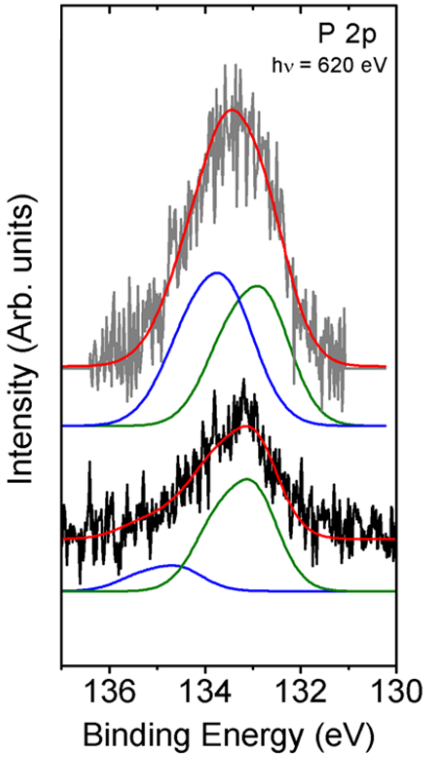

Figure 3.7. *P 2p region acquired for rod-like (upper gray line) and pyramidal NPs (lower black line) by XPS (hv = 620 eV). The P 2p peaks can be deconvoluted in two components with different binding energies (green and blue lines for* $ODPA^{2-}$ *and anhydrides respectively, see text).*

Its symmetric appearance can be well reproduced by assuming two different and equally populated chemical environments for P at the surface of the rods, leading to two components with similar intensities in the XPS signal, but different binding energies (green and blue lines in the fitting of the grey curve at 132.92 and 133.74 eV, respectively).[22] In the case of pyramidal NPs not only the P *2p* signal position is slightly shifted to higher binding energy values but also its shape is much more asymmetric, which is consistent with the contribution of a main single environment of P (green component in the lower black line fitting in Figure 3.7). The lack of symmetry of this signal points to a major displacement of the ligands associated to the highest-energy component by chloride. Moreover, the inclusion of chloride

causes a displacement of 0.1 eV of both components to higher binding energies (133.11 and 134.71 eV, respectively).

These results indicate that the ligand shell of NPs synthesized in the absence of chloride is composed by two different chemical species of P and that they are not equally affected by the incorporation of chloride.

3. 4. 3. 2. Solid ^{31}P NMR analysis

With the aim to investigate the chemical composition of the ODPA based ligands present in the surface of NPs, solid ^{31}P NMR studies of the different shape NPs have been performed. This technique allows for the characterization of the surface ligands without previous digestion of the inorganic CdSe NPs core. In Figure 3.8 the solid ^{31}P NMR spectra of pure ODPA (inset), rod-like (upper gray line) and pyramidal shaped NPs (lower black line) are depicted. As previously reported, a solution ^{31}P NMR spectrum of ODPA capped CdSe NPs presents two broad signals centered at 20 and 30 ppm.[13, 31] The spectra shown in Figure 3.8 show distinct sets of well-defined signals both for rod-like and pyramidal NPs.

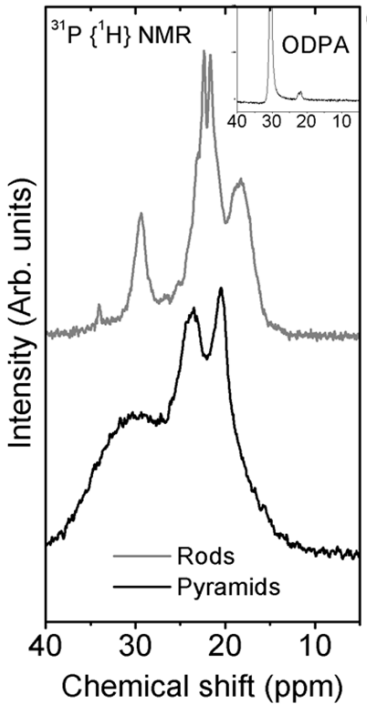

Figure 3.8. *Solid ^{31}P NMR of rod-like (upper gray line) and pyramidal NPs (lower black line). Inset: Pure ODPA spectrum.*

Comparison between them reveals that the transformation from rod to pyramids involves a shift and/or broadening of the signals. This indicates a different chemical environment for P in rod-like and pyramidal NPs, and might thus be interpreted as a fingerprint for the incorporation of chloride in the ligand shell. The remarkable resolution in the solid ^{31}P NMR spectra enables the assignment of the signals to different chemical environments for P. We believe this resolution is related to the size of the NPs showing relatively large crystallographic facets and allowing for a high structural order of the surface. In particular, the ^{31}P NMR spectrum of rod like NPs (Figure 3.8, upper line) shows a peak at 18.3 ppm; a prominent signal around 22.2 ppm terminated in two narrow peaks at 21.7 and 22.4 ppm, and two additional signals at 29.3 and 34.0 ppm. The absence of peaks at higher chemical shifts (>35ppm) discards the presence of TOPO bonded to the NP surface, in agreement with previous studies.[18] Three of such signals (29.3, 22.4, and 21.7 ppm) can also be found in the solid ^{31}P NMR spectrum of pure ODPA (see inset). The dominating contribution at 30.4 ppm is similar to the value reported for solution ODPA ^{31}P NMR.[18, 23] The signals observed at 22.2 ppm and 18.3 ppm can be assigned to ODPA species directly bound to Cd in the form of octadecylphosphonates (double deprotonated $ODPA^{2-}$) and anhydrides of phosphonic acids (ODPA anhydrides), respectively,[13, 26, 31, 32] formed during the reaction between the Se precursor (TOPSe) and the $Cd(ODPA)_2$ complex, according to reaction 2.[23] The presence of ODPA (neutral molecule) could be related with the hydrolysis of anhydrides, and hydrogen bonding between ODPA molecules might be the origin of the peaks at 22.4 and 21.7 ppm, according to previous work.[23] Finally, we attribute the small signal at 34 ppm to a small contribution of TOPSe. Similar values have been obtained for this molecule in the characterization of different Se precursors (TOPSe, TBPSe…) in solution ^{31}P NMR experiments.[23]

Thus, out of all the contributions found in the solid ^{31}P NMR spectra, the two main components that can be unambiguously attributed to species in the ligand shell are those corresponding to $ODPA^{2-}$ and ODPA anhydrides. For pyramidal NPs (Figure 3.8, lower line), the peaks previously assigned to $ODPA^{2-}$ and ODPA anhydrides are slightly shifted downfield when compared to the spectrum of rod-like NPs. Furthermore, a slight downfield shift is also observed by solid state ^{1}H MASS NMR experiments in the pyramidal NPs compared to rod-like. The shift in the whole spectrum could be attributed to the influence of adjacent chloride atoms in the shell. Alternatively, this shift may be related to a slightly different binding against the predominant (1101) polar facets terminated in Cd in the case of pyramids[1, 2] compared to the predominant nonpolar (0110) facets in rods. The range between 25 and 40 ppm shows a

broad undefined peak, and the two contributions at 21.7 and 22.4 ppm are not observed, which may indicate breaking of the hydrogen bonds in the presence of chloride. Typically, the ^{31}P NMR signals of phosphonic acid chlorides are shifted 14 to 20 ppm downfield from the corresponding phosphonic acids.[33] Thus, the relatively small chemical shift observed in Figure 3.8 discards the halogen substitution within the ODPA molecule (i.e., P-Cl bound).

These results along with the XPS analysis show that the surface of rod-like NPs is capped by $ODPA^{2-}$ and ODPA anhydrides. Furthermore it is evidenced that the incorporation of chloride in the ligand shell displaces one of these types of ligands selectively (Scheme 3.2). As it is shown in the XPS experiments (Figure 3.7) the component at higher binding energy values decreases when chlorine is incorporated in the ligand shell.

3. 4. 3. 3. DFT simulations

In order to identify and correlate the RMN and the XPS results, DFT simulations about the geometry adsorption, the adsorption energy and the partial charge of the P atoms of the ligands that binds to the Cd rich (000-1) crystal facets of the CdSe NPs were done by our collaborators in the Institute of Physical Chemistry of the University of Hamburg.[22] To reduce the simulations time the alkyl chain of the ODPA based molecules was reduce to 3 instead 18 C atoms. The simulations results show that the adsorption energy and the partial charge on the P atoms of the $ODPA^{2-}$ are 11.4 eV and 1.64 e, respectively, whereas for the ODPA anhydrides (calculated for a molecule formed by the condensation of two ODPA molecules, Scheme 3.2) are 10.4 eV and 1.66 e. Since the adsorption energy on the (000-1) facet is higher for the $ODPA^{2-}$ than for the ODPA anhydrides it can be suggested that the $ODPA^{2-}$ molecules binds to the CdSe NP surface strongly than the ODPA anhydrides. Moreover, these results entail that the P atoms of the ODPA anhydrides are more positively charged than those of the $ODPA^{2-}$, which suggests that higher binding energy values are expected for ODPA anhydrides (more unscreened) than for $ODPA^{2-}$ in the XPS experiment shown in Figure 3.7.

Taking into account all the results presented in this chapter, in Scheme 3.2 the modification of the surface composition when chloride is incorporated in the ligand shell is depicted. Chloride ions displaces ODPA anhydride ligands that are weakly bind to NP surface while phosphonate ligands remain anchored to the NPs surface.

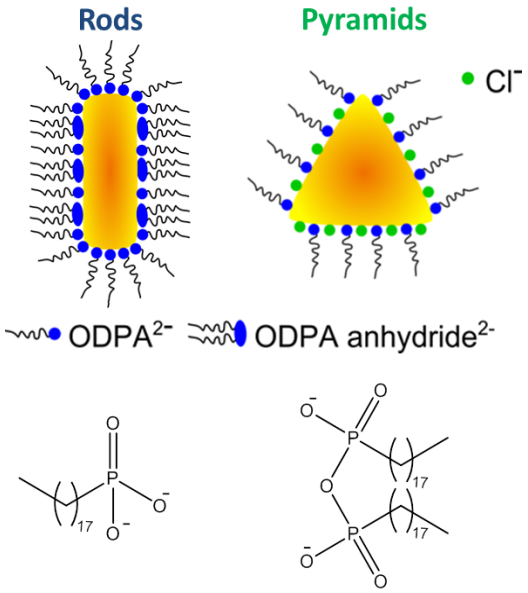

Scheme 3.2. *Images of the ligand shell composition of rod-like and pyramidal shaped NPs. In this image the displacement of the ODPA anhydrides ligands by chloride ions remaining the phosphonates ligands anchored to the surface is shown.*

3. 5. Conclusions

In this chapter the synthesis and a detailed characterization of the different morphology and surface chemistry of rod-like CdSe NPs that evolve into pyramidal shaped in the presence of chlorinated co-solvents have been performed. By means of XPS and ^{31}P NMR it has been found that the shape transformation is caused by the incorporation of chloride in the ligand shell, displacing selectively phosphonic acid anhydrides present in the original ligand sphere of rod-like NPs. As has been evidenced by ^{1}H NMR and EIS-TOF mass spectrometry, the chorinated specie formed *in situ* during the NPs synthesis due to the reaction between TOP and DCE is the ethane-1,2-dyilbys(trioctylphophonium)dichloride, which release the chloride ions responsible for the NPs reshaping.

3. 6. References

1. B. H. Juárez, C. Klinke, A. Kornowski and H. Weller, *Nano Letters*, 2007, **7**, 3564-3568.
2. A. B. Hungría, B. H. Juárez, C. Klinke, H. Weller and P. A. Midgley, *Nano Research*, 2008, **1**, 89-97.
3. B. H. Juárez, M. Meyns, A. Chanaewa, Y. Cai, C. Klinke and H. Weller, *Journal of the American Chemical Society*, 2008, **130**, 15282-15284.
4. M. R. Kim, K. Miszta, M. Povia, R. Brescia, S. Christodoulou, M. Prato, S. Marras and L. Manna, *ACS Nano*, 2012, **6**, 11088-11096.
5. M. Saruyama, M. Kanehara and T. Teranishi, *Journal of the American Chemical Society*, 2010, **132**, 3280-3282.
6. C. Schliehe, B. H. Juarez, M. Pelletier, S. Jander, D. Greshnykh, M. Nagel, A. Meyer, S. Foerster, A. Kornowski, C. Klinke and H. Weller, *Science*, 2010, **329**, 550.
7. X. Li, Y. Qin, S. T. Picraux and Z.-X. Guo, *Journal of Materials Chemistry*, 2011, **21**, 7527-7547.
8. N. C. Anderson and J. S. Owen, *Chemistry of Materials*, 2013, **25**, 69-76.
9. J. S. Owen, J. Park, P.-E. Trudeau and A. P. Alivisatos, *Journal of the American Chemical Society*, 2008, **130**, 12279-12281.
10. A. H. Ip, S. M. Thon, S. Hoogland, O. Voznyy, D. Zhitomirsky, R. Debnath, L. Levina, L. R. Rollny, G. H. Carey, A. Fischer, K. W. Kemp, I. J. Kramer, Z. Ning, A. J. Labelle, K. W. Chou, A. Amassian and E. H. Sargent, *Nature Nanotechnology*, 2012, **7**, 577-582.
11. J. Tang, K. W. Kemp, S. Hoogland, K. S. Jeong, H. Liu, L. Levina, M. Furukawa, X. Wang, R. Debnath, D. Cha, K. W. Chou, A. Fischer, A. Amassian, J. B. Asbury and E. H. Sargent, *Nature Materials*, 2011, **10**, 765-771.
12. J. T. Kopping and T. E. Patten, *Journal of the American Chemical Society*, 2008, **130**, 5689-5698.
13. R. Gomes, A. Hassinen, A. Szczygiel, Q. Zhao, A. Vantomme, J. C. Martins and Z. Hens, *The Journal of Physical Chemistry Letters*, 2011, **2**, 145-152.
14. W. K. Bae, J. Joo, L. A. Padilha, J. Won, D. C. Lee, Q. Lin, W.-k. Koh, H. Luo, V. I. Klimov and J. M. Pietryga, *Journal of the American Chemical Society*, 2012, **134**, 20160-20168.
15. M. Meyns, F. Iacono, C. Palencia, J. Geweke, M. D. Coderch, U. E. A. Fittschen, J. M. Gallego, R. Otero, B. H. Juárez and C. Klinke, *Chemistry of Materials*, 2014, **26**, 1813-1821.
16. Z. A. Peng and X. Peng, *Journal of the American Chemical Society*, 2001, **123**, 183-184.
17. Z. A. Peng and X. Peng, *Journal of the American Chemical Society*, 2001, **123**, 1389-1395.

18. Z. A. Peng and X. Peng, *Journal of the American Chemical Society*, 2002, **124**, 3343-3353.

19. C. Palencia, K. Lauwaet, L. de la Cueva, M. Acebron, J. J. Conde, M. Meyns, C. Klinke, J. M. Gallego, R. Otero and B. H. Juarez, *Nanoscale*, 2014, **6**, 6812-6818.

20. M. Zanella, L. Maserati, M. Pernia Leal, M. Prato, R. Lavieville, M. Povia, R. Krahne and L. Manna, *Chemistry of Materials*, 2013, **25**, 1423-1429.

21. S. J. Lim, W. Kim, S. Jung, J. Seo and S. K. Shin, *Chemistry of Materials*, 2011, **23**, 5029-5036.

22. F. Iacono, C. Palencia, L. de la Cueva, M. Meyns, L. Terracciano, A. Vollmer, M. J. de la Mata, C. Klinke, J. M. Gallego, B. H. Juarez and R. Otero, *ACS Nano*, 2013, **7**, 2559-2565.

23. H. Liu, J. S. Owen and A. P. Alivisatos, *Journal of the American Chemical Society*, 2007, **129**, 305-312.

24. L. Manna, Wang, R. Cingolani and A. P. Alivisatos, *The Journal of Physical Chemistry B*, 2005, **109**, 6183-6192.

25. S. A. Blanton, R. L. Leheny, M. A. Hines and P. Guyot-Sionnest, *Physical Review Letters*, 1997, **79**, 865-868.

26. A. J. Morris-Cohen, M. D. Donakowski, K. E. Knowles and E. A. Weiss, *The Journal of Physical Chemistry C*, 2010, **114**, 897-906.

27. F. Iacono, Ph. D. thesis, Universidad Autónoma de Madrid, 2013.

28. S. J. Lim, W. Kim and S. K. Shin, *Journal of the American Chemical Society*, 2012, **134**, 7576-7579.

29. L. Qu, Z. A. Peng and X. Peng, *Nano Letters*, 2001, **1**, 333-337.

30. R. D. Seals, R. Alexander, L. T. Taylor and J. G. Dillard, *Inorganic Chemistry*, 1973, **12**, 2485-2487.

31. G. Ohms, G. Großmann, B. Schwab and H. Schiefer, *Phosphorus, Sulfur, and Silicon and the Related Elements*, 1992, **68**, 77-89.

32. L. R. Becerra, C. B. Murray, R. G. Griffin, M. G. Bawendi, *Journal of Chemical Physics*, 1994, **100**, 3297–3300.

33. R. S. Rogers, *Tetrahedron letters*, 1992, **33**, 7473-7474.

4. Effect of Chloride Ligands on CdSe Nanoparticles by Cyclic Voltammetry and X-ray Photoelectron Spectroscopy

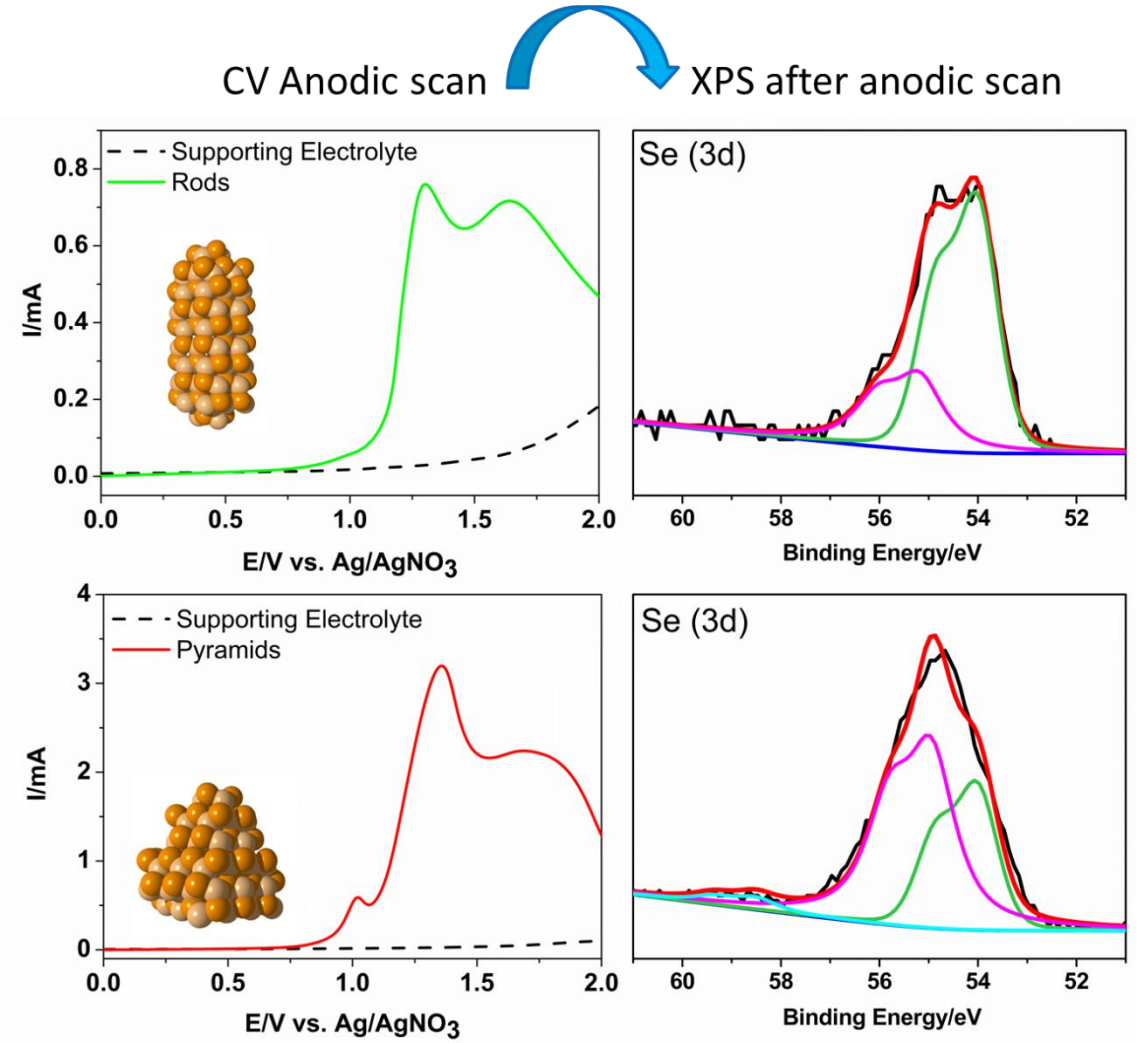

4. Effect of Chloride Ligands on CdSe Nanoparticles by Cyclic Voltammetry and X-ray Photoelectron Spectroscopy

4. 1. Abstract

In this chapter surface chemistry studies of rod-like and pyramidal CdSe NPs have been carried out. Correlated cyclic voltammetry (CV) and X-ray photoelectron spectroscopy (XPS) characterizations have been performed to address the effect of the incorporation of chloride ligands on the NPs surface. In contrast to ODPA capped rod-like NPs, the XPS studies confirm that, during the oxidation of pyramidal NPs capped by phosphonates ($ODPA^{2-}$) and chloride ligands, not only the oxidation of Se surface atoms, but also of Cd atoms takes place. Furthermore, XPS studies also confirm the partial reversibility of the Se oxidation in the presence of chloride. Both CV and subsequent XPS measurements allows identifying chemical environments and surface site modifications, essential to understand the stability and performance of NPs acting as active layers in optoelectronic devices.

4. 2. Introduction

Semiconductor NPs show tunable optical properties as a result of quantum confinement, which has triggered numerous optical studies.[1] Some spectroscopic techniques like absorption spectroscopy (AS), photoluminescence spectroscopy (PS), X-ray photoelectron spectroscopy (XPS), ultraviolet photoelectron spectroscopy (UPS), scanning tunneling spectroscopy (STS), deep-level transient spectroscopy (DLTS) and photoemission spectroscopy in air (PESA) provide information about the energy bandgap of the semiconductor NPs. With this same purpose, during the last decades Cyclic voltammetry (CV) has also been used to determine the electrochemical bandgap as the potential difference between the oxidation and reduction processes, which has activated many studies to match the optical and electrochemical gaps.[2, 3] As it will be shown in this chapter and, supported by other works, this correlation between the optical and the electrochemical band gaps is disputed.[4-7]

The A. J. Bard group was the first one to study the quantum-size effect of CdS NPs dispersed in DMF by CV obtaining good trends (larger potential differences between the redox processes as the NP size decreases) but lower values than the optical bandgaps.[2] Similar studies of CdTe NPs in aqueous solutions were performed by Poznyak et al. finding that the peak positions depend on the NPs size,[8] while Kuçur et al. carried out electrochemical studies of CdSe NPs in ionic liquids to enhance the media conductivity and observed the influence of the defect states and the NPs aggregation.[9] Afterwards, several groups have performed electrochemistry studies of semiconductor NPs not only to observe the effect of the NPs size, but also to investigate the relevance of other features of the NPs in the electrochemical response.[10, 11] Among them, several groups studied different surface composition NPs and observed that for ternary alloy semiconductor NPs ($CdS_{1-x}Se_x$ and $CdSe_{1-x}Te_x$) the redox onsets shift to more positive values as the concentration of Se increases.[10, 12, 13] Other features of the NPs that influence the electrochemical response are the presence of surface trap states that provoke the appearance of new redox processes that are thermodynamically and kinetically favored compared to those locating in the NP core,[11, 14, 15] or the presence of a shell around the semiconductor NPs that shift the oxidation processes to more anodic potential values avoiding the oxidation of the surface trap states.[16] Moreover, it has been reported that changes of the surface ligand composition also modify the position of the redox processes.[5, 6, 17-19] Since there are factors like the number of purification steps or the thickness of the NPs deposits on the electrodes that influence the electrochemical measurements, the relevance to establish an

optimal protocol to measure the CV response of semiconductor NPs has been recently emphasized.[10]

In this chapter a study of semiconductor NPs with different size, morphology and surface composition has been done by means of CV and correlated XPS. Different voltammetric responses have been recorded depending on the scan potential direction and capping ligand shell composition. Correlated CV and XPS measurements allow both to observe the difference in the electrochemical response of differently capped NPs and to identify chemical processes that Cd and Se surface atoms undergo under electrochemical treatments. The combination of these techniques may be very useful to identify undesirable effects on NPs-based devices affected by non-optimized charge injection/separation of charges.[20] Furthermore, the effect of the NPs organization around the electrode surface on the CV response has also been evaluated.

4. 3. Results and discussion

4. 3. 1. Cyclic voltammetry studies of different size CdSe NPs: Size-dependent electrochemical band-gap?

To study in detail the influence of the NPs size and the correlation between the optical and the electrochemical band gap (measured as the potential difference between the oxidation and reduction onsets), several aliquots taken at different reaction times of both, rod-like and pyramidal NPs, were measured by CV. Since the NP morphology does not change with the reaction time for CdSe rod-like NPs, in these samples the effect of the NPs size in the voltammetry can be evaluated. With this aim, during the synthesis, four aliquots taken at 5 min, 30 min, 2 h, and 21 h whose sizes are 4 ± 1 nm, 11 ± 1, 17 ± 1 and 18 ± 2 nm long and 2.1 ± 0.4, 3.3 ± 0.2, 4.1 ± 0.5 and 5.3 ± 0.7 nm wide were measured. The cyclic voltammograms of these aliquots initially scanned in cathodic direction (a), along with their absorption and emission spectra (b and c, respectively) are shown in Figure 4.1. As expected, the absorption edges and the emission peaks shift to longer wavelengths as the rod size increases due to the loss of the quantum confinement. The absorption edge and emission peak values vary from 561 nm to 655 nm and from 568 nm to 663 nm for the shortest and the longest reaction time aliquots, respectively. The cyclic voltammograms of the different size rod-like NPs show similar behaviors for each aliquot: In the first cathodic scan, from 0 to -2 V, no reduction processes are observed for any NP size and, in a further anodic scan from -2 V to 2 V, an oxidation peak can

be observed for every sample. These results are in agreement with an unfavorable cathodic reduction and a favorable anodic oxidation of CdSe at room temperature.[21-23] Afterwards, in the second cathodic scan from 2 V to -2 V a reduction peak appears for each sample at similar peak potential values regardless the NP size. Moreover, the cyclic voltammograms of the different size NPs present similar oxidation and reduction onsets. These onsets are commonly assigned to the injection of holes and electrons in the valence and conduction band, respectively and used to calculate the electrochemical gap, as previously mentioned.[3, 4]

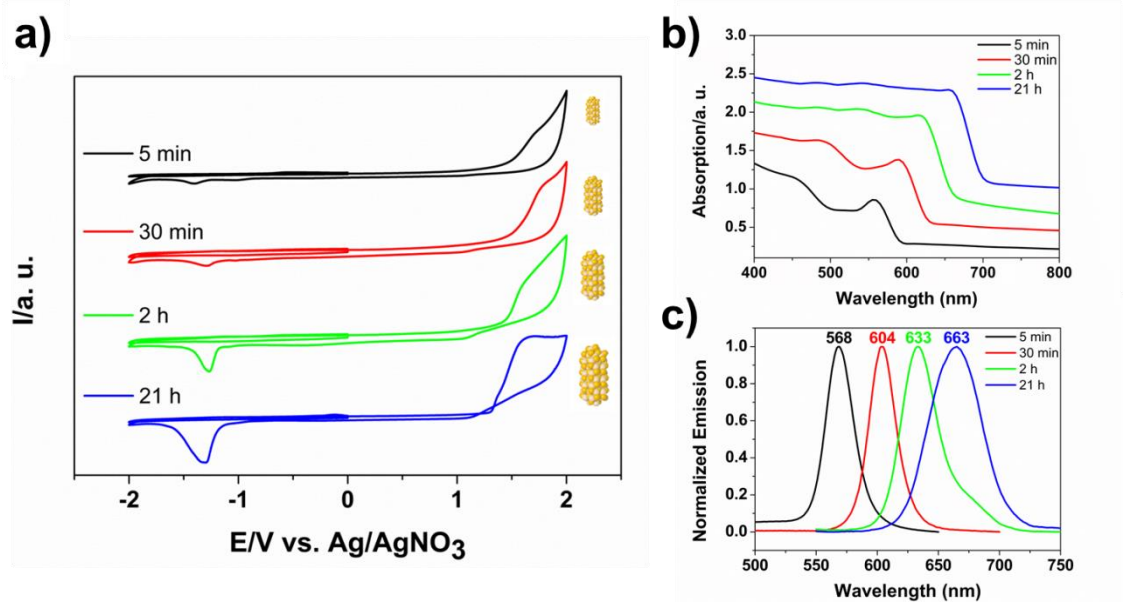

Figure 4.1. *a) Cyclic voltammograms of four aliquots taken at 5 min (black line), 30 min (red line), 2 h (green line) and 21 h (blue line) of reaction in the synthesis of rod-like NPs. Electrolyte solution: 0.1 M TBAP in acetonitrile; v = 0.1 Vs^{-1}. Absorption (b) and normalized emission (c) spectra of the corresponding aliquots.*

Table 4.1 summarizes the bandgap energy of the different size NPs calculated from the voltammograms showing that these values are similar for all samples, excluding any tendency related to the NP size. These results suggest that the redox processes cannot be associated with the bandgap of the NPs, not only because the reduction processes exclusively appear upon previous oxidation, but also because the oxidation and reduction onsets are similar for every aliquot.

Aliquot Reaction Time	Rod-like NPs	Pyramidal NPs
5 min	2.4 eV	-
30 min	2.4 eV	2.1 eV
2 h	2.5 eV	2.1 eV
21 h	2.2 eV	1.9 eV

Table 4.1. *Bandgap energy calculated electrochemically from the potential difference between the oxidation and reduction onsets.*

As it was shown in Chapter 3, during the synthesis of pyramidal NPs not only the size but also the morphology of the NPs changes from rods to pyramids as chloride anions are incorporated into the ligand shell. Thus, in these samples, differences in size, morphology and surface chemistry can be studied. To this aim, four aliquots were taken at the same reaction times than in the synthesis of rod-like NPs (5 min, 30 min, 2 h and 21 h) corresponding to dot-like NPs of 3.2 ± 0.6 nm, to rod-like NPs of 6.2 ± 0.7 nm long and 3.1 ± 0.4 nm wide, to bullet-shaped NPs of 4.5 ± 0.7 nm in their larger axis and to pyramidal shaped NPs of 8 ± 1 nm in diameter, respectively. The cyclic voltammograms of these aliquots initially scanned in cathodic direction (a), along with their absorption and emission spectra (b and c, respectively) are shown in Figure 4.2. As in the previous case, the absorption edges and the emission peaks of the different morphology and size NPs are shifted to longer wavelengths as the NPs grow (Figure 4.2b,c). The absorption edge and emission peak values vary from 579 nm to 675 nm and from 591 nm to 684 nm for the shortest to the longest reaction time aliquiots, respectively.

As in the case of rod-like NPs, in the voltammograms of every sample shown in Figure 4.2a no reduction peaks are recorded in the first cathodic scan from 0 to -2 V and different oxidation processes appear in the subsequent anodic scan from -2 V to 2 V. Afterwards, in the second cathodic scan from -2 V to 2 V a reduction peak appears for each aliquot except for the first one taken after 5 min of reaction. Taking into account the potential value tendency for the different aliquots, the absence of a peak after 5 min of reaction may be related to the limited available potential window. Conversely to the different size rod-like NPs, in this case the reduction peaks shift to less cathodic potentials as the reaction time increases and the

morphology and the surface composition of the NPs change (marked with a grey arrow in Figure 4.2a).

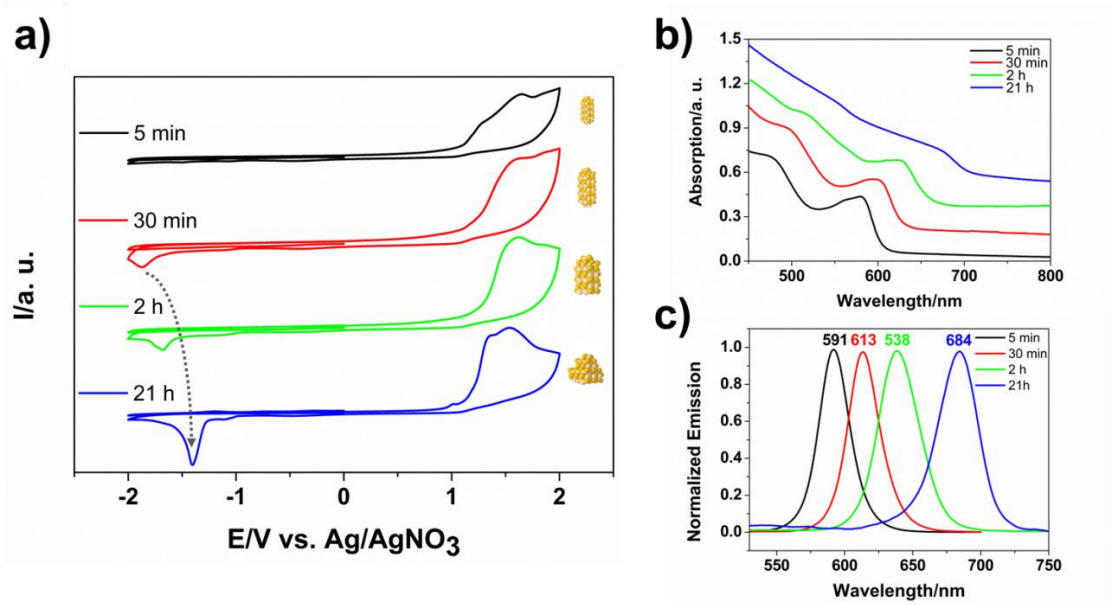

Figure 4.2. *a) Cyclic voltammograms of four aliquots taken at 5 min (black line), 30 min (red line), 2 h (green line) and 21 h (blue line) of reaction in the synthesis of pyramidal NPs. Electrolyte solution: 0.1 M TBAP in acetonitrile; v = 0.1 Vs^{-1}. Absorption (b) and normalized emission (c) spectra of the corresponding aliquots.*

Furthermore, the oxidation and reduction onsets for the aliquots taken at 30 min and 2 h are similar, and the electrochemically calculated bandgap is similar even though their optical properties are very different (Table 4.1). Moreover, it is important to mention that the CV of pyramidal shaped NPs (21 h of reaction) shows an extra oxidation peak at 1 V, which will be further discussed. These results evidence that, the voltammetric response depends on the ligand shell composition of the NPs, and that the recorded reduction peaks are related to previously oxidized species. Thus, according to these results, the redox processes cannot be assigned to the ionization potential (or injection of holes in the valence band) and the electronegativity (or injection of electrons in the conduction band).

4. 3. 2. Cyclic voltammetry studies of rod-like and pyramidal shaped CdSe NPs: effect of chloride ligands and scan direction

In order to analyze in detail the effect that the presence of chlorine on the NPs surface generates on the electrochemical response, both rod-like and pyramidal NPs of 21 hours of reaction (produced following the synthetic procedure described in Chapter 3) have been

characterized by CV as a function of the initial scan direction, whose effect has been previously underlined for electrochemical studies of water-soluble CdTe NPs.[8] Figure 4.3a shows the voltammetry response of pyramids (red line) and rods (green line) when the initial scan direction is anodic (0 to +2 V) followed by a cathodic scan (+2 V, −2 V). For comparison Figure 4.3b shows in the same color code the corresponding characterization when the initial scan direction is cathodic (0 to −2 V) followed by a complete cycle (−2 V, 2 V, −2 V). Two schemes depict the range of employed potentials.

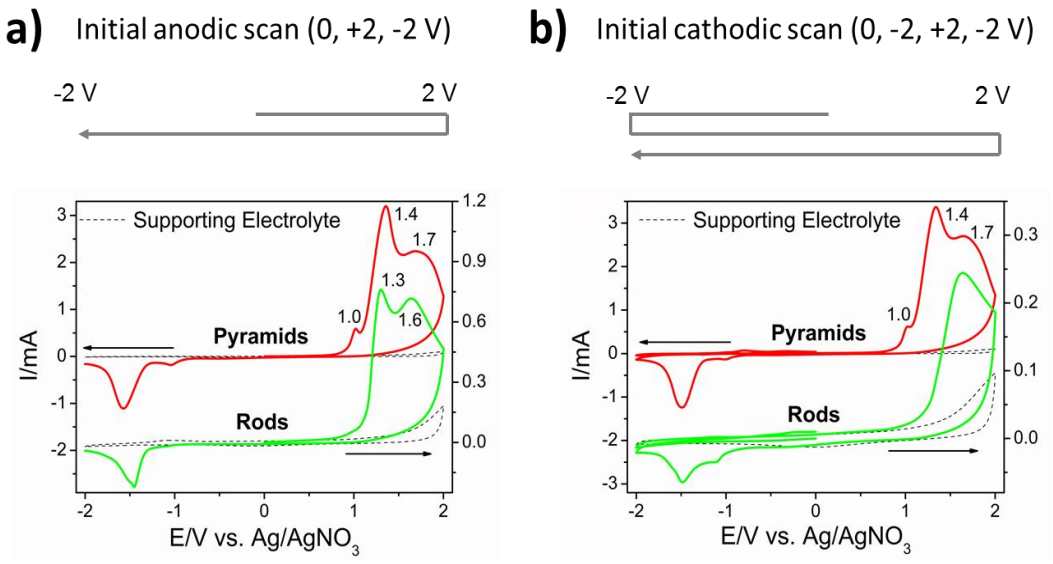

Figure 4.3. *a) CV of pyramidal shape and rod-like NCs where the potential was initially cycled in anodic direction. The complete cycle includes (0, +2V, -2V). b) CV of pyramidal shape and rod-like NCs initially cycled in cathodic direction. The complete cycle includes (0, -2, +2V, -2V). Electrolyte solution: 0.1 M TBAP in acetonitrile; v = 0.1 Vs^{-1}. Grey arrows with scan directions are added as guides. Black arrows indicate the axis of each voltammogram.*

As previously mentioned, upon the first cathodic scan (from 0 to −2 V) (Figure 4.3b) no reduction peaks are recorded regardless of size, shape, or concentration of NPs on the electrode. On the contrary, in the subsequent anodic scan to +2 V, clear oxidation processes can be recorded in the voltammogram for all samples. A second cathodic scan to −2 V after previous oxidation is characterized by a reduction peak centered at −1.4 V. In all cases, since the reduction peaks are only obtained upon previous anodic oxidation, they can be exclusively assigned to the reduction of previously oxidized species on the surface of the NPs and will be further characterized in detail by XPS.

From the voltammograms shown in Figure 4.3 two remarkable facts can be extracted: (i) the potential difference between the anodic and cathodic processes is about 2 V in all cases and (ii) the anodic area, obtained by subtraction of the background current, is higher than the area corresponding to the cathodic processes. These results confirm that the electrochemical response of semiconductor CdSe NPs at room temperature is a nonreversible process, in agreement with previous reports.[2] However, as it will be shown later, the presence of chloride forming part of the capping ligand shell allows for partial reversibility of anodically corroded Se sites. The voltammograms for pyramidal NPs (Figure 4.3, red lines) are similar regardless of the initial scan direction and are composed of two defined peaks at 1.4 and 1.7 V and a small peak centered at 1 V. The same characterization is depicted for rod-like NPs where, in contrast to the case of pyramidal NPs, the voltammograms differ notably depending on the initial scan potential direction. If the initial scan direction is anodic (Figure 4.3a , green line), a well-defined wave composed of two peaks at 1.3 and 1.6 V resembling those observed for pyramidal NPs at 1.4 and 1.7 V is obtained. The two observable peaks separated 0.3−0.4 V in the anodic scans might be related to the oxidation of two different atomic chemical environments. This potential difference is about 57 $KJmol^{-1}$ for the electronic transference of n = $2e^-$. Therefore the peaks at 1.3−1.4 and 1.6−1.7 V may correspond to the oxidation of Se located in different NPs facets for both rods and pyramids. Alternatively, these peaks can be assigned to different oxidation states of Se.[8] However, when the scan direction is initially cathodic the peak at 1.3 V is strongly attenuated in the case of rods (Figure 4.3b, green line) but not in the case of pyramids (Figure 4.3b, red line). We ascertained that in rods the process taking place at this potential (1.3 V) is a slow charge transfer process since the current intensity increases with decreasing scan rate (not shown). The higher density of long alkyl chain molecules (ODPA) capping the surface of rods compared to that of pyramids[24] may act as an insulating barrier. Moreover, these ligands protect the rod surface from the voltammetric oxidation and produce much lower current intensities than for the less ligand capped pyramidal NPs. It is also possible that the process taking place at this potential could be influenced by the previous electron filling of free or trapped holes taking place in the previous cathodic scan.[25]

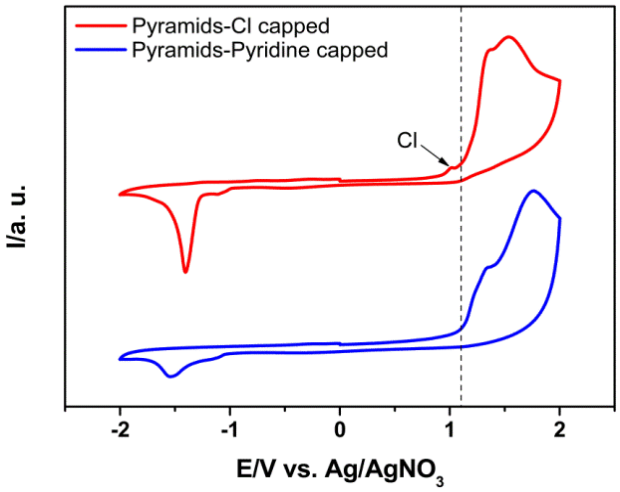

Figure 4.4. *Cyclic voltammograms of pyramidal shaped NPs capped with chloride (red line) and with pyridine (blue line). Electrolyte solution: 0.1 M TBAP in acetonitrile; v = 0.1 Vs^{-1}.*

Finally, a clear peak of low intensity at 1 V is observable exclusively in samples of NPs showing pyramidal shape and may be considered as a fingerprint of the presence of chloride on the NPs surface. Further evidence can be observed when treating ODPA+Cl^-capped CdSe pyramids with pyridine, a well-known displacing molecule anchoring Cd sites. In this case, the peak at 1 V cannot be observed while the rest of the oxidation processes remain in the CV (see voltamograms of Figure 4.4).

4. 3. 3. Stability studies in consecutive Cyclic voltammetry cycles.

With the aim to study the stability of the NPs to the CV potential, several cycles have been applied. Figure 4.5 shows the first five consecutive scans recorded for, rod-like and pyramidal NPs produced after 21 h of reaction (a and b, respectively), along with a representation of the potential value of the reduction peak versus the scan number (insets).

As previously shown for one cycle, for every consecutive one, the anodic charge is always higher than the cathodic charge, pointing to a favorable oxidation and a partial or incomplete reduction of previously oxidized products. Also, the oxidation and therefore the reduction charge decrease as the number of scans increases for both type of samples showing the already mentioned irreversibility of the redox processes. Furthermore, the cathodic peak of the pyramidal shaped NPs is shifted to more cathodic potential values as the number of scans increases while for rod-like NPs the reduction peak remains constant or slightly varies after the first scan.

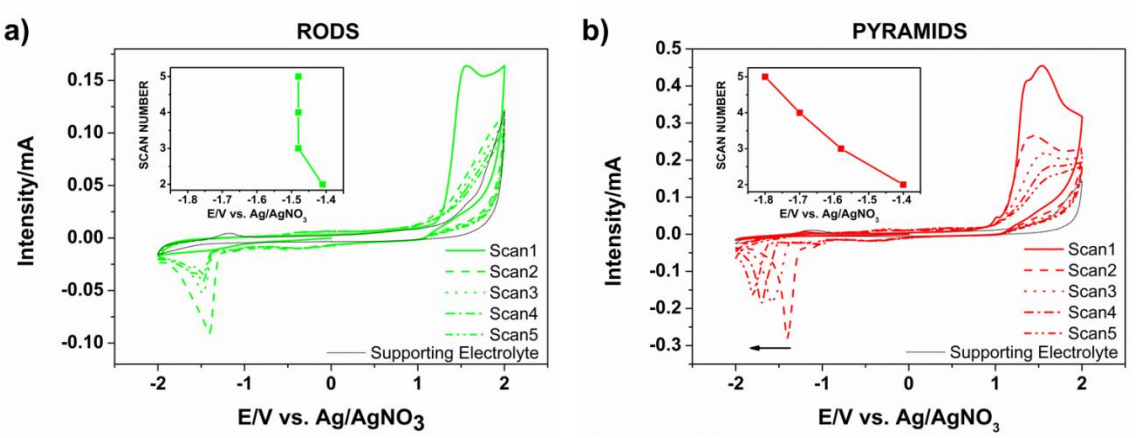

Figure 4.5. *First five consecutive CV scans for rod-like shaped (a) and pyramidal NPs (b). Insets: Potential value of the reduction peak as a function of the scan number. Electrolyte solution: 0.1 M TBAP in acetonitrile. v = 0.1 Vs^{-1}.*

In order to prove that changes in the cathodic peak are not related with a change in the particle size (and thus, in the electrochemical response), the NPs sizes were measured before and after the 5 CV cycles. As it can be observed in Figure 4.6, the histograms reveal similar sizes in both cases. Thus, this is another hint pointing that the cathodic peak and its shift must be related to the nature of the oxidation products of pyramidal NPs, which differ from those of rod-like NPs.

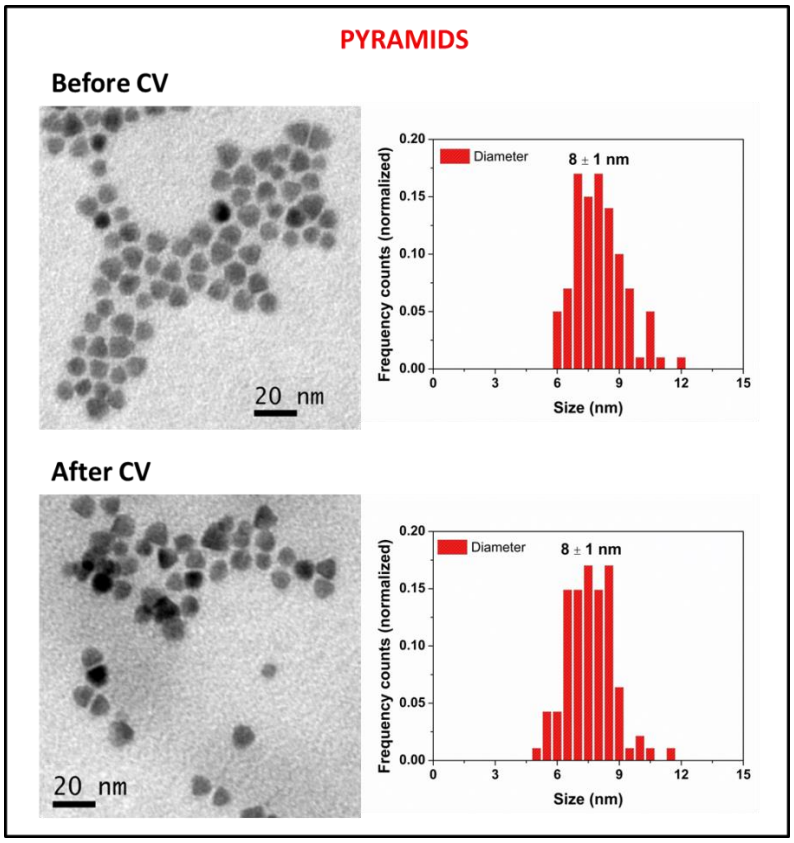

Figure 4.6. *TEM images and normalized size distribution histograms of pyramidal shaped NPs before and after five consecutive voltammetric cycles.*

4. 3. 4. XPS surface characterization of rod-like and pyramidal CdSe NPs after different voltammetric scans

From the results shown above, it is clear that the surface lattice is altered by the presence of chloride, and thus, correlated XPS measurements have been employed to characterize the different NPs surfaces and to understand the changes produced during the oxidation and reduction processes. To this aim, thin films of NPs of 21 h of reaction were deposited by drop-casting on glassy carbon electrodes. Thin deposits are essential to avoid charging effects that may alter the energetic position of the peaks. Figure 4.7 shows Se *3d* spectral regions of modified electrodes by deposition of different shaped NPs (pyramidal and rod-like shaped). The first row includes XPS spectra of pyramidal (a) and rod-like NPs (b) prior to the application of any electrochemical treatment. It is worth mentioning that these spectra correspond to samples that have been previously immersed in the electrolyte solution. Thus, it has been checked that this simple immersion does not affect the Se (or Cd) peaks.

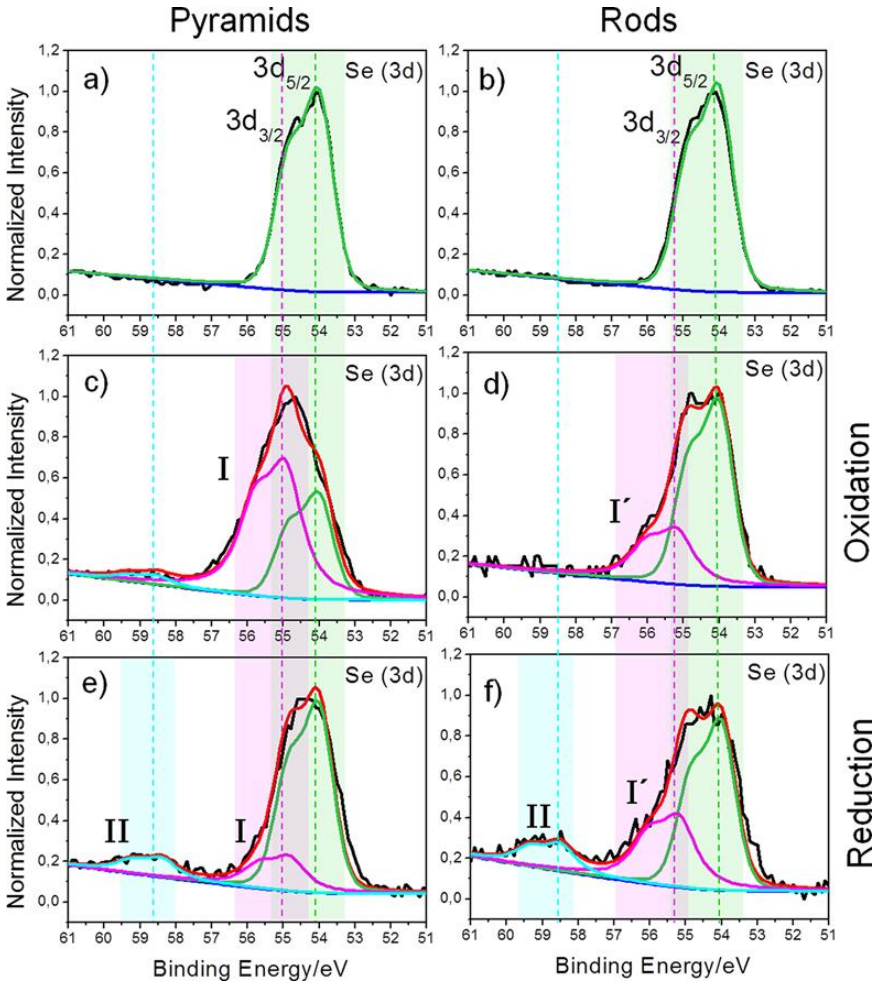

Figure 4.7. *XPS spectra of Se 3d regions of pyramidal shaped and rod-like CdSe NCs without electrochemical treatment (a and b), after first oxidation (c and d), and further reduction (e and f). The labeled components I and I´ are products generated upon electrochemical oxidation than remain stable in ODPA capped rod-like NCs (I´ in 2d compared to I´ in 2f) but can be partially reduced in a further cathodic scan in the case of ODPA+Cl capped pyramidal NCs (I in 2c compared to I in 2e). Component II corresponds to oxidation products in air (see text).*

The Se *3d* signal is composed of two contributions, according to the spin orbit splitting in Se $3d_{5/2}$ and Se $3d_{3/2}$ whose binding energies are centered at 54.1 and 54.6 eV, respectively. When the potential is initially scanned in the cathodic direction (0 to −2 V), the corresponding XPS spectra acquired after this step (not shown) are similar to those obtained for the initial, nonbiased NPs (Figure 4.7(a,b)), in agreement with the absence of peaks in the voltammograms. Hence, both techniques, CV and XPS are not sensitive enough to record changes on the chemical environments (if any) during the application of a cathodic sweep from 0 to −2 V to CdSe NPs on glassy carbon electrodes. Significant changes in the energetic position

and width of the elements composing the ligand shell (C, P, and elements) have also been discarded (spectra not shown). There are, however, differences between the oxidation response of rods and pyramids according to the XPS results, corresponding to the changes observed in CV. First, new oxidized components can be found in the XPS Se spectra at higher binding energies than that of no oxidized CdSe NPs both for pyramids and rods (component I at a binding energy of 55.0 eV in Figure 4.7c for pyramids, and I´ at a binding energy of 55.4 eV in Figure 4.7d for rods). The intensity of the oxidized component is larger for pyramids than for rods, indicating that the oxidation proceeds faster in pyramids. In other words, the oxidation is less effective for Se sites in rods than in pyramids, what highlights that the presence of chloride capping the NPs surface must also have an influence over the redox reactions of Se sites.

In order to further characterize the changes produced in the samples during the anodic process, the potential was subsequently scanned in the cathodic direction. For a further reduction treatment (Figure 4.7(e,f)), the previously oxidized Se sites in the rods (component I´) remain constant both in binding energy position and intensity demonstrating that the anodic oxidation of the rod-like CdSe NPs capped with ODPA and without Cl is irreversible. In contrast, the previously oxidized Se component for pyramids clearly shows a partial reversibility, with a drastic decrease in intensity (component I in panel e vs I in panel c in Figure 4.7). This suggests that the oxidation mechanism for the Cl-capped pyramidal NPs must be essentially different than the one taking place for rod-like NPs, involving the formation of a Se product which does not result in the oxidation of rod-like NPs. This different mechanism may end up in different oxidation products, which would explain the different cathodic peak behavior of pyramidal NPs compared to rod-like ones shown in sections 4. 4. 1. and 4. 4. 3. It is proposed that species such as Se_2Cl_2, known to exist in equilibrium with $SeCl_2$, $SeCl_4$, chlorine, and elemental Se,[26] modify the electrochemical response of CdSe. The expected Se XPS peak for elemental Se, $SeCl_2$ (Se^{2+}), and $SeCl_4$ (Se^{4+}) must be oxidized with respect to Se^{2-} in CdSe, in good agreement with the higher energy position of the recorded peak. Furthermore, a new component is observed both for rods and pyramids (component II in Figure 4.7(e,f) respectively). In this case, since the sample has been reduced during this step (cathodic scan) this peak can only be the result of unavoidable environmental oxidation when samples are transferred from the electrochemical cell to the XPS chamber.

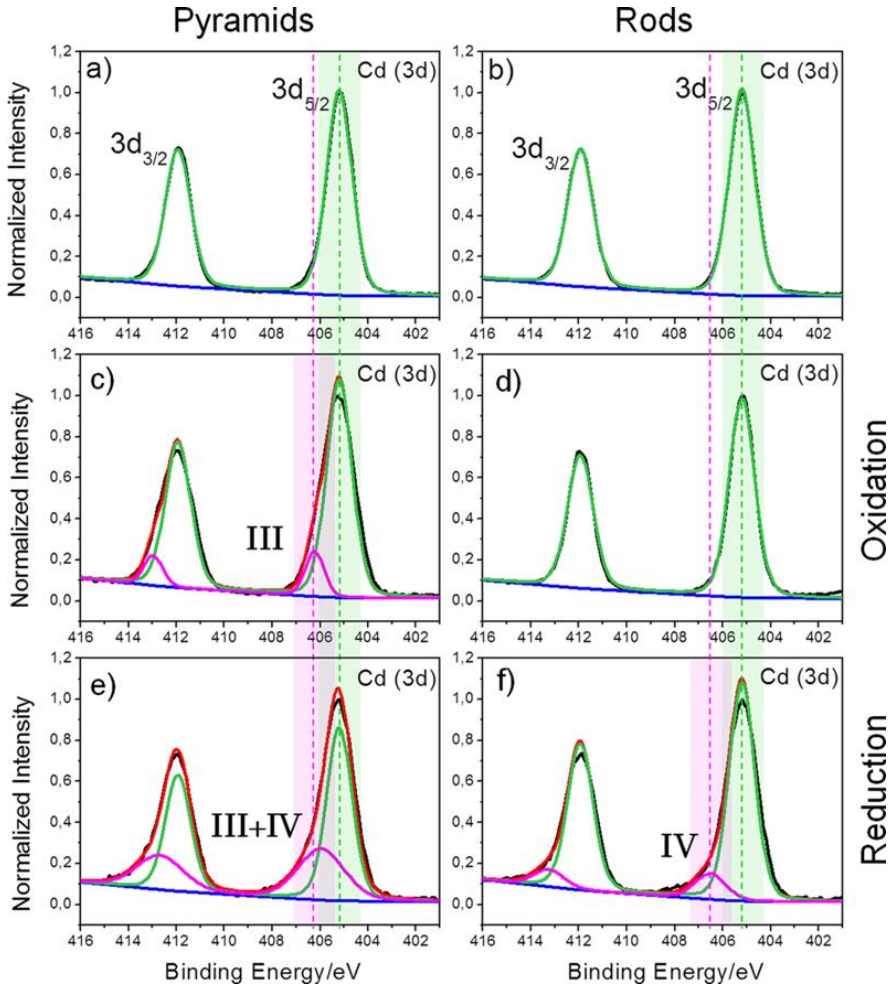

Figure 4.8. *XPS spectra of Cd 3d regions of pyramidal shaped and rod-like CdSe NCs without electrochemical treatment (a and b), after first oxidation (c and d), and further reduction (e and f). The component labeled with III corresponds to oxidation products obtained upon electrochemical oxidation occurring exclusively in ODPA+Cl capped pyramidal NCs (c) but not in ODPA capped rod-like NCs (d). Component IV corresponds to the reduction of Cd^{2+} to Cd^{0} upon electrochemical cathodic scan and further oxidation to Cd^{0} in air (see text).*

XPS spectra shown in Figure 4.8 correspond to the Cd core levels. As in Figure 4.7, the first row corresponds to the spectra of pyramidal (a) and rod-like NPs (b) prior to the application of any electrochemical treatment. The Cd *3d* region shows two peaks centered at 405.2 and 411.9 eV, corresponding to the Cd $3d_{5/2}$ and Cd $3d_{3/2}$ spin orbit split signals. The second row corresponds to Cd spectra obtained upon the application of an anodic scan from 0 to +2 V according to the voltammograms depicted in Figure 4.3a. As it can be clearly observed, the Cd signal remains constant for rod-like NPs (Figure 4.8d), while a new contribution at higher binding energies relative to the Cd $3d_{5/2}$ and Cd $3d_{3/2}$ peaks is recorded for pyramidal

ones (component III in Figure 4.8c). Since the main difference between rods and pyramids when it comes to the chemical properties of the surface, is the presence of chloride ions attached to Cd sites, we conclude that the appearance of this extra contribution must arise from such Cd sites indicating its oxidation. In rods, however, the Cd sites remain unchanged. The binding energy position of the new Cd contribution is in good agreement with the formation of more oxidized Cd species. Similar peak contributions in XPS were also observed in nonstoichiometric CdSe surfaces and interpreted as Cd-rich surfaces.[22] In any event this component does not appear in samples that have not been electrochemically oxidized. The voltammetric response of rods and pyramids differ mainly in the peak recorded at 1 V suggesting that the new Cd contribution can indeed be considered as a fingerprint of the oxidation of the Cd sites capped with Cl.

As in the case of Se sites, the third row in Figure 4.8 depicts the XPS measurements upon reduction of the previously oxidized sample. For Cd sites in rods the reduction process yields a higher binding energy component (component IV in Figure 4.8f). Similarly to the effect observed for Se sites, since the sample has been reduced during this step (cathodic scan), this peak can only be the result of unavoidable environmental oxidation to CdO when samples are transferred from the electrochemical cell to the XPS chamber.

Scheme of the Cd surface atoms oxidation of pyramidal shaped NPs:

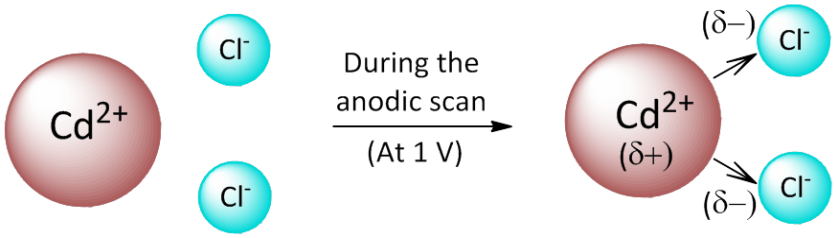

Proposed Cd redox reactions:

- Anodic scan: $Cd^{2+} + 2Cl^- \longrightarrow Cd^{2+(\delta+)} + Cl_2 + 2e^-$
- Cathodic scan: $Cd^{2+(\delta+)} + 2e^- \longrightarrow Cd^0$
- Subsequent environmental oxidation: $2Cd^0 + O_2 \longrightarrow 2CdO$

Scheme 4.1. *Picture of the Cd^{2+} and Cl oxidation at 1 V during the anodic scan and proposed Cd redox reactions after the electrochemical treatment (0 – 2 – -2 V) and its further environmental oxidation for pyramidal shaped NPs.*

The oxidation must proceeds from Cd^{2+} previously reduced to Cd^0 in the cathodic scan (see Scheme 4.1). This effect is also observed for pyramids, where the new component must be added to the previous one obtained upon the anodic scan in the presence of chloride (sum of components III + IV in Figure 4.8e).

Further information can be extracted by the comparison of the ratio between Cd and Se peak areas obtained from CdSe NPs before and after the electrochemical treatments, as shown in Table 4.2. The Cd/Se XPS peak area ratio after the anodic scan changes dramatically for pyramids while is almost constant for rods (19 and 35 respectively). In ODPA capped NPs regular oxidation proceeds according to the well-known anodic decomposition:[22]

$$CdSe \rightarrow Cd^{2+} + Se^0 + 2e^-$$

where Cd^{2+} may remain on the NPs surface. However, in the case of ODPA+Cl CdSe NPs, not only Se sites but also Cd−Cl sites are oxidized (these last ones at 1 V). The oxidation products of the latter reaction are removed from the NPs surface and released to the electrolyte when samples are washed after the first oxidation and before the XPS measurement. Thus, the Cd/Se ratio decreases due to a reduction in the Cd content. This ratio is recovered if samples are not washed after oxidation and are further reduced, what indicates that the oxidation products remain in the interface. This result can be related with the stability of the size of the NPs with the successive scans described in section 4. 4. 3. In that case the NPs size remains unaltered after 5 voltammetric cycles; although during the anodic scan the Cd atoms of the NPs are removed from the NP surface in the following cathodic scan they are incorporated again in the NP surface keeping the size of the NPs constant.

XPS peak area ratio	**Cd/Se initial**	**Cd/Se peaks ratio after 1st oxidation**	**Cd/Se peaks ratio after 2nd reduction**
Rods	38	35	37
Pyramids	36	19	38

Table 4.2. *Relative Cd/Se XPS peak areas for rods and pyramids before and after the application of a first anodic and further cathodic scans.*

Summarizing, by XPS we have identified three different oxidation processes for rod-like and pyramidal NPs: At the Se sites, the oxidation is irreversible for rods, while it is partially

reversible in pyramids. We attribute the reversibility in the pyramids to the formation of Se-Cl species in the presence of Cl. On the other hand, pyramids also show an oxidation process that takes place at the Cd sites. Thus, while oxidation at the Se sites occurs both for pyramids and rods, the oxidation at the Cd sites takes place only in pyramids. In comparison with the CV, the only oxidation process that takes place exclusively in pyramids corresponds to the peak at 1 V, which is attributed to the oxidation of the Cd-Cl sites. On the other hand, the peaks at 1.3-1.4 and 1.6-1.7 V can be attributed to the oxidation of Se, possible in different crystallographic planes or different atomic sites on the surface. Such a process is very efficient in pyramids, corresponding to the larger intensity of the oxidized component in the Se XPS spectra and also to the larger oxidation charge for pyramids.

4.3. 5. Difference between a monolayer and multilayer modified electrodes

As it has been mentioned in Chapter 3, pyramidal NPs capped by chloride anions are prone to decorate Csp^2 surfaces. Owing to the Csp^2 regions present in the glassy-carbon surface it is possible to modify the working electrodes with an ordered monolayer of pyramidal NPs in which the base of the pyramids (the (000-1) facets) interact with the electrode surface by means of chloride ligands (ref). To reach this electrode a glassy-carbon bar was introduced in the pot during 21 hours of reaction.

In order to study the effect of the organization of the NPs on the electrochemical response the electrode modified with an ordered monolayer of pyramidal NPs was compared with a working electrode modified by drop-casting with multilayers of randomly distributed NPs on its surface (Figure 4.9). In Figure 4.9b the CV of the electrode modified with an ordered monolayer of NPs is depicted. As it was expected, no reduction processes were observed in the first cathodic scan. In the following anodic scan three different oxidation peaks appear at 0.9, 1.1 and 1.2 V while for the electrode modified with multilayers of NPs only one oxidation process is recorded around 1 V. Probably the extra oxidation processes are also present in the voltammograms of the multilayers electrodes but cannot be observed due to the large current increase produced by the selenium oxidation. This result proves that the organization of NPs around the electrode has an enormous influence in the position of the recorded peaks by CV.[27] Thus, this is other evidence proving that the determination of an electrochemical band-gap correlated to an optical band-gap cannot be done.

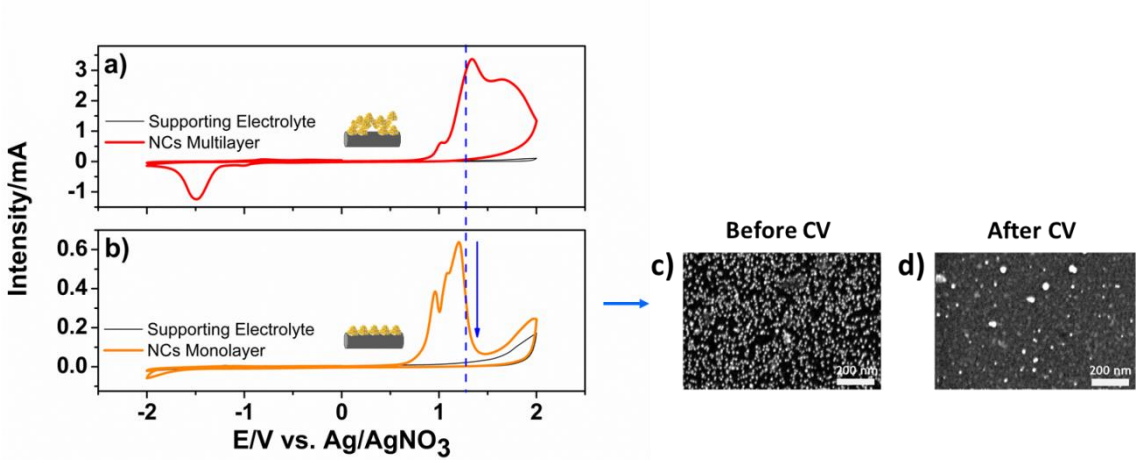

Figure 4.9. *Cyclic voltammogram of a glassy-carbon electrode modified with multilayers of randomly oriented CdSe NPs (a) and with an order monolayer of CdSe NPs (b). Electrolyte solution: 0.1 M TBAP in acetonitrile; v = 0.1 Vs^{-1}. (c) and (d) SEM micrographs of the monolayer modified electrode before and after cyclic voltammetry, respectively.*

After these oxidation processes the current intensity drastically decreases and the Se oxidation peaks were not recorded, contrary to what was observed for an electrode modified with multilayers of NPs randomly distributed (Figure 4.9a). This fact may be due to the oxidation of chloride ligands producing the detachment of the monolayer NPs from the electrode surface avoiding the Se oxidation and the subsequent reduction processes. To verify this result, SEM images were taken before and after the cyclic voltammetry. As can be observed in Figure 4.9d, the NPs amount over the electrode surface is much lower after the electrochemical measurement than in the initial electrode (Figure 4.9c), corroborating the previous hypothesis.

4. 4. Conclusions

The results obtained in the electrochemical studies of different size, morphology and surface composition CdSe NPs evidence that the redox processes depend on several factors: i) The surface composition, ii) the initial scan direction, iii) the number of cycles and iv) the NPs organization around the electrode. According to our evidences, the electrochemical response of semiconductor NPs is due to the redox processes on the surface of the NPs and is not related with the injection of holes and electrons in the valence and conduction band, respectively. It is then demonstrated that, contrary to extensive previously published results, cyclic voltammetry is not a suitable technique to calculate the electrochemical bandgap as a comparable value to the optical one, for CdSe NPs. Moreover, the combination of CV and XPS

allows for the identification of different Cd and Se environments and for testing the stability of CdSe NPs under different electrochemical treatments. The incorporation of chloride to the ligand shell modifies the surface chemical environment of Cd surface sites as well as the redox response of the NPs. XPS ascertains that applying an anodic scan produces irreversible corrosion of Se in rods, but certain reversibility in pyramidal NPs capped with chloride ligands.

4. 5. References

1. A. L. Rogach, ed., *Semiconductor Nanocrystals Quantum Dots. Synthesis, Assembly, Spectroscopy and Applications.*, SpringerWienNewYork, 2008.
2. S. K. Haram, B. M. Quinn and A. J. Bard, *Journal of the American Chemical Society*, 2001, **123**, 8860-8861.
3. E. Kucur, J. Riegler, G. A. Urban and T. Nann, *The Journal of Chemical Physics*, 2003, **119**, 2333.
4. S. K. Haram, A. Kshirsagar, Y. D. Gujarathi, P. P. Ingole, O. A. Nene, G. B. Markad and S. P. Nanavati, *The Journal of Physical Chemistry C*, 2011, **115**, 6243-6249.
5. A. Lefrancois, E. Couderc, J. Faure-Vincent, S. Sadki, A. Pron and P. Reiss, *Journal of Materials Chemistry*, 2011, **21**, 11524-11531.
6. M. Amelia, S. Impellizzeri, S. Monaco, I. Yildiz, S. Silvi, F. M. Raymo and A. Credi, *Journal of Chemical Physics and Physical Chemistry*, 2011, **12**, 2280-2288.
7. A. S. Cuharuc, L. L. Kulyuk, R. I. Lascova, A. A. Mitioglu and A. I. Dikusar, *Surface Engineering and Applied Electrochemistry*, 2012, **48**, 193-211.
8. S. K. Poznyak, N. P. Osipovich, A. Shavel, D. V. Talapin, M. Gao, A. Eychmüller and N. Gaponik, *The Journal of Physical Chemistry B*, 2005, **109**, 1094-1100.
9. E. Kuçur, W. Bücking, S. Arenz, R. Giernoth and T. Nann, *Journal of Chemical Physics and Physical Chemistry*, 2006, **7**, 77-81.
10. J. Liu, W. Yang, Y. Li, L. Fan and Y. Li, *Physical Chemistry Chemical Physics*, 2014, **16**, 4778-4788.
11. M. Amelia, T. Avellina, S. Monaco, S. Impellizzeri, I. Yildiz, F. M. Raymo and A. Credi, *Pure and Applied Chemystry*, 2011, **83**, 1-8.
12. Y. C. Li, H. Z. Zhong, R. Li, Y. Zhou, C. H. Yang and Y. F. Li, *Advanced Functional Materials*, 2006, **16**, 1705-1716.
13. B. Hou, D. Parker, G. P. Kissling, J. A. Jones, D. Cherns and D. J. Fermín, *The Journal of Physical Chemistry C*, 2013, **117**, 6814-6820.
14. S. N. Inamdar, P. P. Ingole and S. K. Haram, *Journal of Chemical Physics and Physical Chemistry*, 2008, **9**, 2574-2579.
15. E. Kuçur, W. Bücking, R. Giernoth and T. Nann, *The Journal of Physical Chemistry B*, 2005, **109**, 20355-20360.
16. S. Impellizzeri, S. Monaco, I. Yildiz, M. Amelia, A. Credi and F. M. Raymo, *The Journal of Physical Chemistry C*, 2010, **114**, 7007-7013.
17. D. Aldakov, C. Querner, Y. Kervella, B. Jousselme, R. Demadrille, E. Rossitto, P. Reiss and A. Pron, *Microchimica Acta*, 2008, **160**, 335-344.

18. M. Soreni-Harari, N. Yaacobi-Gross, D. Steiner, A. Aharoni, U. Banin, O. Millo and N. Tessler, *Nano Letters*, 2008, **8**, 678-684.

19. C. Querner, P. Reiss, S. Sadki, M. Zagorska and A. Pron, *Physical Chemistry Chemical Physics*, 2005, **7**, 3204-3209.

20. P. V. Kamat, *The Journal of Physical Chemistry C*, 2008, **112**, 18737-18753.

21. A. J. Bard and M. S. Wrighton, *Journal of The Electrochemical Society*, 1977, **124**, 1706-1710.

22. J. Jasieniak and P. Mulvaney, *Journal of the American Chemical Society*, 2007, **129**, 2841-2848.

23. J. H. Engel, Y. Surendranath and A. P. Alivisatos, *Journal of the American Chemical Society*, 2012, **134**, 13200-13203.

24. F. Iacono, C. Palencia, L. de la Cueva, M. Meyns, L. Terracciano, A. Vollmer, M. J. de la Mata, C. Klinke, J. M. Gallego, B. H. Juarez and R. Otero, *ACS Nano*, 2013, **7**, 2559-2565.

25. A. L. Weaver and D. R. Gamelin, *Journal of the American Chemical Society*, 2012, **134**, 6819-6825.

26. M. Lamoureux and J. Milne, *Polyhedron*, 1990, **9**, 589-595.

27. G. Zotti, B. Vercelli, A. Berlin, P. T. K. Chin and U. Giovanella, *Chemistry of Materials*, 2009, **21**, 2258-2271.

5. Precursor Controlled Morphology of Au-Se Deposits on CdSe Nanoparticles (NPs)

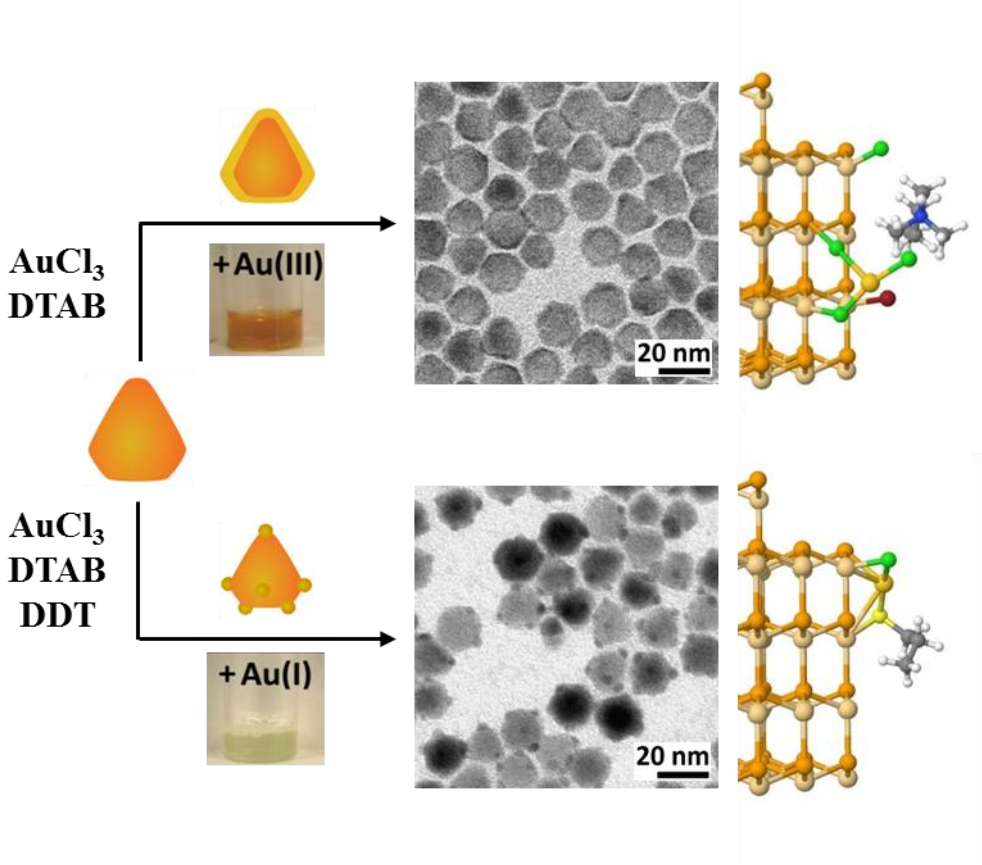

5. Precursor Controlled Morphology of Au-Se Deposits on CdSe Nanoparticles (NPs)

5. 1. Abstract

In this chapter the synthesis and characterization of different Au-CdSe hybrid nanoparticles (HNPs) has been done. On the basis of a system with only three reaction components, pyramidal shaped CdSe seeds, n-dodecyltrimethylammonium bromide complexed $AuCl_3$, and dodecanethiol, it has been demonstrated that the morphology of Au deposits on the semiconductor NPs, either in the form of dots on the vertices or in the form of a shell around the NP surface, can be determined by controlling the oxidation state of the metal precursor. Furthermore, X-ray photoelectron spectroscopy has been applied to show that the resultant deposits are composed of partially oxidized Au, corresponding to a Au-Se compound regardless the deposit morphology. To obtain a detailed characterization of the HNPs with different morphologies and to gain mechanistic insights into the deposition process, (cryogenic) high-resolution transmission electron microscopy, mass spectrometry, cyclic voltammetry, and computational simulations have been performed. These results emphasize that the knowledge of the surface chemistry of the seed particles as well as a defined picture of the metal precursors is necessary to understand heterodeposition processes.

5. Precursor Controlled Morphology of Au-Se Deposits on CdSe Nanoparticles (NPs)

5. 2. Introduction

The small dimensions and the high chemical reactivity of nanoparticles (NPs) have opened the door to a whole universe of new material combinations, compositions, and architectures. The growth of multidomain semiconductor-metal hybrid nanoparticles (HNPs) by colloidal seeded growth techniques (consisting essentially of the reduction of a metal complex on the surface of semiconductor NPs used as a seeds) has attracted particular interest.[1–4] By taking advantage of the different surface chemistries of the two components, metallic domains can act as anchor points for biofunctionalization or help to direct the self-assembly of the HNPs.[5,6] With respect to the physical properties, the growth of Au or Pt metallic contacts on individual semiconducting CdSe NPs increases their conductance and enables charge separation of generated electron-hole pairs, finding applications in photocatalysis and hydrogen generation.[7–14] The reduction process of the metal precursor depends on the surface chemistry of the semiconductor seeds, including for example the presence of polar or nonpolar facets, the type of atoms, dangling bonds, etc.[15,16] Besides, the interaction of the precursor with ligands having different length and ligand density on a particular facet and, especially, the oxidation state of the precursor and its concentration play important roles.[17,18] In general, the reduction of metal complexes in organic media results in elemental metal deposits, as in the case of phosphonic acid-capped CdSe, which are held responsible for increasing the electrical conductivity in the final HNPs.[19] In most cases the metallic deposits grow exclusively in the form of spherical dots, on the tips, apexes, or defects on the different NP facets.[6,15,20] While a commonly applied strategy involving a mixture of $AuCl_3$, a complex agent in the form of alkylammonium bromides and alkylamines as mild reducing agent frequently results in dumbbell or matchstick-like morphologies with CdSe (or CdS) nanorods as the center domain,[6,20] a distinctly different behavior was observed with hexagonal pyramidal CdSe NPs.[17] Instead of well-defined and stable spherical Au domains, a shell-like structure that evolved into irregular Au dots upon exposure to the electron beam during transmission electron microscopy (TEM) inspections was observed. The possibility to precisely adjust the final morphology of the Au domain (either shell or dots) by selectively adding strong reducing agents to the reaction solution suggested that the change of the HNP morphology during TEM inspection was due to an observer problem the interaction with the electron beam, ultimately modifying its oxidation state.[30, 44–46]

5. Precursor Controlled Morphology of Au-Se Deposits on CdSe Nanoparticles (NPs)

In this chapter it has been demonstrated that the question of whether dots or a shell are formed during Au deposition not only is grounded on an observer effect or postsynthetic reduction. By slightly varying the synthetic protocol, in particular the oxidation state of the Au precursor, it is possible to control the morphology of the Au deposits in HNPs. On the seed side, the particular morphology and surface chemistry of pyramidal wurtzite CdSe NPs also comes into play. As has been showed in Chapter 3, rod-like CdSe NPs are capped by a high density of long-alkyl chain phosphonates ($ODPA^{2-}$) and ODPA anhydrides molecules while pyramidal shaped NPs synthesized in the presence of chlorinated co-solvents are capped by a mixed ligand sphere with a relatively low density of phosphonates ($ODPA^{2-}$) molecules and chloride ions.[21-26] Furthermore, {101} planes terminated either by Cd or Se are favored.[24] The aim of this chapter is to understand the mechanistic aspects of Au deposition and to identify differences in the nature of the Au deposits, which has been found not to be elemental Au but Au in a higher oxidation state. To this aim, the role of all reactants has been investigated and a comprehensive combination of analytical tools such as (cryogenic) high-resolution electron microscopy (HR-TEM), X-ray photoelectron spectroscopy (XPS), mass spectrometry (MS), X-ray diffraction (XRD), cyclic voltammetry (CV), and computational modelling have been applied.

5. 3. Synthesis of different Au-CdSe HNPs

5. 3. 1. Synthesis of pyramidal CdSe seed NPs

The synthesis of these HNPs were performed by our collaborator Mychaela Meyns, at the University of Hamburg. CdSe NPs synthesis was performed following the methodology described for pyramidal shaped NPs in section 3.3 in Chapter 3 with slight variations. In this case 1-chlorooctadecane (ODC) is used as halogenated source. The reason is that due to its high boiling point (330 °C; 760 mmHg) it is not necessary to decrease the temperature to 80 °C to inject it. Once the $Cd(ODPA)_2$ complex was formed the temperature was set to 265 °C and 43 µL (0.13 mmol) of ODC were injected. After 25 min, 0.43 mL (0.4 mmol) of 1 M TOPSe solution were injected before reducing the temperature to 255 °C for NPs growth and the reaction was continued as described in the case of pyramidal CdSe NPs in Chapter 3.

5. 3. 2. Preparation of Au(III)-Stock Solution

A 4.4 mM Au(III)-stock solution was prepared by mixing gold(III) chloride (20 mg, 66 µmol) and n-dodecyltrimethylammonium bromide (DTAB, 32 mg, 104 µmol) in 15 mL of toluene in a nitrogen atmosphere. After mild sonication and slight warming (heating plate, 50

°C) a clear, orange-red solution was obtained. It was stored in darkness under ambient conditions until further use.

5. 3. 3. Synthesis of Au-CdSe HNPs

We added the Au solutions to CdSe seeds dispersed in 4 mL of toluene with an optical density of 0.27 at the first absorption maximum. Au solutions with different contents of Au were injected under stirring in ambient conditions. For easy comparison, the ratio Au/CdSe was defined as the molar amount (n) of Au in µmol divided by the product of volume CdSe stock solution and the optical density ($V_{CdSe\ solution} \times OD_{CdSe}$) in substitution for the exact molar amount of CdSe. After the reactions, all samples were precipitated by centrifugation (3 min, 7000 rpm), separated from the supernatant, and redispersed in toluene three times. The first time, toluene/ethanol (1:1) was enough to precipitate the particles, and the second and third times methanol had to be used to provoke precipitation.

a) Au-Shell Deposition with Au(III)-Stock Solution. For shell deposition appropriate amounts of Au(III)-stock solution were diluted to 2.0 mL with toluene and added to the CdSe NP dispersion. To obtain a thin Au shell with a Au/CdSe = 2, 474 µL of the Au solution, containing 0.64 mg (2.1 µmol) of $AuCl_3$ and 0.96 mg (3.1 µmol) of DTAB, was injected. A thick Au shell with Au/CdSe = 2.9 was obtained with 684 µL of the Au solution containing 0.91 mg (3.0 µmol) of $AuCl_3$ and 1.5 mg (4.8 µmol) of DTAB. HNPs with a Au shell formed within 10 min and became instable in the solution in toluene. By adding dodecanethiol DDT (at least 18-fold with regard to Au) they can be stabilized again in the same solution and remain dispersible even after purification.

b) Au-Dot Deposition with Au(I)-DDT. To obtain different Au/CdSe ratios the concentration of the Au precursor was adjusted. For an Au/CdSe ratio of 1.3, 4.2 mg (20 µmol) of dodecanethiol and the Au(III)-stock solution containing 0.43 mg (1.4 µmol) of $AuCl_3$ and 0.68 mg (2.2 µmol) of DTAB were mixed with toluene to a total volume of 2.0 mL and shaken for 5 min (no sonication in order to prevent preliminary Au nucleation). After injecting the colorless solution, the reaction was left to stir at room temperature for 1 h.

5. 3. 4. Synthesis of Au nanoparticles

The synthesis of Au dots was done in a similar manner to the Au-dot deposition but without CdSe seeds and adding a reducing agent to favour the Au reduction.[47] In this case, 474 µL of

the Au(III)-stock solution, containing 0.64 mg (2.1 µmol) of $AuCl_3$ and 0.96 mg (3.1 µmol) of DTAB, were diluted to 2.7 mL and 5 mL (20 µmol) of dodecanethiol were added. When the solution turns colourless 3.3 mL of a prepared solution of 10.1 mg (39.3 µmol) tetrabutylammonium borohydride and 14.1 mg (4.57 µmol) DTAB in toluene were injected into the solution to start the Au nucleation.

5. 4. Results and discussion

5. 4. 1. Synthesis and morphological characterization

We followed a seeded-growth approach based on a straight forward method applied to deposit Au on Cd chalcogenides NPs in organic solution.[6] $AuCl_3$ was solubilized with dodecyltrimethylammonium bromide (DTAB) in toluene forming an orange complex (named Au(III)-stock solution in the following).[27] To reduce Au(III) to Au(I) before deposition on the seed NPs, this complex is usually mixed with mild reducing agents such as amines or thiols.[28,29] In this case, an excess of dodecanethiol (DDT) was added to the Au(III)-stock solution. These two solutions, with different oxidation states, namely Au(III)-stock solution and Au(I)−DDT, were employed to examine their effect on the Au deposition onto CdSe pyramidal NPs.

The incubation of CdSe NPs in the Au(III)-stock solution results in the formation of a shell around the whole NP (Figure 5.1(a,b)). The thickness of the shell can be controlled by simply changing the concentration of the Au stock solution (see synthetic details in section 5.3). This shell is similar to that observed in an earlier study, where the formation of a Au shell on hexagonal pyramidal CdSe NPs with Au-DTAB solutions containing amines was reported.[17] Making this shell visible proved intricate, as it was readily destroyed by interaction with the electron beam in the TEM and lasted only for seconds after focusing. In Figure 5.1a the formation of metal deposits with a globular morphology on one or several sides of the seed NP produced by the effect of the beam exposure is shown. Such destructive interactions are known from Au NPs characterization where precursor complexes can be reduced from Au(III) to Au(I) or even Au clusters during inspection.[30] Both electron beams and heat (due to thermal stress) may induce structural rearrangements and even degeneration of the original structure in HNPs of CdSe-Au and CdS-Au. However, by reducing the temperature during inspection (96 K), atomic migration can be slowed down so that high resolution recordings and STEM micrographs of the shell can be obtained, as it is shown in Figure 5.1b. On the contrary, the incubation of CdSe NPs with the Au(I)−DDT precursor solution leads to the formation of dot-

shaped deposits. These deposits, that are stable during TEM inspection, are spherical and differ notably from those evolving from the Au-shell TEM inspection (Figure 5.1c). The TEM images were acquired by Andreas Konowski, from Prof. Horst Weller group at the University of Hamburg.

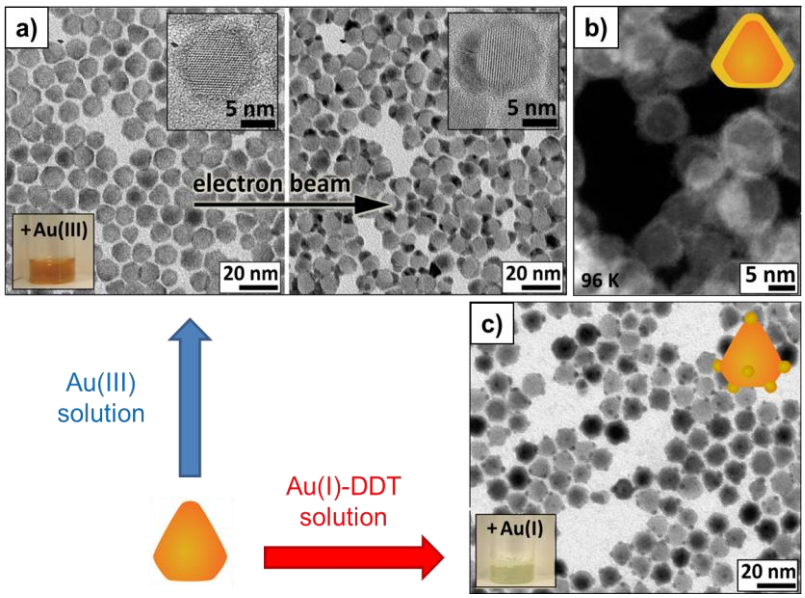

Figure 5.1. *(a) TEM images of pyramidal CdSe NPs incubated with Au(III)-stock solution and taken immediately after focusing (Au/CdSe: 2.8). Within seconds to minutes, depending on the beam intensity and the amount of Au, the interaction with the electron beam induces migration of the Au atoms previously distributed over the surface of CdSe and its merging into Au clusters (200 kV acceleration voltage, 3 min between left and right). The insets show two representative particles at the corresponding stage. (b) At reduced temperature (96 K) the movement of the Au atoms is slowed down, which allows the visualization of the shell-like morphology of the Au deposits in STEM mode. (c) By adding Au(I)–DDT precursor spherical Au deposits are obtained (Au/CdSe: 1.4).*

The size of the initial CdSe NPs is around 12 nm, and it is reduced to approximately 10 nm after the Au(III) deposition process. In the case of the dot-like deposits, this reduction is only around 0.5 nm. We also observe a slight reduction in the Cd content of the samples upon Au deposition, ascertained by EDX analysis (Table 5.1).

Material	Cd (atomic %)	Se (atomic %)	Au (atomic %)
CdSe	47.6	52.4	-
CdSe + dots	40.9	53.6	5.5
CdSe + Au-shell (thin)	35.1	51.2	13.8
CdSe-Au + shell (thick)	30.0	55.8	14.2

Table 5. 1. *EDX analysis of CdSe NPs after Au deposition: etching effect.*

The EDX results show two opposing tendencies: the Cd (atomic %) content decreases whereas the Au (atomic %) content increases as the NPs are incubated with Au, leaving the Se content practically constant. Mechanistically, the final size of the resultant particle is determined by two competing processes, namely, the growth of the Au deposit in the form of dots or a shell and an etching of the CdSe NPs, an effect also observed previously.[9] This etching effect might be caused by bromide or chloride ions released from the precursors (DTAB and $AuCl_3$),[31] which would react with the Cd surface atoms, leaving free Se sites behind to interact with the Au cations.

5. 4. 1. XPS surface characterization of the different Au-CdSe HNPs

In order to account for differences in the CdSe NPs upon Au deposition, XPS analyses have been carried out. Figure 5.2 shows the XPS analysis (C *1s*, Cd *3d*, and Se *3d* regions) performed on plain pyramidal CdSe NPs (first row), CdSe NPs exhibiting dot-shaped deposits (second row), and NPs with a thin (Au/CdSe: 2.0, see section 5.3) and a thick Au shell (Au/CdSe: 2.9) (third and fourth row, respectively). As it can be seen, in all C *1s* spectra (Figures 5.2(a-d)) there is one signal at 284.5 eV, corresponding to the Csp^2 contribution of the HOPG substrate, which has been used as a reference for binding energy calibration. For pure CdSe NPs (Figure 5.2a) the C *1s* signal shows another well-defined contribution, centered at 285.3 eV, corresponding to the long alkyl chains of the initial ligands. This Csp^3 contribution decreases dramatically for every hybrid system regardless the morphology of the Au deposits (either dots or shell), indicating a partial or total displacement of phosphonic ligands upon Au growth.

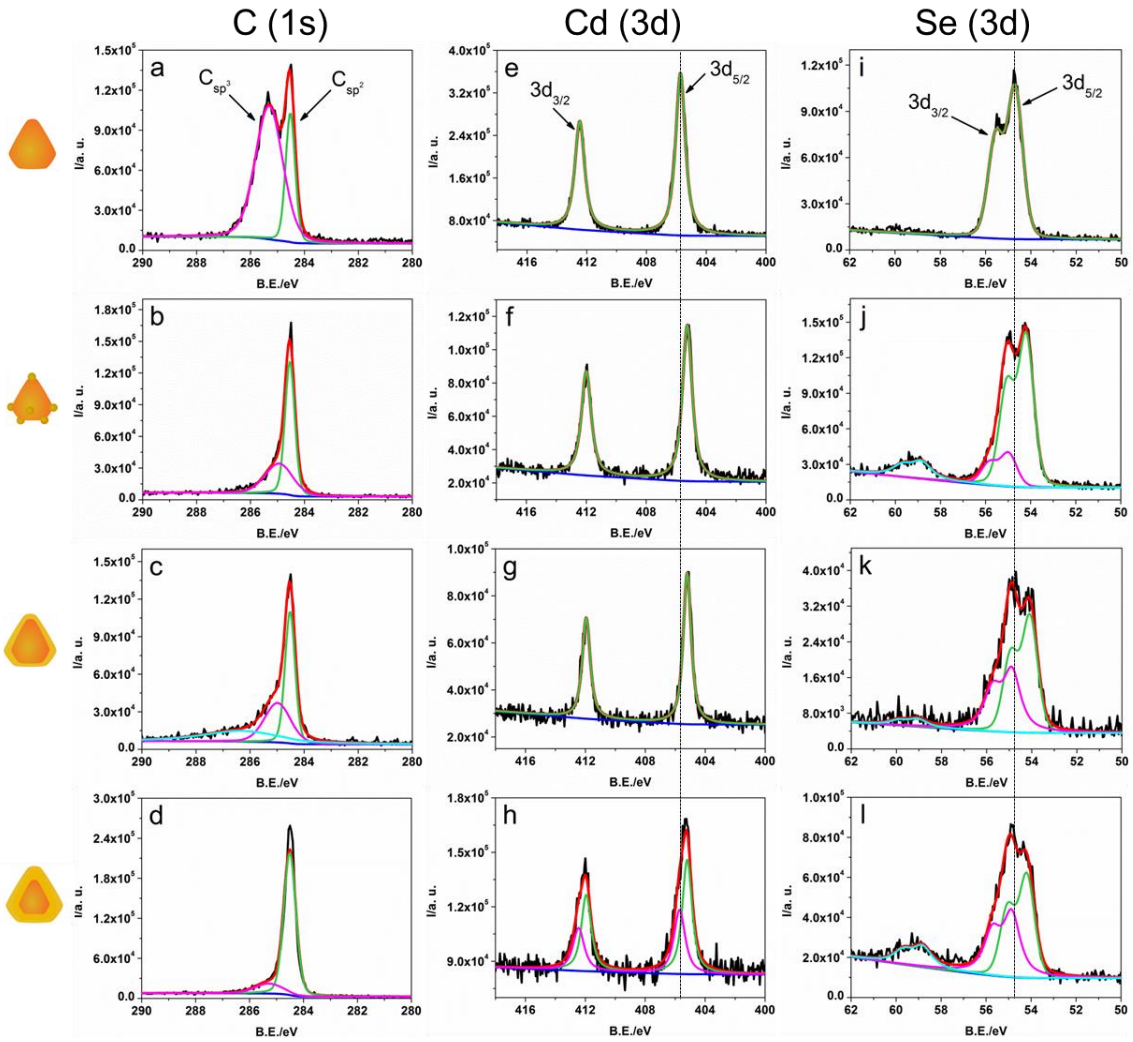

Figure 5.2. *XPS spectral regions of C 1s, Cd 3d, and Se 3d for pure CdSe NPs (first row), CdSe NPs with spherical gold deposits (second row), and CdSe NPs covered with a thin gold shell (third row) and with a thicker Au shell (fourth row).*

The second column of Figure 5.2 shows the Cd *3d* spectra (e-h). Two peaks can be observed in these spectra due to the spin-orbit splitting, Cd $3d_{5/2}$ and Cd $3d_{3/2}$, at 405.7 and 412.5 eV, respectively, related to Cd in CdSe. As it can be seen in spectra f, g, and h, the core Cd *3d* signals are shifted to smaller binding energies (405.2 and 412.0 eV) for the Cd $3d_{5/2}$ and Cd $3d_{3/2}$, respectively) upon Au growth. Similar effects have been observed in PbSe nanocrystal thin films upon ligand removal and have been attributed to the modification of the electronic density and, hence, of the local dielectric constant.[32] This interpretation is in good agreement with the elimination of the alkyl chains contribution evidenced by the C *1s* core level analysis. An alternative explanation could be the changes in the oxidation state (or in the chemical environments) of Cd and Se atoms,[19] due to the formation of Au-Se bonds. In the case of the

HNPs with the thickest shell (2 h), the Cd *3d* spectrum shows an additional oxidized component centered at higher binding energy (for a better display the comparison between the raw and fitted data is depicted in Figure 5.3).

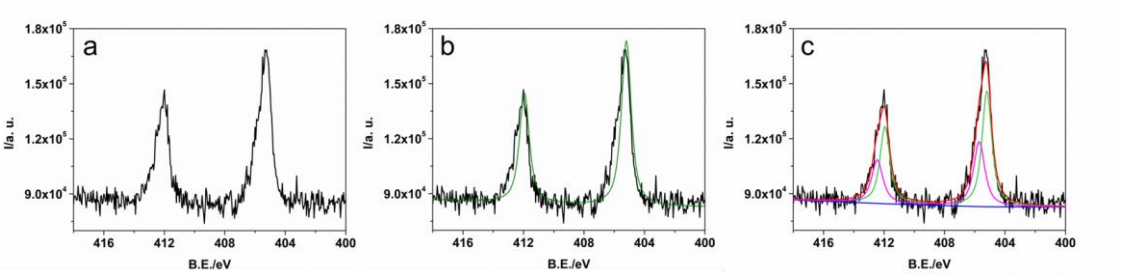

Figure 5.3. *XPS raw data before fitting (a), fitting with one component (b) and fitting with two components (c) of the Cd 3d region of the HNPs covered with a thick Au shell.*

Rather than considering this component as new, it is understood as a change in the electronic density due to unbounded Cd atoms. The absence of Cd oxidized components for CdSe covered by dotted Au (2f) and thin Au shell (2g) might be the result of sensitivity limitations. In the third column of Figure 5.2 the spectra of the Se *3d* peak are represented (i-l). This peak is also composed of two contributions (Se $3d_{5/2}$ and $3d_{3/2}$) due to the spin-orbit coupling.

In the case of pyramidal CdSe NPs, the Se $3d_{5/2}$ is localized at 54.7 eV and is related to the Se^{2-} contribution of bulk CdSe.[33] Upon Au growth, two different changes in the Se peaks can be observed: The first one corresponds to a shift to lower binding energy values (from 54.7 to 54.2 eV), as previously described for the Cd signal and probably also related to the removal of ligands. The second change consists on the appearance of a new contribution at higher binding energy (54.9 eV) assigned to the oxidized Se sites involved in the Au(III) reduction to form Au-Se bonds. A similar Se binding energy (around 55.2 eV) assigned to covalent Au-Se bonds for Au NPs stabilized with alkaneselenate ligands has been previously recorded.[34] While the new Se contribution is visible for the three Au-CdSe hybrid systems at the same binding energy, higher intensity is recorded for NPs covered by a gold shell, indicating a higher oxidized surface in this case. Furthermore, an oxidized Se contribution appears at 58.8 eV in the spectra of every hybrid system resulting from unavoidable environmental oxidation during sample preparation and insertion in the XPS chamber.[35]

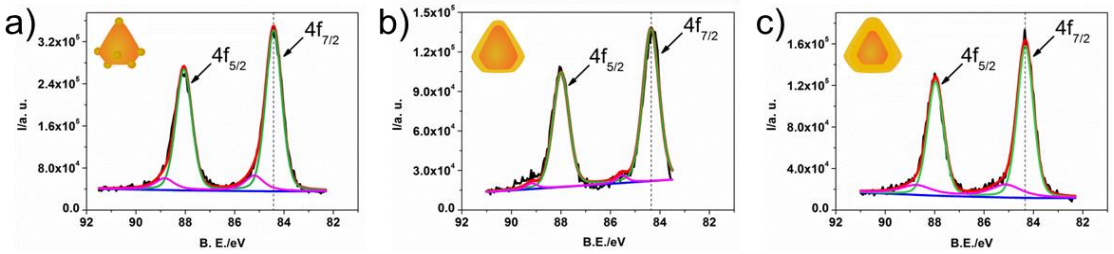

Figure 5.4. *XPS spectra of Au 4f for CdSe NPs with spherical Au deposits (a) and CdSe NPs covered with a thin Au shell (b) and with a thicker Au shell (c).*

To account for differences in the Au deposits, Au *4f* signals were also recorded and are shown in Figure 5.4 Au *4f* signals are composed of two contributions, corresponding to the Au $4f_{7/2}$ and $4f_{5/2}$ energy levels at 84.4 and 88.0 eV, respectively. Interestingly, since the binding energy of metallic Au is 84.0 eV, this data indicates that Au deposits must not be in elemental form but in a higher oxidation state, such as that reported for Au-Se bonds.[34]

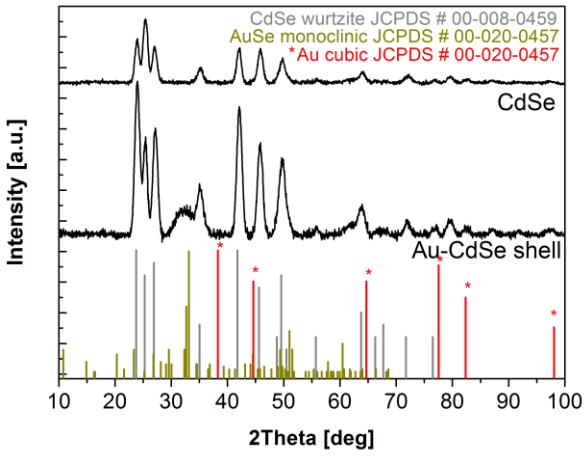

Figure 5.5. *The XRD of plain CdSe and HNPs with the thickest shell deposit are compared with wurtzite CdSe, AuSe and Au. The diffractogram of HNPs with the thickest Au shell does not contain reflexes of elemental gold deposits. Instead, a broad peak can be found centered at 2ϑ = 33°, at the position of the most prominent reflex of monoclinic AuSe. For CdSe NPs covered with thin shell or dotted deposits, no difference in the XRD pattern was recorded. This might be due to sensitivity limitations related to their small size/thickness. The appearance of this new phase of Au-Se in the XRD patterns along with the Au* $4f_{7/2}$ *binding energy evidences that the gold is not in elemental form.*

Furthermore, as it can be seen in Figure 5.4, for all CdSe-Au HNPs an extra component at higher binding energies is observed. This small contribution has a binding energy of 84.9 eV for

the CdSe NPs decorated with Au dots and 85.5 and 85.1 eV for the NPs covered with a thinner and thicker Au shell, respectively. Rather than assigning these higher binding energy components to an extra higher oxidation state of Au, this component is understood as the contributions of Au surface atoms with different environments. The presence of a Au-Se bond (and not metallic Au(0)) is also supported by the X-ray diffractograms shown in Figure 5.5.

Thus, if the final composition of the Au deposits is similar regardless the oxidation state of the precursor, the question that arises is why they grow as dots or as a shell. To obtain more information and clear this question up the different precursor solutions, HNPs and deposition processes have been studied by several methods.

5. 4. 2. Precursor solutions characterization by Mass Spectrometry and Cyclic Voltammetry

Despite the common notion that DDT reduces Au(III) in halide complexes, we intended to obtain a detailed characterization of the two gold precursor solutions. To this aim we have performed mass analysis and cyclic voltammetry. Figure 5.6(a,b) corresponds to the positive and negative ion parts of the mass spectra of the complex formed from $AuCl_3$ and DTAB (Au(III)-stock solution) and Figure 5.6(c,d) to those of the compound formed by adding DDT to this complex (Au(I)-DDT). The m/z values can be also found in Table 5.2.

Au(III)	Structure	$[AuBr_4]^-$	$[AuClBr_3]^-$	$[AuCl_2Br_2]^-$	$[AuCl_3Br]^-$	$[AuCl_4]^-$	$AuBr_2^{2\bullet}$	$AuClBr^{2\bullet}$	$AuCl_2^{2\bullet}$
	m/z	514.66	468.72	424.76	380.81	354.82	336.86	310.85	266.92
Au(I)	Structure	$C_{12}H_{25}S^\bullet$	$[FeCl_3Br]^-$	$[FeClBr_2]^-$	$[FeCl_2Br_2]^-$				
	m/z	201.17	241.76	250.73	285.70				

Table 5.2. *Parameters of the peaks found in the negative-ion mode of the Au precursor solutions used in the synthesis of HNPs with a shell deposit (Au(III)-stock solution) and with dots deposits on the corners (Au(I)-DDT precursor solution).*

The mass analysis of the positive-ion mode of the spectra (Figure 5.6(a,c)) exhibits a similar and intense peak at m/z: 228.2, which can be assigned to the alkylammonium cation ($[CH_3(CH_2)_{11}N(CH_3)_3]^+$) in both complexes. However, very different spectra are acquired in the negative-ion mode. In Figure 5.7b the molecular ion peaks of every possible combination of Au with halides complexes ($AuCl_xBr_{4-x}^-$) is evidenced, confirming that the oxidation state of Au is Au(III) (see peak details in Table 5.2).

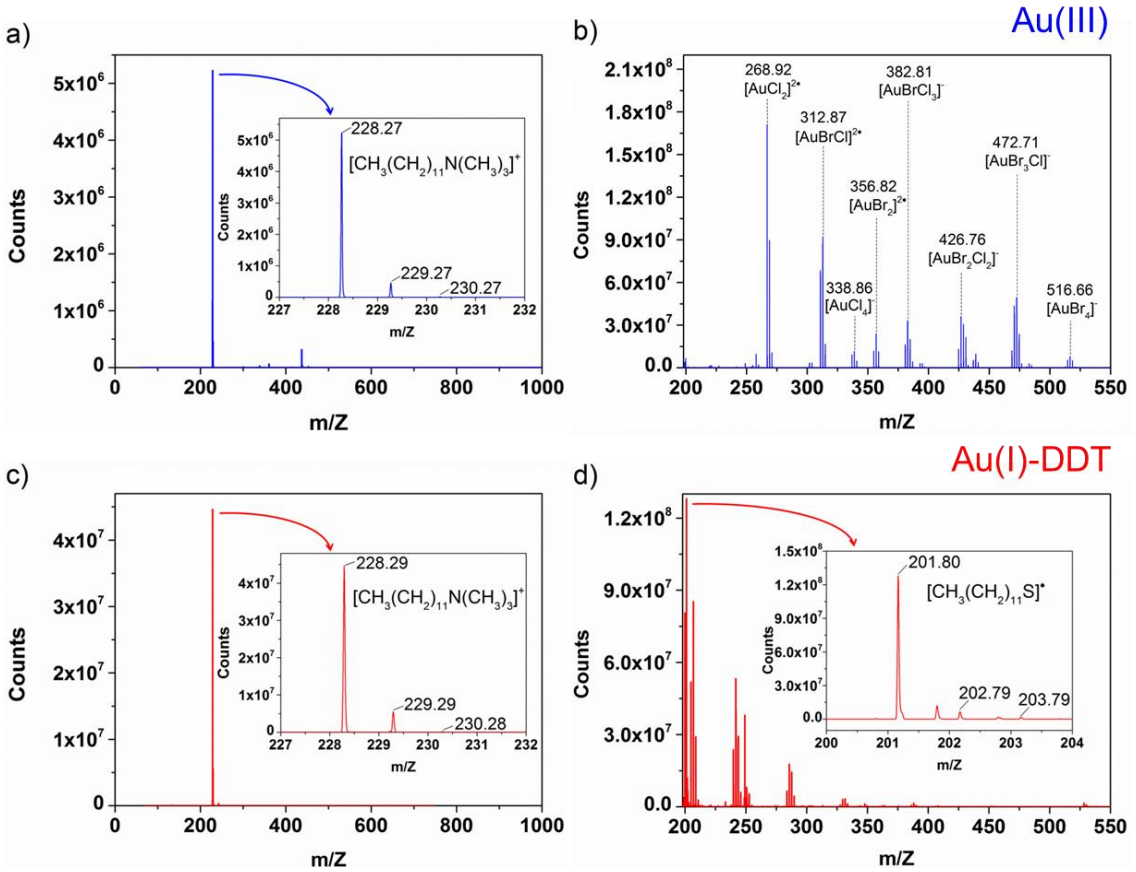

Figure 5.6. *Mass spectra of the Au precursors used to form shell (Au(III)-stock solution, $AuCl_3$ + DTAB; up, blue) or dot-like deposits (Au(I)-DDT precursor solution, $AuCl_3$ + DTAB + DDT; down, red) on CdSe NPs. (a) and (c) correspond to the positive-ion mode and (b) and (d) to the negative-ion mode of the mass spectra.*

After addition of DDT (Figure 5.6d), the molecular ion peaks related to the $[AuCl_xBr_{4-x}]^-$ complexes are not detected, and a new peak corresponding to the radical breakup of DDT at m/z=201.1 can be found (Table 5.2). This result points to the reduction of Au(III) to Au(I) in which the thiol group of the DDT acts as reducing agent. Thus, the MS results support that the oxidation state of the Au precursors differs.

According to these MS results we propose the following reactions to form the Au(III)-stock solution (1) and Au(I)-DDT precursor solution (2), according to Scheme 5.1.

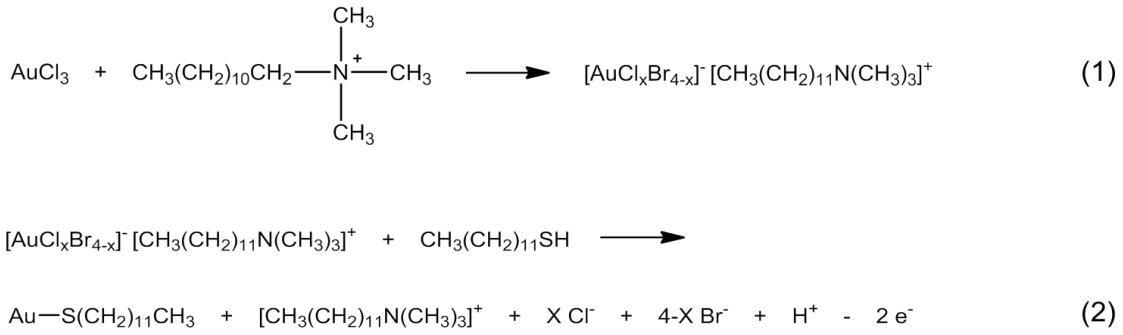

Scheme 5.1. *Reactions for Au(III)-Stock Solution (1) and Au(I)-DDT (2).*

In order to further verify the different oxidation states of the Au precursors and test their electrochemical response, cyclic voltammetry (CV) was applied. Figure 5.7(a,b) shows the obtained voltammograms of the pure Au(III)-stock solution and the Au(I)-DDT precursor solution, respectively. For the former (Figure 5.7a), the first reduction peak at -0.1 V corresponds to the Au(III) to Au(I) reduction process and the second reduction peak at -1.1 V corresponds to Au(0) metallic deposit formed by the reduction of Au(I) to Au(0).

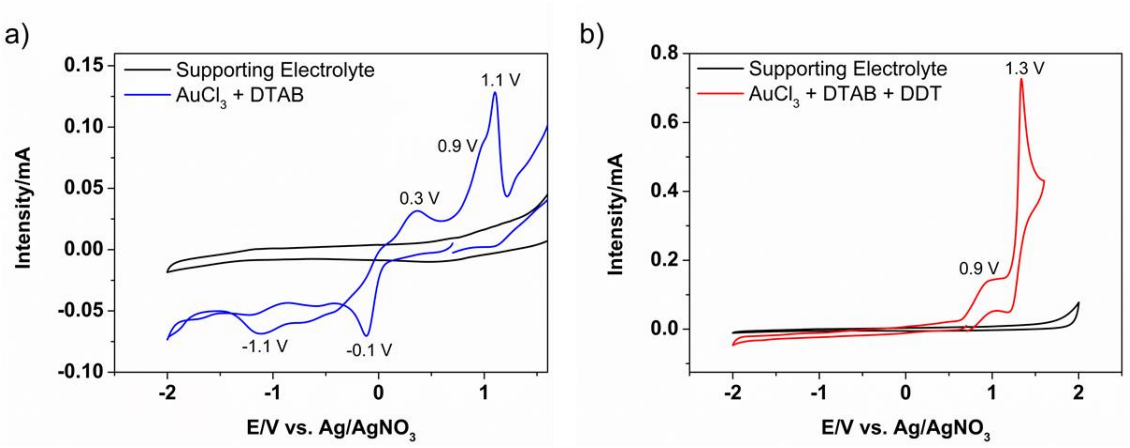

Figure 5.7. *Cyclic voltammograms of (a) Au(III)-stock solution ($AuCl_3$ and DTAB) and (b) Au(I) solution formed by adding DDT to the previous Au(III)-stock solution. Electrolyte solution: 0.1 M TBAP in acetonitrile; v = 0.1 Vs^{-1}.*

Scanning further, the oxidation of halides (Cl^- and Br^-) over the Au metallic deposit (peaks at 0.3 and 0.9 V) and over the glassy-carbon electrode at more anodic potentials (around 1.1 V) can be clearly identified.[36-40] However, in the voltammogram obtained with the precursor solution used to grow dots, Au(I)-DDT (Figure 5.7b), no reduction process can be recorded, which supports the absence of Au(III) and the high stability of the Au-S bond in the compound (no reduction of Au(I) to Au(0) is recorded).

These characterizations of the precursor solutions show that the main difference in the incubation reactions must be related with the oxidation state of Au. The addition of DDT to the Au precursor solution reduces Au(III) to Au(I) changing the deposition mechanism and the final morphology of the deposits.

5. 4. 3. Electrochemical characterization Au-CdSe HNPs

In order to evaluate differences in the Au-CdSe HNPs with dots or shell, they have also been characterized by CV and compared with both pure CdSe and pure Au NPs (prepared from the Au(III) stock solution by reduction with tetrabutylammonium borohydride, see section 5.3). Figure 5.8 shows the voltammograms of pyramidal CdSe NPs (a), NPs with Au-Se dot-like deposits (b), with a thin Au-Se shell deposit (c) and the voltammogram of pure Au dots (d). For the plain CdSe pyramidal NPs, a first cathodic scan does not show any charge transfer process. This is in good agreement to the previous results described in Chapter 4 which showed that the cathodic response in the voltammogram is exclusively related to the reduction of previously oxidized species.[35] However, the anodic part of the voltammogram exhibits two well-defined peaks at 1.2 and 1.5 V, which correspond to the Se oxidation and might be related to different atomic chemical environments or Se atoms located in different NPs facets.[35] When Au is added to the CdSe seed NPs, regardless the morphology of Au deposits, the oxidation onset is shifted from 1.0 V to less anodic potentials (to ∼0.6 V, blue arrow in Figure 5.8(b,c)) with respect to bare CdSe NPs (blue arrow in Figure 5.8a). In the voltammogram of Au NPs (Figure 5.8d) we can observe the oxidation of Au at those potentials (∼0.6 V). Thus, the shift of the oxidation onset for the HNPs may be due to Au oxidation. We can also observe that the peaks attributed to the Se oxidation (initially at 1.2 and 1.5 V) are shifted to more anodic potentials for every HNPs system (see dotted arrows from part a to part c of Figure 5.8). This fact is only the consequence of the higher overpotential required to oxidize Se in the presence of Au. Interestingly, the oxidation charges for the HNPs are lower than the oxidation charge of CdSe NPs in the absence of Au. The voltammetric charge is 5356.12 μC for the pure CdSe seed NPs, 4423.47 μC for the CdSe NPs with deposited Au dot, and 3535.71 μC for CdSe NPs covered by an Au shell, which means that the charge decreases by 17% for the HNPs with Au-Se dots and by 34% for the HNPs with a Au-Se shell.

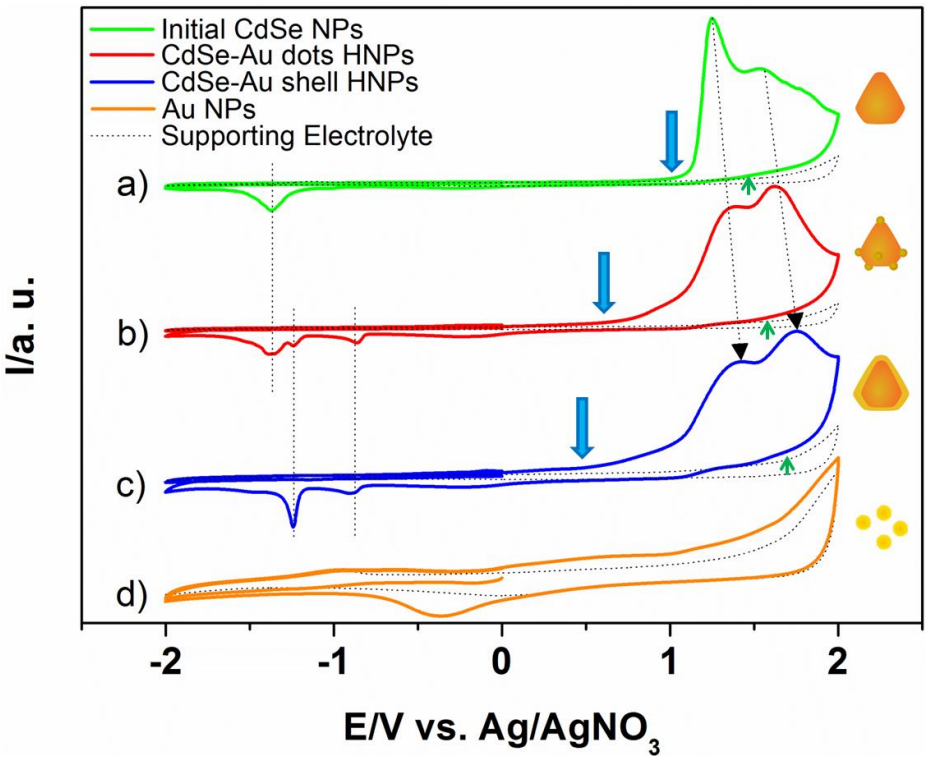

Figure 5.8. *Cyclic voltammograms of seed pyramidal CdSe NPs (a), CdSe HNPs decorated with dot-like deposits on the vertices of the pyramids (b), CdSe HNPs covered by a shell deposit (c), and Au NPs (d) deposited on a glassy carbon electrode. Electrolyte solution: 0.1 M TBAP in acetonitrile; v = 0.1 Vs^{-1}. Dotted black arrows mark the shifts in the oxidation peaks. Blue arrows point out the differences in the oxidation onset. Green arrows designate the Se oxidation current obtained during the cathodic scan.*

Since all voltammograms were recorded for the same NP concentration, the oxidation charges can be directly compared. Remarkably enough, in the Se *3d* spectra previously shown (Figure 5.2(j,k)), the area corresponding to the oxidized $Se_{Au\text{-}Se}$ component in the HNPs with Au-Se dots and Au-Se thin shell is 18% and 40% of the total Se area of that of the HNPs, respectively. These values are in good agreement with the decrease of charge in the corresponding voltammograms mentioned previously. This indicates that during an anodic scan only those Se atoms bonded to Cd can be oxidized, since Se in the Au-Se deposits is already oxidized. In fact, if the Au-Se was oxidized during the anodic scan, the total voltammetric charge of CdSe NPs covered by a thin Au-Se shell would increase compared to CdSe NPs with Au-Se dots and the latter compared to the bare CdSe NPs. On the other hand, it must be taken into account that Au atoms of the deposits are susceptible to be oxidized. If that would be the case, the oxidation charge should increase with increasing Au concentration from pure CdSe NPs, to HNPs covered with dots or shell deposits, in contrast to the obtained results. For these reasons

it can be concluded that Au atoms in Au-Se deposits are very stable, i.e., are not oxidized in the applied potential range, and only unbounded Au could be oxidized, its charge contribution being negligible as indicated by the reduction charge. In the cathodic scan from +2 V to the negative direction, an oxidation current (indicated with green arrows in Figure 5.8) was observed at anodic potentials around 1.5 V. In HNPs this current is the balance of two different redox processes that take place simultaneously, namely, the oxidation of Se of CdSe NPs and the partial reduction of Au (Au oxides) at the expense of the Se oxidation. This process produces a shift to less cathodic potentials for the reduction of Au oxides, as confirmed in Figure 5.9. Notably there is no evidence of adsorption/desorption of thiols in the cathodic scan of HNPs which is further supported by the voltammogram of Au dots in which we only observed the reduction of Au oxides (Figure 5.8d).[41]

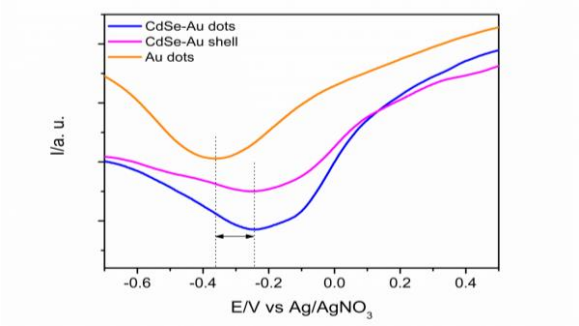

Figure 5.9. *Reduction of Au oxides of Au dots (orange line), CdSe NPs with dots deposits (blue line) and CdSe NPs covered with a thin shell deposit (magenta). Electrolyte solution: 0.1 M TBAP in acetonitrile; v = 0.1 Vs^{-1}.*

For negative potentials, both pure CdSe NPs and HNPs show a reduction peak centered at -1.37 V whose intensity decreases from pure CdSe NPs to HNPs with Au-Se dots and practically vanishes for HNPs with an Au-Se shell. This peak can be attributed to the simple reduction of oxidized Se species formed in the previous anodic scan. Moreover, an extra reduction peak at -1.2 V appears for HNPs whose contribution becomes higher as the amount of Au increases (from dots to shell deposits). To understand the presence of this peak, the reduction of the Au(III)-stock solution shown in Figure 5.7a should be taken into account. As previously shown, the reduction takes place in different steps. First Au(III) is reduced to Au(I) and finally to Au(0) in a further step. The reduction peak at -1.1 V corresponds to the mass deposit formed by the reduction of Au(I) to Au(0). These results suggest that the reduction peak at -1.2 V might be related to the reduction of Au(I) atoms that are not bonded to Se.

Gathering the characterization of the precursors with the CdSe HNPs by means of XPS, MS, and electrochemistry, it is clear that the different morphologies of the deposits are not only related to the different oxidation states of the Au precursor solutions but also the surface composition of the NP play an important role, driving the final morphology of the deposits and their final oxidation state. For this reason the deposition mechanisms of Au on CdSe NPs taking into account all these factors has been studied by molecular dynamics simulations.

5. 4. 4. Molecular dynamics simulations of the different deposition processes

In the literature, the very first step of the deposition process of the metal on the NP surface is a matter of discussion. Some authors argue that crystalline metal domains form after precursor molecules adsorb on the surface and are reduced by anions on the seed.[9, 42] Others assume an attachment and growth of metal clusters formed in solution by reduction with added amines or other mild reducing agents.[1, 3] In order to understand the possible deposition mechanism and the formation of dots or a shell, molecular dynamics simulations were carried out by our colleague, Prof. Christian Klinke, from the University of Hamburg. They have been performed considering (i) a noncapped CdSe NPs surface and (ii) CdSe with preadsorbed Cl on the surface, to simulate a closest scenario of the pyramidal NPs surface, according to the previous results.[25, 26] Figure 5.10 shows the simulations for CdSe NPs incubated with the Au(III)-stock solution, whose ionic form corresponds to the complex $[AuCl_xBr_{4-x}]^-$ $[CH_3(CH_2)_{11}N(CH_3)_3]^+$. Figure 5.10(a,b) correspond to the plain non-capped CdSe NPs and Figure 5.11(c,d) to CdSe NPs capped with Cl. For charge and spin neutrality two Cl atoms on opposite sides of the NP have been simulated, although only one is visible in the images. The simulations show several differences. In the case of non-capped NPs the Cl atom of the complex interacts first electrostatically with the surface (Figure 5.10a, after 1 ps). We hypothesize that this first interaction (involving Cl^- and Br^- anions reacting with the surface) may cause the release of surface atoms, which would explain the decrease in the Cd content (proven by EDX) and the related etching effect (see Figure 5.1). After 10 ps (Figure 5.10b) the complex fully decomposes, releasing the alkylammonium cation ($[CH_3(CH_2)_{11}N(CH_3)_3]^+$). At the same time, Au gets adsorbed on the NP surface, and the initial Au(III) is reduced at the expense of Se^{2-}. The picture differs substantially when CdSe NPs are capped with Cl anions (Figure 5.10(c,d)): in this case, the electrostatic repulsion of the complex approaching the Cl capped surface slows down the interaction with the CdSe surface, hindering the decomposition of the complex at a similar time.

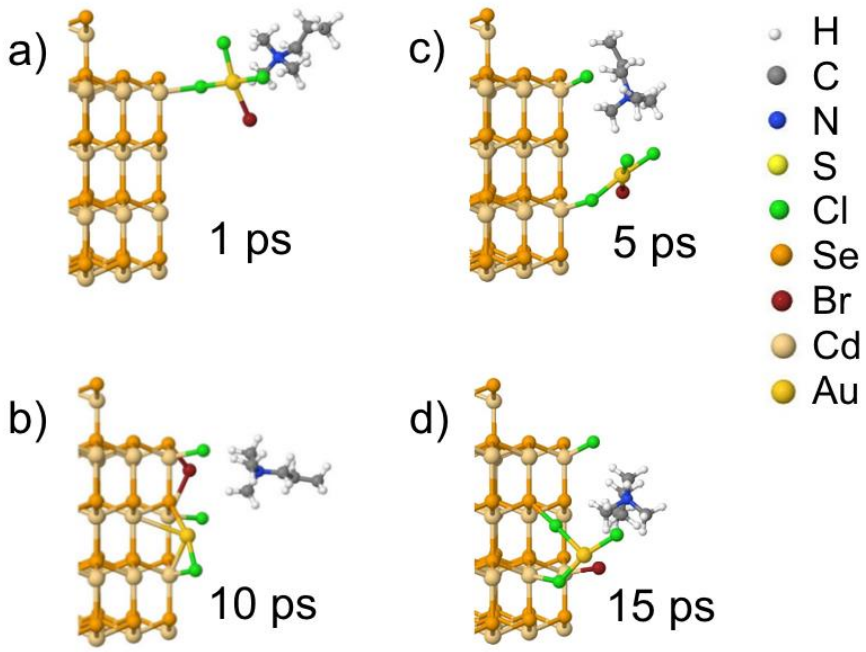

Figure 5.10. *Molecular dynamic simulations of non-capped CdSe NPs (a, b) and Cl-capped CdSe (c, d) incubated with Au(III)-stock solution at 300 K.*

For this reason Figures 5.10(c,d) depict the molecular dynamics after 5 and 15 ps, respectively, where the final configuration shows Au interacting with the NP surface mediated by Cl atoms from the complex. Although a simplification, this simulation confirms that the reduction of the Au precursor on the NP surface takes place in a different way depending on the surface constitution. For non-capped CdSe NCs, further Au(0) would nucleate on the Au-Se interface, while in the case of Cl-capped CdSe NCs, the first interaction is mediated by Cl and further nucleation (not shown) follows a similar behavior, where Cl is always involved in the reaction between Au and Se surface atoms. This result is in good agreement with the formation of a Au-Se compound with a possible SeClAu composition.

To explain the formation of dots, the simulation was performed with $AuS(CH_2)_2CH_3$ as precursor solution instead of the longer DDT, to reduce the simulation time (Figure 5.11). After 1 ps the simulations show that for non-capped CdSe NPs (Figure 5.11(a,b)) Au interacts first with Se. In contrast, for NPs capped with Cl (Figure 5.11(c,d)), the Au(I) precursor interacts with that Cl. In both cases, the interaction takes place with atoms on the vertices, contrary to the preceding case where those sites were not favorable for the complex. After 10 ps (Figure 5.11d), the final configurations show that for Cl capped NPs Cl is involved in the interaction between the Au(I) precursor and the surface. In both cases the Au(I) precursor does not

decompose but gets absorbed on the NP surface. As previously mentioned, in this case the CdSe NPs also reduce their initial size. This etching effect might be related in this case to halogens and/or halides free in solution produced as byproducts when the Au(III)-stock solution is reduced to Au(I) by the presence of the thiol (DDT) (see equation 2 in Scheme 5.1). As in the former case, these different interactions may account for the absence of elemental Au on the surface of pyramidal CdSe capped with chloride anions, as confirmed by XPS.

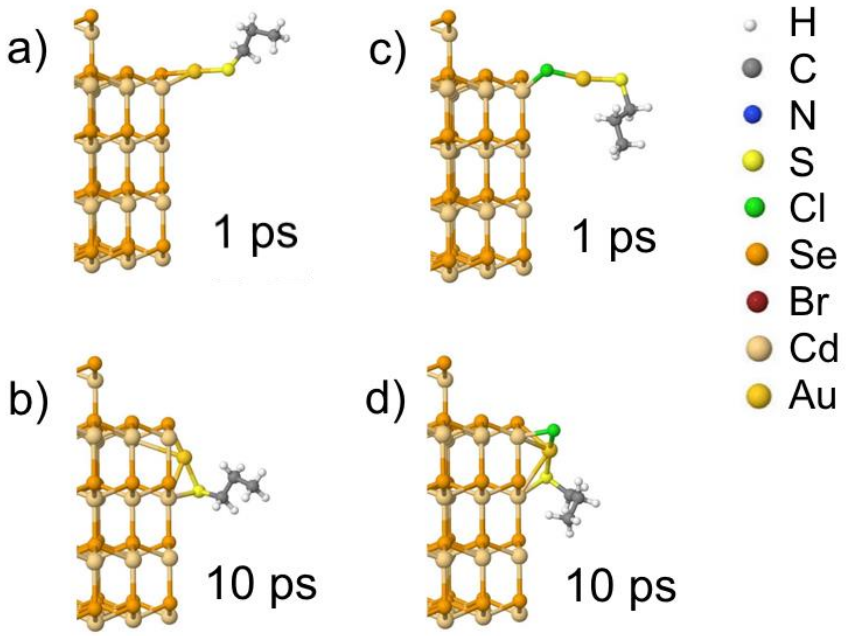

Figure 5.11. *Molecular dynamic simulations of noncapped CdSe NPs (a, b) and Cl-capped CdSe (c, d) incubated with Au(I)−DDT precursor solution at 300 K.*

Assuming the limitations of the simulations, which are performed considering perfect and stoichiometric crystals in vacuum, these results along with the HRTEM, XPS, and CV characterizations provide an accurate picture of the deposition process as well as a comprehensive understanding of the final composition and morphology of the deposits. We believe that this type of study is necessary to correlate potential synergetic properties (for example, conductivity or reactivity) obtained from the combination of materials in hybrid structures.

5. 5. Conclusions

In this work, metal-semiconductor hybrid nanoparticles (HNPs) containing Au and CdSe were characterized by HRTEM (including low temperature STEM), XPS, MS, cyclic voltammetry, and molecular dynamics simulations. Differences in the reactivity of the distinct Au oxidation states of Au precursor solutions induce preferential deposition of dot-like deposits on the vertices of the CdSe seeds or a shell covering the whole NP surface. Evidenced by XPS and supported by molecular dynamics simulations, the Au deposits are not elemental, but most probably AuSe or AuSeCl. Such a composition may explain the instability of deposited Au shells and their transformation into dot-shaped deposits under the e-beam. The incomplete reduction of Au is driven by the surface chemistry of the CdSe seeds, which is composed of both phosphonates ($ODPA^{2-}$) and chloride ligands. The results show that the deposition mechanism as well as the final morphology and composition of the deposits depend on two important factors: (i) the oxidation state of the Au precursor and (ii) the surface chemistry. Both are essential issues to address in order to understand the deposition process and the key factors determining the evolving interface and related properties in a heterodeposition process. Such knowledge is not only valuable in regard to the formation and stability of hybrid nanostructures but also with respect to the fabrication of other heterostructures applied, for example, in catalytic processes.

5. 6. References

1. J. Zeng, J. Huang, C. Liu, C. H. Wu,Y. Lin, X. Wang, S. Zhang, J. Hou, Y. Xia, *Advanced Materials,* **2010,** *22,* 1936-1940.

2. R. Costi, A. E. Saunders , U. Banin, *Angewandte Chemie International Edition,* **2010,** *49,* 4878 - 4897.

3. L. Carbone, P. D. Cozzoli, *Nano Today,* **2010,** *5,* 449-493.

4. U. Banin ,Y. Ben-Shahar, K. Vinokurov, *Chemistry of Materials,* **2014,** *26,* 97-110.

5. A. Salant, E. Amitay-Sadovsky, U. Banin, *Journal of the Americal Chemical Society,* **2006,** *128,* 10006-10007.

6. T. Mokari, E. Rothenberg, I. Popov, R. Costi, U. Banin, *Science,* **2004,** *304,* 1787-1790.

7. M. Meyns, S. Willing, H. Lehmann, C. Klinke, *ACS Nano* **2015,** *9* (6), 6077-6087.

8. A. Vaneski, A. S. Susha, J. Rodríguez-Fernández, M. Berr, F. Jäckel, J. Feldmann, A. L. Rogach, *Advanced Functional Materials,* **2011,** *21,* 1547-1556.

9. R. Costi, A. E. Saunders, E. Elmalem, A. Salant, U. Banin , *Nano Letters,* **2008,** *8* (2), 637-641.

10. F. Schweinberger, M. J. Berr, M. Döblinger, C. Wolff, K. E. Sanwald, A. S. Crampton, C. J. Ridge, F. Jäckel, J. Feldmann, M. Tschurl, U. Heiz, *Journal of the Americal Chemical Society,* **2013,** *135,* 13262-13265.

11. R. Costi, G. Cohen, A. Salant, E. Rabani, U. Banin, *Nano Letters,* **2009,** *9* (5), 2031-2039.

12. L. Amirav, P. A. Alivisatos, *Journal of Physical Chemistry Letters,* **2010,** *1,* 1051-1054.

13. M. J. Berr, F. F. Schweinberger, M. Döblinger, K. E. Sanwald, C. Wolff, J. Breimeier, A. S. Crampton, C. J. Ridge, M. Tschurl, U. Heiz , F. Jäckel, J. Feldmann, *Nano Letters,* **2012,** *12,* 5903-5906.

14. S. Naskar, A. Schlosser, J. F. Miethe, F. Steinbach, A. Feldhoff, N. C. Bigall, *Chemistry of Materials,* **2015,** *27,* 3159-3166.

15. A. E. Saunders, I. Popov, U. Banin, *Journal of Physical Chemistry B,* **2006,** *110,* 25421-25429.

16. L. Carbone , S. Kudera, C. Giannini, G. Ciccarella, R. Cingolani, P. D. Cozzoli, L. Manna, *Journal of Materials Chemistry,* **2006,** *16,* 3952-3956.

17. M. Meyns, N. G. Bastus, Y. Cai, A. Kornowski, B. H. Juárez, H. Weller, C. Klinke, *Journal of Materials Chemistry,* **2010,** *20,* 10602-10605.

18. I. J.-L. Plante, S. E. Habas, B. D. Yuhas, D. J. Gargas, T. Mokari, *Chemistry of Materials,* **2009,** *21,* 3662-3667.

19. M. T. Sheldon, P.-E. Trudeau, T. Mokari, L.-W. Wang, A. P. Alivisatos, *Nano Letters,* **2009,** *9* (11), 3676-3682.

20. T. Mokari, C. G. Sztrum, A. Salant, E. Rabani, U. Banin, *Nature Materials,* **2005,** *4,* 855-863.

21. B. H. Juárez, M. Meyns, A. Chanaewa, Y. Cai, C. Klinke , H. Weller, *Journal of American Chemical Society,* **2008,** *130,* 15282-15284.

22. B. H. Juárez, C. Klinke, A. Kornowski, H. Weller, *Nano Letters,* **2007,** *7* (12), 3564-3568.

23. A. B. Hungría, B. H. Juárez, C. Klinke, H. Weller, P. A. Midgley, *Nano Research,* **2008,** *1,* 89-97.

24. M. Meyns, F. Iacono, C. Palencia, J. Geweke, M. D. Coderch, U. E. A. Fittschen, J. M. Gallego, R. Otero, B. H. Juárez, C. Klinke, *Chemistry of Materials,* **2014,** *26,* 1813-1821.

25. F. Iacono, C. Palencia, L. de la Cueva, M. Meyns, L. Terracciano, A. Vollmer, M. J. de la Mata, C. Klinke, J. M. Gallego, B. H. Juárez, R. Otero, *ACS Nano,* **2013,** *7* (3), 2559-2565.

26. C. Palencia, K. Lauwaet, L. de la Cueva, M. Acebrón, J. J. Conde, M. Meyns, C. Klinke, J. M. Gallego, R. Otero, B. H. Juárez, *Nanoscale,* **2014,** *6,* 6812-6818.

27. R. Puddephatt, *The Chemistry of Gold;* Elsevier: Amsterdam, 1978.

28. J. Yang, Y. Ying, *Nature Materials,* **2009,** *8,* 683-689.

29. Z. Huo, C.-K. Tsung, W. Huang, X. Zhang, P. Yang, *Nano Letters,* **2008,** *8* (7), 2041-2044.

30. J. G. Goulet, A. Leonardi, R. B. Lennox, *Journal of Physical Chemistry C,* **2012,** *116,* 14096-14102.

31. S. J. Lim, W. Kim, S. Jung, J. Seo, S. K. Shin, *Chemistry of Materials,* **2011,** *23,* 5029-5036.

32. L. Rosen, A. M. Sawvel, D. J. Milliron, B. A. Helms, *Chemistry of Materials,* **2014,** *26,* 2214-2217.

33. M. Shenasa, S. Sainkar, D. Lichtman, *Journal of Electron Spectroscopy and Related Phenomena,* **1986,** *40,* 329-337.

34. C. K. Yee, A. Ulman, J. D. Ruiz, A. Parikh, H. White, M. Rafailovich, *Langmuir,* **2003,** *19,* 9450-9458.

35. L. de la Cueva, K. Lauwaet, R. Otero , J. M. Gallego, C. Alonso, B. H. Juárez, *Journal of Physical Chemistry C,* **2014,** *118,* 4998-5004.

36. L. Aldous, D. Silvester, C. Villagrán, W. R. Pitner, R. G. Compton, M. C. Lagunas, C. Hardacre, *New Journal of Chemistry,* **2006,** *30,* 1576-1583.

37. M. Ongaro, A. Gambirasi, M. Favaro, A. Kuhn, P. Ugo, *Electrochimica Acta,* **2014,** *116,* 421- 428.

38. U. Koelle, A. Laguna, *Inorganica Chimica Acta,* **1999,** *290,* 44-50.

39. C. Villagrán, C. E. Banks, C. Hardacre, R. G. Compton, *Analytical Chemistry,* **2004,** *76* (7), 1998-2003.

40. L. M. A. Monzón, F. Byrne, J. M. D. Coey, *Journal of Electroanalytical Chemistry,* **2011,** *657,* 54-60.

41. P. G. Lustemberg, C. Vericat, A. Benitez, E. Vela, N. Tognalli, A. Fainstein, M. L. Martiarena, R. C. Salvarezza, *Journal of Physical Chemistry C,* **2008,** *112,* 11394-11402.

42. C. O´Sullivan, R. D. Gunning, A. Barret, A. Singh, K. M. Ryan, *Journal of Materials Chemistry,* **2010,** *20,* 7875-7880.

43. cp2k.org; J. VandeVondele, M. Krack, F. Mohamed, M. Parrinello, T. Chassaing, J. Hutter, *Computer Physics Communications,* **2005**, *167*, 103-128.

44. A. Halder, N. Ravishankar, *Journal of Physical Chemistry B,* **2006**, *110*, 6595-6600.

45. T. Mokari, R. Costi, C. G. Sztrum, E. Rabani, U. Banin, *Physica Status Solidi B,* **2006**, *15*, 3952-3958.

46. E. Khon, N. N. Hewa-Kasakarage, I. Nemitz, K. Acharya, M. Zamkov, *Chemistry of Materials,* **2010**, *22*, 5929–5936.

47. N. R. Jana, X. Peng, *Journal of the American Chemical Society,* **2003**, *125*, 14280-14281.

6. Conclusions

6. Conclusions

The most relevant conclusions obtained during the course of this thesis are summarized below.

- CdSe NPs with different morphology can be synthesized by the *hot injection method.* The shape transformation from rod-like to pyramidal shaped NPs is obtained including a chlorinated co-solvent in the reaction media. It has been found that during the reaction the ethane-1,2-dyilbys(trioctylphosphonium)dichloride is formed releasing chloride ions that causes the morphology changes.
- The cyclic voltammetry characterization of CdSe NPs with different morphology, size and surface composition reveals that the redox processes depend on the NP surface composition, the scan direction, the number of cycles and the NP organization around the electrode surface.
- The cyclic voltammetry results obtained in this thesis evidence that the electrochemical response of CdSe NPs is due to the redox processes on the surface of the NPs and are not related with the injection of holes and electrons in the valence and conduction bands, respectively. It is then demonstrated that cyclic voltammetry is not a suitable technique to calculate the electrochemical bandgap as a comparable value to the optical one, for CdSe NPs.
- Combining CV and XPS techniques it has been shown that the presence of chloride ligands changes the redox response and its oxidation also modifies the chemical environment of Cd surface sites. The surface studies performed by XPS after an anodic scan evidence the irreversible oxidation of Se in rod-like NPs whereas certain reversibility has been observed for pyramidal shaped NPs capped with chloride.
- For the synthesis of Au-CdSe NPs by the *seeded-growth method* it has been demonstrated that the final morphology of the deposits (rod-like or shell) is driven by the initial oxidation state of the Au precursors (Au(I) or Au(III)).
- It has been verified that the chemical composition of the Au deposits depends on the surface composition of the seed NPs. For pyramidal shaped CdSe NPs capped with phosphonates ($ODPA^{2-}$) and chloride ligands the Au deposits are not composed of elemental Au but most probably of AuSe or AuSeCl.

6. Conclusiones

A continuación se resumen las conclusiones más relevantes obtenidas durante el curso de esta tesis.

- Mediante el método de inyección en caliente es posible sintetizar nanopartículas de CdSe con diferente morfología. La transformación morfológica desde nanopartículas con forma cilíndrica a nanopartículas con forma piramidal se obtiene incluyendo disolventes clorados en el medio de reacción. Se ha demostrado que el dicloruro de etano-1,2-diilbis(trioctilfosfonio) se forma durante la reacción desprendiendo iones cloruros responsables del cambio de morfología.
- Mediante la caracterización de nanopartículas de CdSe de diferentes tamaños, formas y composición química se ha comprobado, por voltametría cíclica, que los procesos redox dependen la composición superficial de las nanopartículas, de la dirección de barrido, del número de ciclos y de la organización de las nanopartículas alrededor de la superficie del electrodo.
- Mediante voltametría cíclica se ha podido demostrar que los procesos redox de nanopartículas de CdSe se producen en la superficie de éstas y no están relacionados con la inyección de huecos y electrones en la banda de valencia y de conducción, respectivamente. Por tanto, la voltametría cíclica no es una técnica adecuada para calcular el intervalo de energías electroquímico de nanopartículas de CdSe y no es posible compararlo con el valor obtenido mediante espectroscopía óptica.
- Mediante la combinación de las técnicas de voltametría cíclica y XPS se ha demostrado que la incorporación de ligandos cloruro modifica la respuesta electroquímica y que su oxidación también produce cambios en el entorno químico de los átomos de Cd superficiales. Además, la aplicación de un barrido anódico provoca la oxidación irreversible del Se en el caso de las nanopartículas con forma cilíndrica mientras que se aprecia cierta reversibilidad en el caso de nanopartículas con forma piramidal.
- En la síntesis de nanopartículas híbridas de Au-CdSe mediante el método de crecimiento sobre semillas se ha comprobado que la morfología final de los depósitos de Au (tipo esferas en los vértices o cobertura alrededor de la NP) depende del estado de oxidación inicial del precursor de Au (Au(I) or Au(III)).

- Se ha elucidado que la composición química de los depósitos de Au depende de la composición química superficial de las nanopartículas utilizadas como semillas. En el

caso de las nanopartículas con forma piramidal, cuyos ligandos son fosfonatos ($ODPA^{2-}$) y cloruros, los depósitos de Au no están compuestos de Au(0) sino probablemente de AuSe o AuSeCl.

ANNEX I.

ANNEX I

I. I. Reagents and materials

Anhydrous acetonitrile (99.8%), 1-chlorooctadecane (ODC; 96.0%), trioctylphosphine (TOP; 97%), methanol (99.8%), tetrabutylammonium perchlorate (TBAB; 99.0%) and gold(III) chloride ($AuCl_3$; 99.0%, storage in a nitrogen filled glovebox) were purchased from Aldrich. Cadmium oxide (CdO; 99.998%), selenium powder (Se; 99.999%), n-dodecyltrimethylammonium bromide (DTAB; 99%) and octadecylphosphonic acid (ODPA, crystalline) were acquired from Alfa Aesar. Toluene (99.5%) and 1,2-dichloroethane (DCE; 99.5%) were procured from Panreac. Trioctylphosphine oxide (TOPO; 98.0%), silver nitrate ($AgNO_3$; 99.8) and pyridine (99.6%) were obtained from Merck. Acros is the producer of 1-dodecanothiol (DDT; 98.0%). All the reagents were used as received without further purification.

The Highly Oriented Pyrolitic Graphite substrates (HOPG) ZYB quality, with 1 cm^2 of size and 2 mm of thickness were purchased from NT-MDT, whereas the glassy-carbon (GC) bars of 1 mm diameter and 15 mm length were acquired from Hochtemperatur-Werkstoffe GmbH (HTW).

I. II. Methodology

I. II. I. Cyclic Voltammetry (CV)

Electrochemical cell

A glass electrochemical cell with a three electrode setup and double wall to allow the solution thermostat was used.

A square platinum sheet (99.998% purity) with a larger area than the working electrode to avoid polarizations served as **counter electrode.**

A glassy-carbon bar of 9 mm length and 1 mm diameter was used as **working electrode**. Two different methods have been used to deposit de CdSe NPs: i) drop-casting of a dispersion of CdSe NPs obtaining a multilayer working electrode of CdSe NPs randomly distributed by solvent evaporation, and ii) pot-deposition of an order CdSe NPs monolayer obtained by including the glassy-carbon bar in the reaction pot. In this case the pyramidal CdSe NPs are always attached to the electrode surface by the same crystallographic face (000-1).

The working electrode potential is measured against a **reference electrode** of $Ag/AgNO_3$ fabricated in the laboratory ($Ag/AgNO_3$ 0.1 M//TBAP 0.1 M in acetonitrile). This electrode consist on a silver wire that is in contact with a solution of $AgNO_3$ 0.1 M and tetrabutylammonium perchlorate (TBAP) 0.1 M in acetonitrile. The solution of the reference electrode is in contact with the supporting electrolyte solution through a porous fiber. This electrode also has a luggin capillary to reduce the potential drop between the working and the reference electrode. All potentials are quoted with respect this electrode, whose potential is 0.5326 V *versus* the Normal Hydrogen Electrode (NHE). This electrode is assembled inside a glove-box.

The **supporting electrolyte solution** consists of a mixture of TBAP 0.1 M in acetonitrile. To avoid the presence of oxygen, the electrolyte solution was done under N_2 atmosphere inside a glove-box. First, the TBAP salt is introduced in a completely dried flask and three cycles of vacuum/nitrogen were done. Finally, the organic solvent was added inside a glove-box filled with N_2.

All the electrochemical measurements were done in organic media at 25 ± 1 °C and in the absence of oxygen, since it is electroactive specie in the range of work potentials. To this end, the solution is saturated by passing an inert gas flow (nitrogen or argon) that displaces the oxygen during a time prior to the measurements. This time depends on the solution volume (around 20 minutes).

Experimental procedure

Glassware pre-treatment

To obtain the glassware clean to perform the electrochemical measurements, all the glass pieces were immersed in a concentrated solution of H_2SO_4 (50 %), heated at 220 °C during 10 min, rinsed with ultrapure water and dried at 80 °C in an oven.

Electrodes cleaning

To clean the counter electrode the platinum sheet is sanded, burned in the Bunsen burner, rinsed with ultrapure water and dried at 80 °C in an oven.

To clean the reference electrode the silver wire is sanded, rinsed with ultrapure water and dried at 80 °C in an oven.

To clean the working electrode the glassy-carbon bar is sonicated 15 minutes in toluene, polished in a microcloth with 1 µm diamond paste (Buehler), sonicated 20 minutes in ultrapure distilled water and dried at 80 °C in an oven.

Samples pre-treatment

Before the electrochemical measurements the samples were purified. For the working electrodes deposited by drop-casting, the NPs batch was purified by centrifugation (5 minutes at 14000 rpm) and re-dispersion processes, using toluene as solvent and methanol as non-solvent. After two purification processes, the NPs batch was re-dispersed in toluene. In the case of the aliquots taken at 5 and 30 minutes of reaction the samples were first filtrate with PTFE filters of 0.45 µm pore size before the purification processes.

For the pot-deposition on glassy-carbon working electrodes, the modified electrodes were purified by washing the substrates in toluene baths to remove the NPs that are not attached to the electrode surface.

CV measurements

Once the electrochemical cell is mounted and deoxygenized, the CV of the glassy-carbon working electrode in the supporting electrolyte is recorded to verify the absence of contaminations. Afterwards, the analyte (NPs) is deposited on the electrode surface by drop-casting. For all CV measurements 50 µL of NPs, storage in batches at the same concentrations, were deposited. Only in the case of the correlated CV and XPS experiments, the electrodes were modified by depositing diluted dispersions of NPs (10 µL of NPs diluted in toluene to a final volume of 50 µL). In this manner, low thickness deposits of multilayer NPs were generated avoiding charge effects during the XPS measurements. On the other hand, to measure the electrode modified with a monolayer of NPs, the electrode fabricated by pot-deposition is used as working electrode.

Afterwards, the cell was deoxygenated again during 5 minutes and the voltammetric response of the NPs was measured. All the voltammograms were recorded at $0.1 V s^{-1}$.

I. II. II. X-ray photoelectron spectroscopy (XPS)

The XPS experiments were performed with tantalum foils as **substrates** that were fixed to the samples holders.

Experimental procedure

To clean the substrates, the tantalum foils were immersed in acetone and sonicated during 10 minutes and dried.

Both the samples of NPs deposited by drop-casting and the NPs attached to HOPG substrates were purified as the samples used in the electrochemical measurements. In the case of the correlated CV and XPS experiments, the glassy-carbon electrodes were washed after the CV measurement by carefully dropping acetonitrile to remove the electrolyte solution salt that may adsorb on the electrode.

The HOPG substrates were fixed to the tantalum foils with conductive carbon ribbon and the electrodes also with carbon ribbon and silver paint to improve the contact between the glassy-carbon bars and the substrates.

XPS measurements

Once the samples were assembled, the holder was introduced and transferred to the prevacuum chamber during 8 hours. Afterwards, the holder was transferred to the XPS chamber to perform the measurements that were done at room temperature in ultrahigh vacuum.

In chapter 3, the spectra of Cd *3d*, Se *3d*, and P *2p* were recorded using a pass energy of 10 eV, whereas spectra for Cl *2p* were recorded with 20 eV. The binding energies were referenced to Cd $3d_{5/2}$ at 405.2 eV.

In chapter 4, the spectra of Cd *3d* were recorded using a pass energy of 20 eV while the Se *3d* were recorded at 10 eV. Using these pass energies we obtained a FWHM for the Se $3d_{5/2}$ and Cd $3d_{5/2}$ lines of 0.9 and 1.3 eV, respectively. The binding energies were referenced to Cd $3d_{5/2}$ at 405.2 eV.

In chapter 5, all the spectra of Cd *3d*, Se *3d*, Au *4f* and C *1s* were recorded using a pass energy of 20 eV. Using these pass energies we obtained a FWHM for both the Cd $3d_{5/2}$ and Se

$3d_{5/2}$ lines of 0.8 eV, respectively. Binding energies were calibrated using the Csp^2 peak of the HOPG substrate at 284.5 eV as reference.

All the raw data were used, with no preliminary smoothing and charge neutralization was deemed to be unnecessary, since no movement of the Cd $3d_{5/2}$ line with time had been detected. Experimental spectra were deconvoluted using the XPSPEAK 4.1 software with symmetric Gaussian-Lorentzian product functions were used to approximate the line shapes of the fitting components. In order to fit the Cd and Se signals in HNPs, the binding energy, width (FWHM), and % of Gaussian-Lorentzian of the initial CdSe NPs have been kept constant.

I. II. III. Nuclear Magnetic Resonance (NMR)

Experimental procedure

All the NPs samples were purified as mentioned above for the other experiments. In the case of the ^1H NMR experiments, the samples were prepared using deuterated chloroform ($CDCl_3$) as solvent. The NMR tubes, containing the precise amount of $CDCl_3$ were purged and filled under nitrogen. For the ^1H MAS and ^{31}P CP/MAS solid state NMR (cross-polarization/magic angle spinning nuclear magnetic resonance) experiments the samples were dried and transferred either to a 4 mm or to 2.5 mm diameter probes.

NMR measurements

^1H NMR spectra were acquired with a sufficient relaxation delay to allow complete relaxation between pulses.

For the 2.5 mm probe ^{31}P CP/MAS experiments, an excitation ^1H $\pi/2$ 2,2 µs pulse was used with 50 kHz spectral width, 4 ms contact time, and high power proton decoupling tppm 15 at 115 kHz. Recycled delay was set at 5 s. For the 4 mm probe experiments, an excitation ^1H $\pi/2$ 3 µs pulse was used with 35 kHz spectral width, 2 ms contact time and high power proton decoupling tppm 15 at 80 kHz. Recycled delay was set at 5 s. All spectra were referenced to 85% phosphonic acid (0 ppm) as standard. The solid ^{31}P CP/MAS NMR spectrum of ODPA was acquired by direct measurement of the purchased product. High spinning speed hinders polarization transfer from ^1H to ^{31}P but, at the same time, it is necessary to obtain better resolution, so the experimental conditions were optimized to balance these effects. The spectrum of rod-like CdSe NC was recorded at a spinning speed of 7 kHz, while it was necessary to increase the spinning speed up to 30 kHz to obtain well resolved peaks in the case of pyramidal CdSe NCs.

I. II. IV. Mass Spectometry (MS)

Experimental procedure

For the MS analysis of the reaction product between TOP and DCE of chapter 3, the reaction was carried out in a three-neck flask coupled to a Schlenk line. An equimolar mixture of DCE and TOP was stirred at room temperature for some minutes. Afterwards, a first aliquot was taken as a representative sample of the direct mixing of DCE and TOP at room temperature. A second aliquot was taken after keeping the temperature at 265 °C for 21 hours. In this case $CHCl_3$ was used as mobile phase.

For the MS analysis of the Au precursor solutions performed in chapter 5, the Au(III)-stock solution was carried out inside a glove-box under N_2 atmosphere by dissolving a mixture of $AuCl_3$ (4.42 mM) and DTAB (6.93 mM) in 15 mL of toluene. In the case of the Au(I)-DDT solution, DDT (75.5 mM) was added to the Au(III)-stock solution.

MS measurements

All the samples solutions were injected via direct infusion in an electrospray source with a flux rate of 20 µL/min, and the spectra were acquired in the positive and negative detection ion modes.

I. II. V. UV-Vis Absorption and fluorescence spectroscopy

Experimental procedure

All the NPs samples were purified as mentioned above for the other experiments. For the UV-Vis absorption and fluorescence measurements presented in chapter 4, diluted dispersions of CdSe NPs were transferred to quartz cuvettes with an optical pathway of 1 cm.

Measurements

All the absorption spectra were recorded from 400 to 800 nm and the wavelength of the first absorption maximum was determined at the crossing of tangents graphically fitted to the sides of the slope. The optical density (OD) is the absorbance registered at this wavelength.

The fluorescence or emission spectra were recorded by exciting the NPs at 400 nm and the acquisition range varies from 500 to 750 nm.

I. II. VI. X-ray Diffraction (XRD)

The purification of the CdSe NPs was done as has been described previously, whereas the purification of the HNPs composed of pyramidal CdSe NPs covered with a Au shell were purified by centrifugation and re-dispersion processes, using toluene as solvent and ethanol as non-solvent the first time and methanol as non-solvent in the following washes. After the purification processes, the samples were deposited by drop-casting onto a polished silicon substrate.

I. II. VII. Transmission Electron Microscopy (TEM)

Purified samples (10 µL) were drop-casted onto carbon covered copper grids. Medium values of nanoparticle dimensions were determined from at least 210 counts with Image-J software.

I. II. VIII. Scanning Electron Microscopy (SEM)

For the SEM analysis, the glassy-carbon electrodes before and after the CV measurements were purified as described above. These electrodes were fixed to the sample holder with conductive carbon tape.

I. II. IX. Molecular dynamic simulations

Simulations based on density functional theory (DFT) employ geometry optimization in order to evaluate the interaction/adsorption of molecules (ligands) on crystals. Such simulations represent the situation at 0 K. Most chemical reactions (also at surfaces) require an activation energy which can be provided by thermal energy. Thus, molecular dynamic simulations are necessary. In order to simulate the adsorption and possible decomposition of precursor molecules on nanoparticles, we employ molecular dynamics simulations within the DFT framework. For that, we used the versatile software package CP2K/QUICKSTEP43 with the PADE LDA functional, the DZVP basis set, and a corresponding GTH-PADE potential. An individual wurtzite-CdSe nanocrystal with 123 Cd and 123 Se atoms and the respective ligand molecules are simulated with periodic boundary conditions where the box dimensions are sufficiently large to avoid interaction between virtual neighboring molecular structures. The atom positions of the CdSe nanocrystal were kept fixed using the corresponding experimental values (a = 0.430 nm, c = 0.702 nm), while the ligand molecules were free to move or decompose. The simulation temperature (NOSE thermostat, time constant 50 fs, NVT ensemble) was 300 K, as in the experiments. All MD simulations ran for 20 ps, after which an additional geometry optimization has been performed at 0 K. In all cases the geometries

before and after this optimization are similar, the main difference being shorter bonds between the adsorbed moieties and the CdSe surface atoms. These simulations were done by Prof. Christian Klinke in the University of Hamburg.

I. III. Apparatus

The electrochemical experiments were performed with an Autolab PGSTAT20 (EcoChemie) with a GPES 4.9 software.

X-ray photoelectron spectroscopy has been performed in two different experimental setups, one at the Universidad Autónoma de Madrid (UAM) in the laboratory of R. Otero composed of a PHOIBOS 150 MCD5 electron hemispherical analyzer and a monochromatic Al Kα source (hv = 1486 eV), and another at the Helmholtz Zentrum Berlin für Materialien and Energie GmbH, BESSY II by the group of Prof. R. Otero and Prof. C. Klinke. All deconvolutions except those of chapter 3 (P signal) were performed by myself.

^{1}H NMR spectra were recorded on a Bruker AMS-300 MHz and the ^{1}H MAS and ^{31}P CP/MAS solid state NMR spectra were collected at room temperature on a Bruker AV 400 WB spectrometer at the SidI at the Universidad Autónoma de Madrid (UAM). These experiments were done by Dr. C. Palencia.

The mass spectrometry analysis was done with a QTOF hybrid analyzer, QSTAR pulsar i model (AB Sciex) at the SidI at the Universidad Autónoma de Madrid (UAM). The MS analysis of chapter 3 was done by Dr. C. Palencia, whereas the MS analyses of chapter 5 were done by myself.

The absorption measurements were carried out in a Varian Spectrophotometer Cary 50 and the photoluminescence spectra were recorded in a spectrofluorometer Horiba Jobin Yvon Fluoromax- 4.

XRD measurements were carried out with a Philips X'Pert PRO MPD with Bragg-Brentano geometry and a Cu (Kα) X-ray source emitting at 0.154 nm. Backgrounds were subtracted with the X'Pert Highscore Plus software. These experiments were done by M. Meyns from Prof. C. Klinke group at the University of Hamburg.

TEM has been performed on a JEOL 1010 with an acceleration voltage of 100 keV and scanning electron microscopy images were acquired in a field emission microscope (FE-SEM) Philips XL30 S-FEG and in a FEI microscope Nova Nanosem 230 model at the SidI at the

Universidad Autónoma de Madrid (UAM). High resolution TEM micrographs at reduced temperature (96 K) were obtained with a JEOL JEM 2200FS (UHR) equipped with a field emitter as well as CESCOR and CETCOR correctors and a cryo sample holder. The high resolution TEM images were acquired by Andreas Konowski, from Prof. Horst Weller group at the University of Hamburg.

ANNEX II.

ANNEX II.

2. 1. Molar amounts of reactants used in the synthesis of CdSe NPs with different Cd/Se ratios.

Cd/Se precursors molar ratio	4	2	1	0.5	0.25
DCE · 10^{-4} (mol)	2.5	0.75	0.38	0.38	0.38
CdO · 10^{-4} (mol)	7.8	3.9	2	2	2
ODPA · 10^{-4} (mol)	24	12	6	6	6
Se@TOP · 10^{-4} (1M) (mol)	2	2	2	4.3	8
DCE/CdO (mol)	0.32	0.19	0.19	0.19	0.19
DCE/Se@TOP (mol)	1.25	0.38	0.19	0.09	0.05
DCE/TOP (mol)	0.62	0.19	0.12	0.06	0.03

Table 1. Molar amounts of precursors used to prepare CdSe NCs from different Cd/Se precursor molar ratios. DCE/CdO and DCE/Se@TOP and DCE/TOP molar ratios are also included.

List of abbreviations

List of abbreviations

CP/MASS	Cross-polarization/magnetic angle spinning
CV	Cyclic voltammetry
DCE	1,2-dichloroethane
DDT	1-dodecanethiol
DMF	N,N-dimethylformamide
DTAB	Dodecyltrimethylammonium bromide
EDX	Energy-dispersive X-ray spectroscopy
E_g	Band gap
ESI	Electrospray ionization
HNPs	Hybrid nanoparticles
HOMO	Highest occupied molecular orbital
HOPG	Highly oriented pyrolytic graphite
HR	High resolution
MS	Mass spectrometry
NMR	Nuclear magnetic resonance
NPs	Nanoparticles
ODC	1-chlorooctadecane
ODPA	Octadecyphosphonic acid
SEM	Scanning electron microscopy
STEM	Scanning transmission electron microscopy
TBAP	Tetra-n-butylammonium bromide
TEM	Transmission electron microscopy

TOF	Time-of-flight
TOP	Trioctylphosphine
TOPO	Trioctylphosphine oxide
XRD	X-ray diffraction

Publications and conference contributions

Publications and conference contributions

List of publications

Thesis related publications:

- F. Iacono, L. de la Cueva, J. M. Gallego, B. H. Juarez, R. Otero. "*Thermal Ligand Desorption in CdSe Quantum Dots by Correlated XPS and STM*" **Particle & Particle Systems Characterization**, 2016.

- L. de la Cueva, M. Meyns, N. G. Bastús, J. Rodríguez-Fernández, R. Otero, J. M. Gallego, C. Alonso, C. Klinke, B. H. Juárez. "*Shell or Dots − Precursor Controlled Morphology of Au−Se Deposits on CdSe Nanoparticles*" **Chemistry of Materials**, 2016, ***28***, 2704−2714.

- C. Palencia, K. Lauwaet, L. de la Cueva, M. Acebrón, J. J. Conde, M. Meyns, C. Klinke, J. M. Gallego, R. Otero, B. H. Juárez. "*Cl-capped CdSe nanocrystals via in-situ generation of chloride anions*" **Nanoscale**, 2014, ***6***, 6812-6818.

- L. de la Cueva, K. Lauwaet, R. Otero, J. M. Gallego, C. Alonso, B. H. Juárez. "*Effect of Chloride Ligands on CdSe Nanocrystals by Cyclic Voltammetry and X-Ray Photoelectron Spectroscopy*" **Journal of Physical Chemistry C**, 2014, ***118***, 4998-5004.

- F. Iacono, C. Palencia, L. de la Cueva, M. Meyns, L. Terracciano, A. Vollmer. M. J. de la Mata, C. Klinke, J. M. Gallego, B. H. Juárez, R. Otero. "*Interfacing Quantum Dots and Graphitic Surfaces with Chlorine Atomic Ligands*" **ACS NANO**, 2013, ***7***, 2559-2565.

Other publications:

- D. H. Ortgies, L. de la Cueva, B. del Rosal, F. Sanz-Rodríguez, N. Fernández, M. C. Iglesias-de la Cruz, G. Salas, D. Cabrera, Francisco J. Teran, D. Jaque, E. M. Rodríguez. "*In Vivo Deep Tissue Fluorescence and Magnetic Imaging Employing Hybrid Nanostructures*" **Applied Materials & Interfaces**, 2016, ***8***, 1406−1414.

- S. M. Ocampo, V. Rodriguez-Fanjul, L. de la Cueva, G. Salas, J. L. Carrascosa, M. J. Rodriguez, N. García-Romero, J. L. Cuñado, J. Camarero, R. Miranda, C. Belda-Iniesta, A. Ayuso-Sacido. "g-*force induced giant efficiency of nanoparticles internalization into living cells*" **Scientific Reports**, 2015, **5**.

- Aires, S. M. Ocampo, D. Cabrera, L. de la Cueva, G. Salas, F. J. Terán, A. L. Cortajarena. *"BSA-coated magnetic nanoparticles for enhanced therapeutic properties"* **Journal of Materials Chemistry B**, 2015, ***3***, 6239-6247.

Conference contributions
Oral contributions:

- Title: “Surface characterization of CdSe-Au hybrid nanoparticles by cyclic voltammetry and X-ray photoelectron spectroscopy”
  Authors: **L. de la Cueva**, M. Meyns, J. M. Gallego, R. Otero, C. Klinke, C. Alonso, B. H. Juárez
  Congress: “5th Early Stage Research Workshop at IMDEA Nanociencia 2015”
  Place: Madrid (España)
  Date: 17-18 Junio, 2015

- Title: “Estudios electroquímicos de nanocristales semiconductores”
  Authors: **L. de la Cueva**, C. Alonso, B. H. Juárez
  Congress: “XXXIII Reunión del Grupo de Electroquímica de la RSEQ”
  Lugar de celebración: Madrid (España)
  Date: 1-4 Julio, 2012

- Title: “Electrochemical studies on CdSe nanocrystals”
  Authors: **L. de la Cueva**, C. Alonso, B. H. Juárez
  Congress: “2nd Early Stage Research Workshop at IMDEA Nanociencia 2012”
  Place: Madrid (España)
  Date: 28-29 Junio, 2012

- Title: “Electrochemical studies on CdSe nanocrystals and CdSe-Carbon Nanotube composites”
  Authors: **L. de la Cueva**, C. Alonso, B. H. Juárez
  Congress: “1st Early Stage Research Workshop at IMDEA Nanociencia 2011”
  Place: Madrid (España)
  Date: 21 Junio, 2011

Posters:

- Title: “Silica encapsulation of magnetic nanoparticles”
  Authors: **L. de la Cueva**, P. Rodríguez, R. Amaro, D. Cabrera, M. Acebrón, B. H. Juárez, F. J. Terán, G. Salas
  Congress: “Physical properties of nanoparticles: Characterization and applications”
  Place: Bad Honnef (Germany)
  Date: 26-31 Julio, 2015

- Title: “Silica encapsulation of magnetic nanoparticles”
  Authors: **L. de la Cueva**, P. Rodríguez, R. Amaro, D. Cabrera, M. Acebrón, B. H. Juárez, F. J. Terán, G. Salas
  Congress: “Final MultiFun 2015 Workshop”
  Place: Madrid (España)
  Date: 23-25 Febrero, 2015

- Title: “Suface characterization of CdSe-Au hybrid nanoparticles by cyclic voltammetry and X-ray photoelectron spectroscopy”
  Authors: **L. de la Cueva**, M. Meyns, K. Klinke, J. M. Gallego, R. Otero, C. Alonso, B. H. Juárez
  Congress: “NaNaX 6”
  Place: Bad Hofgastein (Austria)
  Date: 18-23 Mayo, 2014

- Title: “Interfacing quantum dots and graphitic surfaces with chloride anions as ligands”
  Authors: C. Palencia, F. Iacono, **L. de la Cueva**, C. Alonso, K. Lauwaet, J. M. Gallego, R. Otero, B. H. Juárez
  Congress: “NaNaX 6”
  Place: Bad Hofgastein (Austria)
  Date: 18-23 Mayo, 2014

- Title: “Surface studies of CdSe-Au hybrid nanocrystals”
  Authors: **L. de la Cueva**, M. Meyns, J. M. Gallego, R. Otero, C. Klinke, C. Alonso, B. H. Juárez
  Congress: “XXXIV Reunión del Grupo de Electroquímica de la RSEQ”
  Place: Valencia (España)
  Date: 15-17 Julio, 2013

- Title: “Suface effects of Chlorine on CdSe nanocrystals”
  Authors: **L. de la Cueva**, C. Palencia, K. Lauwaet, J. M. Gallego, R. Otero, C. Alonso, B. H. Juárez
  Congress: “XXXIV Reunión del Grupo de Electroquímica de la RSEQ”
  Place: Valencia (España)
  Date: 15-17 Julio, 2013

- Title: “Electrochemical studies on CdSe nanocrystals”
  Authors: **L. de la Cueva**, C. Palencia, K. Lauwaet, F. Iacono, M. Meyns, C. Klinke, J. M. Gallego, R. Otero, C. Alonso, B. H. Juárez
  Congress: “3rd Early Stage Research Workshop at IMDEA Nanociencia 2011”
  Place: Madrid (España)
  Date: 27-28 Junio, 2013

- Title: “Electrochemical studies on semiconductor nanocrystals”
  Authors: **L. de la Cueva**, C. Alonso, B. H. Juárez
  Congress: “NaNaX 5”
  Place: Fuengilora (España)
  Date: 7-11 Mayo, 2012

Particle
& Particle Systems Characterization
www.particle-journal.com
Materials Views
www.MaterialsViews.com

Thermal Ligand Desorption in CdSe Quantum Dots by Correlated XPS and STM

Fabiola Iacono, Leonor de la Cueva, José María Gallego, Beatriz H. Juarez, and Roberto Otero**

The last decades have witnessed a significant progress in the colloidal synthesis of size, shape, and composition-controlled semiconductor nanocrystals (NCs), also called colloidal quantum dots.[1,2] Out of these studies a set of concepts has emerged as guideline for the rational design of novel colloidal NCs and complex hybrid systems with synergetic functionalities.[3]

In order to produce complex structures as a result of the interaction between different materials, one of the most critical issues to be addressed is the detailed characterization of the organic–inorganic interfaces of each counterpart. This knowledge is essential in order to postulate reaction mechanisms that allow full control and reproducibility over the preparation of complex structures.

As a matter of course, the surface characterization of NCs has been formerly tackled by several means, including analytical techniques, imaging, mainly performed by transmission electron microscopy (TEM), and traditional surface science techniques. Advances in XPS (X-ray photoelectron spectroscopy), SAXS (small-angle X-ray spectroscopy), EXAFS (extended X-ray absorption fine structure), etc., and scanning probe techniques, such as AFM (atomic force microscopy) or STM (scanning tunneling microscopy), allow for in situ characterization of nanoscaled materials, molecules (or atoms) treated under singular conditions. Thus, complex characterization under high pressure conditions, composition controlled atmosphere, high or low temperatures, permits to mimic the behavior of these entities in scenarios close to real working conditions. As a result, valuable knowledge is obtained to shed light into the development of these materials, focus of a myriad of applications, from catalysis to aerospace technology.

Imaging, along with spectroscopical information at a single particle level, has been previously reported by STM in combination with STS (scanning tunneling spectroscopy), revealing a quantized density of states in different size, shape, and composition-controlled NCs, including hybrid metal–semiconductor structures.[4–7] Imaging of NCs by STM requires reducing the tunnel barriers, from the STM tip to the NCs surface and from the NCs surface to the substrate,[8] by desorption of solvents and/or ligands that passivate the NCs surface. This is usually performed by gently heating the samples at temperatures around 150 °C for several hours.[9] Furthermore, to avoid NCs displacement during imaging, they must be tightly anchored to the surface, which can be resolved by passivating the NP surface with a ligand that binds covalently to the substrate.[10] Alternatively, imaging can also be controlled by taking advantage of ordered arrangements, where tip effects over the movement of NCs are minimized.[5]

In this work, we report STM and synchrotron XPS studies of pyramidal CdSe NCs self-assembled on highly oriented pyrolytic graphite (HOPG) substrates. The samples have been characterized by STM after different annealing treatments from 80 to 400 °C, evidencing a soft intra-particle ripening at moderate temperatures (up to 200 °C) and a severe inter-particle ripening (Ostwald Ripening) at higher ones. While these effects, studied in detail for colloidal semiconductor quantum dots in solution,[11] were also previously well known in nanoparticle systems grown by MBE on solid surfaces,[12] our system, consisting on colloidal NCs deposited on the surface is different at least regarding the presence of the capping ligands. Synchrotron-based, high-resolution XPS experiments reveal indeed that the activation of the ripening processes is correlated with the sequential desorption of the different chemical components of the ligand shell. The adsorption/desorption of ligands in colloidal NCs is regularly investigated by NMR spectroscopy[13] but rarely in ultrahigh vacuum conditions. In this work correlated synchrotron XPS performed after the annealing treatments allows studying the desorption dynamics of the different ligands. While degradation enhanced by temperature has been widely studied in supported NCs to study the loss of active surface area,[14] our studies give emphasis to the effects that each ligand desorption at different temperatures provokes on the NC's morphology. The methodology followed in this work can be very valuable to correlate the performance of nanoscale supported materials (i.e., heterogeneous catalysis, fuel cells, etc.) working under high temperature real conditions with modifications on their surface, taking also organic capping ligands into account.

Dr. F. Iacono, Dr. R. Otero
Departamento de Física de la Materia Condensada and Instituto Nicolás Cabrera
Facultad de Ciencias
Universidad Autónoma de Madrid
Avenida Francisco Tomás y Valiente 7, 28049 Madrid, Spain
Dr. F. Iacono, L. de la Cueva, Dr. B. H. Juarez, Dr. R. Otero
IMDEA Nanoscience
Faraday 9, 28049 Madrid, Spain
E-mail: beatriz.hernandez@imdea.org; Roberto.otero@imdea.org
Dr. J. M. Gallego
Instituto de Ciencia de Materiales de Madrid (ICMM-CSIC)
Calle Sor Juana Inés de la Cruz, 3, Cantoblanco, 28049 Madrid, Spain
Dr. B. H. Juarez
Departamento de Química-Física Aplicada
Facultad de Ciencias
Universidad Autónoma de Madrid
Avenida Francisco Tomás y Valiente 7, 28049 Madrid, Spain

DOI: 10.1002/ppsc.201600027

CHEMISTRY OF MATERIALS

Article

pubs.acs.org/cm

Shell or Dots – Precursor Controlled Morphology of Au–Se Deposits on CdSe Nanoparticles

Leonor de la Cueva,[†,¶] Michaela Meyns,[‡,▽,¶] Neus G. Bastús,[§] Jonathan Rodríguez-Fernández,[∥] Roberto Otero,[†,∥] José M. Gallego,[†,⊥] Concepción Alonso,[#] Christian Klinke,[*,‡] and Beatriz H. Juárez[*,†,#]

[†]Madrid Institute of Advanced Studies in Nanoscience, IMDEA Nanoscience, Faraday 9, Cantoblanco, 28049 Madrid, Spain

[‡]Institute of Physical Chemistry, University of Hamburg, Grindelallee 117, 20146 Hamburg, Germany

[§]Institut Català de Nanociència i Nanotecnologia (ICN2), CSIC and The Barcelona Institute of Science and Technology, Campus UAB, Bellaterra, 08193 Barcelona, Spain

[∥]Physics Condense Matter Department, Universidad Autónoma de Madrid, 28049 Madrid, Spain

[⊥]Instituto de Ciencia de Materiales de Madrid, Consejo Superior de Investigaciones Científicas (ICMM-CSIC), Sor Juana Inés de la Cruz 3, Cantoblanco, 28049 Madrid, Spain

[#]Department of Applied Physical Chemistry, Universidad Autónoma de Madrid, Cantoblanco, 28049 Madrid, Spain

Supporting Information

ABSTRACT: The most prevalent image of the morphology of Au–CdSe hybrid nanoparticles (HNPs) is that of dumbbells or matchsticks with CdSe nanoparticles (NPs) acting as seed material onto which spherical Au dots are deposited. On the basis of a system with only three reaction components, CdSe seeds, *n*-dodecyltrimethylammonium bromide-complexed $AuCl_3$, and dodecanethiol, we demonstrate how the morphology of the Au deposits on the semiconductor NPs, either in the form of dots on the vertices or in the form of a shell around the NP surface, can be determined by controlling the oxidation state of the metal precursor. Furthermore, we apply X-ray photoelectron spectroscopy to show that the resultant deposits are composed of partially oxidized Au, corresponding to a Au–Se compound regardless the deposit morphology. To obtain a detailed characterization of the HNPs with different morphologies and to gain mechanistic insights into the deposition process, (cryogenic) high-resolution transmission electron microscopy, mass spectrometry, cyclic voltammetry, and computational simulations have been performed. Our results emphasize that the knowledge of the surface chemistry of the seed particles as well as a defined picture of the metal precursors is necessary to understand heterodeposition processes.

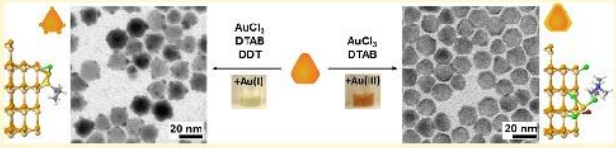

INTRODUCTION

The small dimensions and the high chemical reactivity of nanoparticles (NPs) have opened the door to a whole universe of new material combinations, compositions, and architectures. The growth of multidomain semiconductor–metal hybrid nanoparticles (HNPs) by colloidal seeded-growth techniques (consisting essentially of the reduction of a metal complex on the surface of semiconductor NPs used as a seeds) has attracted particular interest.[1−4] By taking advantage of the different surface chemistries of the two components, metallic domains can act as anchor points for biofunctionalization or help to direct the self-assembly of the HNPs.[5,6] With respect to the physical properties, the growth of Au or Pt metallic contacts on individual semiconducting CdSe NPs increases their conductance and enables charge separation of generated electron–hole pairs, finding applications in photocatalysis and hydrogen generation.[7−14] The reduction process of the metal precursor depends on the surface chemistry of the semiconductor seeds, including for example the presence of polar or nonpolar facets, the type of atoms, dangling bonds, etc.[15,16] Besides, the interaction of the precursor with ligands having different length and ligand density on a particular facet and, especially, the oxidation state of the precursor and its concentration play important roles.[17,18] In general, the reduction of metal complexes in organic media results in elemental metal deposits, as in the case of phosphonic acid-capped CdSe, which are held responsible for increasing the electrical conductivity in the final HNPs.[19] In most cases the metallic deposits grow exclusively in the form of spherical dots, on the tips, apexes, or defects on the different NP facets.[6,15,20]

While a commonly applied strategy involving a mixture of $AuCl_3$, a complex agent in the form of alkylammonium bromides, and alkylamines as mild reducing agent frequently results in dumbbell or matchstick-like morphologies with CdSe (or CdS) nanorods as the center domain,[6,20] a distinctly different behavior was observed with hexagonal pyramidal CdSe NPs.[17] Instead of well-defined and stable spherical Au domains, a shell-like structure that evolved into irregular Au dots upon exposure to the electron beam during transmission electron microscopy (TEM) inspections was observed. The possibility

Received: January 21, 2016
Revised: March 31, 2016
Published: March 31, 2016

DOI: 10.1021/acs.chemmater.6b00287
Chem. Mater. 2016, 28, 2704−2714

Nanoscale

PAPER

View Article Online
View Journal | View Issue

Cite this: *Nanoscale*, 2014, **6**, 6812

Cl-capped CdSe nanocrystals *via in situ* generation of chloride anions†

Cristina Palencia,‡*[a] Koen Lauwaet,[a] Leonor de la Cueva,[a] María Acebrón,[a] Julio J. Conde,[a] Michaela Meyns,[b] Christian Klinke,[b] José M. Gallego,[ac] Roberto Otero[ad] and Beatriz H. Juárez‡*[ae]

Received 22nd January 2014
Accepted 30th March 2014

DOI: 10.1039/c4nr00431k

www.rsc.org/nanoscale

Halide ions cap and stabilize colloidal semiconductor nanocrystal (NC) surfaces allowing for NCs surface interactions that may improve the performance of NC thin film devices such as photo-detectors and/or solar cells. Current ways to introduce halide anions as ligands on surfaces of NCs produced by the hot injection method are based on post-synthetic treatments. In this work we explore the possibility to introduce Cl in the NC ligand shell *in situ* during the NCs synthesis. With this aim, the effect of 1,2-dichloroethane (DCE) in the synthesis of CdSe rod-like NCs produced under different Cd/Se precursor molar ratios has been studied. We report a double role of DCE depending on the Cd/Se precursor molar ratio (either under excess of cadmium or selenium precursor). According to mass spectrometry (ESI-TOF) and nuclear magnetic resonance (^{1}H NMR), under excess of Se precursor (Se dissolved in trioctylphosphine, TOP) conditions at 265 °C ethane-1,2-diylbis(trioctylphosphonium)dichloride is released as a product of the reaction between DCE and TOP. According to XPS studies chlorine gets incorporated into the CdSe ligand shell, promoting re-shaping of rod-like NCs into pyramidal ones. In contrast, under excess Cd precursor (CdO) conditions, DCE reacts with the Cd complex releasing chlorine-containing non-active species which do not trigger NCs re-shaping. The amount of chlorine incorporated into the ligand shell can thus be controlled by properly tuning the Cd/Se precursor molar ratio.

Introduction

Colloidal semiconductor nanocrystals (NCs) show tunable and photostable luminescence properties along with broadband absorption and narrow emission, which makes them suitable for optoelectronic and photovoltaic applications.[1,2] For these purposes, fine control over the synthetic procedure to obtain monodisperse, robust and highly emissive semiconductor NCs is required. The development of the hot-injection method[3] provides high control over size, shape, shape distribution and NCs surface composition for semiconductor materials such as CdSe,[4,5] PbSe[6,7] or PbS.[8,9] This method also allows fine control over the NCs growth, which is achieved by the use of long alkyl chain surfactants acting as both metal complexing agents and ligands. These ligands form an insulating layer between NCs, restricting the charge transport between them and, as a consequence, devices containing such NCs (solar cells and photodetectors[10,11]) may show low conversion efficiencies. A less insulating ligand shell is obtained by the exchange of these long alkyl chain molecules for shorter ones, including thiols[12,13] or amines,[14–16] in post-reaction treatments. The use of halides to perform ligand exchange reactions has recently been proposed.[11,17–19] Halide anions can be considered as the shortest X type (ionic) ligands, facilitating charge transport among NCs. The passivating role of halide anions in PbS systems has been reported[11] and other reports have evidenced the passivation effect of chlorine in CdSe NCs, highlighting the possibility of using halogenated molecules to efficiently displace both L (coordinative) and/or X type ligands.[18,19] Post-reaction treatments with chlorine-containing solutions seem to provide some benefits to certain colloidal NCs, such as more robust optical

[a]*IMDEA Nanoscience, c\Faraday 9, Campus de Cantoblanco, 28049 Madrid, Spain. E-mail: cristina.palencia.ramirez@chemie.uni-hamburg.de; beatriz.hernandez@imdea.org*

[b]*Institute of Physical Chemistry, University of Hamburg, Grindelallee 117, 20146 Hamburg, Germany*

[c]*Instituto de Ciencia de Materiales de Madrid, ICMM, CSIC, Sor Juana Inés de la Cruz s\n, 28049 Madrid, Spain*

[d]*Dpto. de Física de la Materia Condensada and Instituto Nicolás Cabrera, Facultad de Ciencias, Universidad Autónoma de Madrid UAM, Avda. Fco. Tomás y Valiente 7, 28049 Madrid, Spain*

[e]*Dpto. de Química Física Aplicada, Facultad de Ciencias, Universidad Autónoma de Madrid UAM, Avda. Fco Tomás y Valiente 7, 28049 Madrid, Spain*

† Electronic supplementary information (ESI) available: Table S1 shows the molar amounts of the precursor used to prepare CdSe NCs from different Cd/Se precursor molar ratios. Fig. S2 shows TEM images of the control experiments. These consist of the synthesis of CdSe NCs from Cd/Se precursor molar ratios of 4, 2, 1, 0.5 and 0.25 in the absence of DCE. Table S3 shows the relative XPS peak areas of CdSe samples synthesized from different Cd/Se precursor molar ratios. See DOI: 10.1039/c4nr00431k

‡ Current address: Institute of Physical Chemistry, University of Hamburg, Grindelallee 117, 20146 Hamburg, Germany.

THE JOURNAL OF PHYSICAL CHEMISTRY C

Article

pubs.acs.org/JPCC

Effect of Chloride Ligands on CdSe Nanocrystals by Cyclic Voltammetry and X-ray Photoelectron Spectroscopy

Leonor de la Cueva,[†] Koen Lauwaet,[†] Roberto Otero,[†,‡] José M. Gallego,[‡,§] Concepción Alonso,[∥,*] and Beatriz H. Juarez*[,†,∥]

[†]Instituto Madrileño de Estudios Avanzados en Nanociencia (IMDEA Nanociencia), C/Faraday 9, Cantoblanco, 28049 Madrid, Spain

[‡]Departamento de Física de la Materia Condensada, Universidad Autónoma de Madrid, Madrid, Spain

[§]Instituto de Ciencia de Materiales de Madrid, ICMM, (CSIC), Sor Ángela de la Cruz, s/n, Cantoblanco, 28049 Madrid, Spain

[∥]Departamento de Química-Física Aplicada, Universidad Autónoma de Madrid, Cantoblanco, 28049 Madrid Spain

Supporting Information

ABSTRACT: Rod-like octadecylphosphonic acid (ODPA) capped CdSe nanocrystals (NCs) produced by hot injection in the presence of chlorinated cosolvents modify their shape and surface properties by incorporation of chloride in the capping ligand shell. Correlated cyclic voltammetry (CV) and X-ray photoelectron spectroscopy (XPS) studies have been performed to address the effect of this incorporation on the NCs surface. In contrast to ODPA capped rod-like NCs, the XPS studies confirm that, during the oxidation of NCs containing chloride, not only the oxidation of Se surface atoms but also of Cd atoms takes place. Furthermore, XPS studies also confirm the partial reversibility of the Se oxidation in the presence of chloride. Both CV and subsequent XPS measurements allows identifying chemical environments and surface site modifications, essential to understand the stability and performance of NCs acting as active layers in optoelectronic devices.

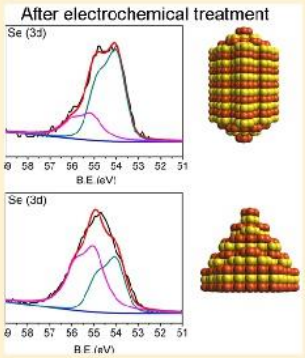

INTRODUCTION

Semiconductor nanocrystals (NCs; colloidal quantum dots) have been employed as harvesters in quantum dot-sensitized solar cells and photodetector devices.[1−5] The performance of such devices is ultimately determined by the structural quality and chemical nature of the interface between neighboring quantum dots, or between a quantum dot and the electric contact. For example, for solar cells, redox-couple species are used as scavengers for holes to prevent irreversible reactions on the surface of the NCs.[6] In photodetector devices, on the other hand, the removal of the usually long insulating organic ligands turns out to be essential to overcome the interface energy barrier, facilitating electrical transport in NCs films. To this aim, ligand exchange by shorter and/or conductive ligands, post physic-chemical treatments,[7] or the use of 2D materials[8] have been performed. Among the possible ligands, the treatment of the NCs with halogen-containing compounds[9,10] (rendering anion halide ligands, considered as atomic)[9] significantly improves the efficiency of devices.[11,12] Furthermore, the presence of such sort ligands on the NCs surface triggers electrostatic interactions between NCs and carbon nanotubes, making possible the photoconductive response.[13]

Cyclic voltammetry (CV) is a technique widely used to determine the stability of NCs as well as the potential difference between the oxidation and reduction processes, what have also triggered many studies to match the optical and electrochemical gaps.[14,15] Previous work reports that the electrochemical response of NCs is not significantly affected by different capping agents,[16] while others remark different band positions depending on chain length[17] or surface defects, which influence the electrochemical measurements.[18] Since the modification of the NCs surface generally causes observable changes in the optical response, i.e., photoluminescence (PL), several research groups have combined electrochemical and optical means to study the NCs.[19] Both CV and step-pulse voltammetry have been employed to investigate the PL of 2D monolayers of CdSe-based NCs as a function of applied potentials under air or N_2 atmospheres.[20] On the other hand, X-ray photoelectron spectroscopy (XPS) measurements have been scarcely employed to understand the possible source of the photoluminescence variations.[21] In this work we have studied the effect that the presence of chloride forming part of the ligand shell generates in the CV response of CdSe NCs. Different voltammetric responses have been recorded depending on the scan potential direction and capping ligand shell composition. Correlated CV and XPS measurements allow both to observe the difference in the electrochemical response of differently capped NCs and to identify chemical processes that Cd and Se surface atoms undergo under electrochemical treatments. We believe that the combination of these techniques is very useful to identify undesirable effects on NCs-based devices affected by nonoptimized charge injection/separation of charges.[22]

Received: December 3, 2013
Revised: February 10, 2014

   dx.doi.org/10.1021/jp4118425 | J. Phys. Chem. C XXXX, XXX, XXX−XXX

Interfacing Quantum Dots and Graphitic Surfaces with Chlorine Atomic Ligands

Fabiola Iacono,[†,●] Cristina Palencia,[‡,●] Leonor de la Cueva,[‡] Michaela Meyns,[§] Luigi Terracciano,[†] Antje Vollmer,[⊥] María José de la Mata,[¶] Christian Klinke,[§] José M. Gallego,[‡,#] Beatriz H. Juarez,[‡,▽,*] and Roberto Otero[†,‡,*]

[†]Departamento de Física de la Materia Condensada and Instituto Nicolás Cabrera, Facultad de Ciencias, Universidad Autónoma de Madrid, UAM, Avd. Fco. Tomás y Valiente 7, 28049 Madrid, Spain, [‡]IMDEA Nanoscience, c\ Faraday 9, Campus de Cantoblanco, 28049 Madrid, Spain, [§]Institute of Physical Chemistry, University of Hamburg, Grindelallee 117, Hamburg, Germany, [⊥]Helmholtz Zentrum Berlin für Materialien und Energie GmbH, BESSY II, Albert-Einstein-Strasse 15, 12489 Berlin, Germany, [¶]Servicio Interdepartamental de Investigación. SIdI. Universidad Autónoma de Madrid UAM, Avd. Fco. Tomás y Valiente 7, 28049 Madrid, Spain, [#]Instituto de Ciencia de Materiales de Madrid, ICMM, CSIC, Sor Ángela de la Cruz s/n, 28049 Madrid, Spain, and [▽]Departamento de Química Física Aplicada, Facultad de Ciencias, Universidad Autónoma de Madrid UAM, Avd. Fco. Tomás y Valiente 7, 28049 Madrid, Spain. [●]Fabiola Iacono and Cristina Palencia have contributed equally to this work.

ABSTRACT The performance of devices based on semiconductor nanocrystals (NCs) improves both with stronger interface interactions among NCs and between NCs and solid electrode surfaces. The combination of X-ray photoelectron spectroscopy (XPS) and solid ^{31}P CP/MAS NMR (cross-polarization/magic angle spinning nuclear magnetic resonance) shows that the selective substitution of long organic chains by chlorine atomic ligands during the colloidal synthesis by the hot injection method promotes the adsorption of CdSe NCs to carbon sp^2 surfaces, leading to the formation of well-ordered NC monolayers on graphitic materials.

KEYWORDS: CdSe nanocrystals · graphitic surface · graphene · atomic ligands · chlorine · interaction

Semiconductor nanocrystals (NCs) have found application as part of the active material in many optoelectronic and photovoltaic devices, due to their very interesting optical and electronic properties.[1] Usually, the performance of such devices is limited by the reduced charge mobility across the NC–NC and/or NC–electrode interfaces, because the surface of the colloidal NCs is stabilized by a shell of organic ligands that are usually long and poor electric conductors. The electronic mobility and thereby the performance of such devices can be enhanced by treatments that substitute the original insulating organic ligands for halides[2,3] or inorganic shells,[4] which improves the electronic NC–NC interface coupling.

Concerning the NC–electrode interface, a significant coupling has been reported for carbon C-sp^2 surface electrodes (carbon nanotubes (CNTs), graphene flakes, and graphitic surfaces covered with NCs).[5−9] These systems have been studied mainly because of their photoconductive response as a result of the possible photoinduced electron transfer across the interface upon optical excitation. Furthermore, for many applications, it is important to preserve the electronic transport properties across the C-sp^2 lattice. This implies that the interface should not be modified by covalent functionalization. One way to obtain noncovalently functionalized C-sp^2 lattices decorated with CdSe NCs is by adding 1,2-dichloroethane (DCE) during the synthesis of rodlike CdSe NCs by hot injection in the presence of such C-sp^2 surfaces.[9] Whether this method leads to chlorine incorporation in the ligand shell, the way in which the halogen could get incorporated to that shell, or the effect that this incorporation could have in mediating the interaction with the surface are questions which remain unexplored. It has been recently reported that molecular chlorine interacts with Se surface atoms of PbSe NCs passivating the surface, and preventing oxidation[11] and chloride ions decisively modifies the growth of branched NCs.[12] Chlorine ligand exchange has been followed by ^{1}H and ^{31}P NMR spectroscopy[13] and the coupling of nuclear magnetic resonance (NMR) and X-ray photoelectron

*Address correspondence to roberto.otero@uam.es.

Received for review December 19, 2012 and accepted February 8, 2013.

Published online February 08, 2013
10.1021/nn305868n